ИНСТИТУТ ЗА ФИЗИКУ
ПРИМЉЕНО: 14 -07- 2017
Рад.јед. | број | Арх.шифра | Прилог
0801 | 967/1

Naučnom veću Instituta za fiziku, Beograd

Pregrevica 118, Zemun

Predmet: Reizbor Nenada Selakovića u zvanje istraživač saradnik

Molba

Molim Naučno veće Instituta za fiziku da pokrene postupak za moj reizbor u zvanje istraživač saradnik.

Prilažem:

- Potpisan zahtev za pokretanje reizbora
- Mišljenje rukovodioca
- Biografiju
- Spisak objavljenih naučnih radova
- Fotokopije objavljenih naučnih radova
- Uverenje o upisanim doktorskim studijama
- Kratak pregled naučne aktivnosti kandidata
- Kopiju rešenja o prethodnom izboru u zvanje istraživač saradnik

U Beogradu

14.7.2017.

S poštovanjem

Nenad Selaković

Naučnom veću
Instituta za fiziku u Beogradu
Pregrevica 118, Zemun

Predmet: Mišljenje rukovodioca projekta o reizboru Nenada Selakovića u zvanje istraživač saradnik

Nenad Selaković je angažovan na projektu III41011 Primene niskotemperatursnih plazmi u biomedicini, zaštiti čovekove okoline i nanotehnologijama. 2011. godine upisao je doktorske studije na Fizičkom fakultetu Univerziteta u Beogradu - smer Fizika jonizovanog gasa, plazme i tehnologije plazme.

Kolega Selaković je, do sada, publikovao četiri rada u međunarodnim časopisima, tri kategorije M_{21} i jedan kategorije M_{23}, a i njegova istraživanja su publikovana na velikom broju međunarodnih konferencija.

Kako kandidat Nenad Selaković, zadovoljava sve formalne i suštinske uslove koji su potrebni za reizbor u zvanje *istraživač saradnik*, kako od strane Ministarstva za nauku, tako i od strane Instituta za fiziku u Beogradu, saglasna sam sa pokretanjem postupka za njegov reizbor u zvanje istraživač saradnik.

Predlažem komisiju u sastavu:
1. Dr Nevena Puač, naučni savetnik Instituta za Fiziku, Beograd
2. Dr Gordana Malović, naučni savetnik Instituta za Fiziku, Beograd
3. Prof. dr Srđan Bukvić, redovni profesor Fizičkog fakulteta Univerziteta u Beogradu

S poštovanjem

U Beogradu 14.7.2017.

Dr Nevena Puač
Rukovodilac projekta III41011

Biografija kandidata

Nenad Selaković je rođen u Beogradu 14.11.1981. godine. Pohađao je Tehničku školu “Petar Drapšin“.

Fizički fakultet je završio u Beogradu 2011. godine odbranom diplomskog rada na temu „Električna karakterizacija i prostorno-vremenski razložena merenja atmosferskog pražnjenja u režimu plazma metka”. Diplomski rad je uradio pod mentorstvom dr Gordane Malović i dr Nevene Puač u Laboratoriji za gasnu elektroniku pod rukovodstvom dr Zorana Lj. Petrovića. Dobitnik je nagrade “Prof. dr Ljubomir Ćirković” za najbolji diplomski rad odbranjen u periodu 2010/2011. Krajem 2011. godine upisuje doktorske studije na Fizičkom fakultetu Univerziteta u Beogradu – smer: Fizika jonizovanog gasa, plazme i tehnologija plazme i položio je sve ispite potrebne za redovan upis treće godine studija sa prosečnom ocenom 10.00.

Nenad Selaković je od 31.12.2011. godine zaposlen u Laboratoriji za gasnu elektroniku Instituta za fiziku, kao istraživač - pripravnik na projektu III41011 "Primene niskotemperaturnih plazmi u biomedicini, zaštiti čovekove okoline i nanotehnologijama" u okviru Centra izuzetnih vrednosti za primenu plazme u nanotehnologijama, biomedicini i ekologiji.

Nenad Selaković je do sada publikovao 3 naučna rada u vrhunskim međunarodnim časopisima (M_{21}) i jedan rad u međunarodnom časopisu (M_{23}). Rezultati njegovih istraživanja prezentovani su na velikom broju međunarodnih konferencija.

Objavljeni radovi kandidata

RAD U VRHUNSKOM MEĐUNARODNOM ČASOPISU M21

1. N. Puač, S. Živković, N. Selaković, M. Milutinović, J. Boljević, G. Malović, and Z. L. Petrović, "*Long and short term effects of plasma treatment on meristematic plant cells*", Applied Phyics. Letters, vol. 104 br. 21, p. 214106, 2014. DOI: 10.1063/1.4880360
2. D. Maletić, N. Puač, N. Selaković, S. Lazović, G. Malović, A. Djordjević and Z: Lj. Petrović, " *Time-resolved optical emission imaging of an atmospheric plasma jet for different electrode positions with a constant electrode gap*", Plasma Sources Science & Technology, vol. 24 br. 2, 2015. DOI: 10.1088/0963-0252/24/2/025006
3. A. Zeniou, N. Puač, N. Škoro, N. Selaković, P. Dimitrakellis, E. Gogolides and Z. Lj. Petrović, "*Electrical and Optical Characterization of an Atmospheric Pressure, Uniform, Large-Area Processing, Dielectric Barrier Discharge",* Journal of Physics D, vol. 50 br. 13, 2017. DOI: 10.1088/1361-6463/aa5d69

RAD U MEĐUNARODNOM ČASOPISU M23

4. J. Čech, A. Brablec, M. Černák, N. Puač, N. Selaković, and Z. Lj. Petrović, *Mass spectrometry of diffuse coplanar surface barrier discharge: influence of discharge frequency and oxygen content in N2/O2 mixture,* European Physical Journal D, vol. 71 br. 2, 2017. DOI: 10.1140/epjd/e2016-70607-5

SAOPŠTENJE SA MEĐUNARODNOG SKUPA ŠTAMPANO U CELINI M33

1. S. Lazović, N. Puač, S. Zivković, S. Jevremović, D. Maletić, N. Selakovlć, G. Malovie, J. Kovae, T. Filipie, M. Mozetič, U. Cvelbar, and Z. Lj. Petrovič, *"Properties and bio-medical applications of non-thermal"*, 69th Iuvsta Workshop On Oxidation Of Organic Materials By Excited Radicals Created In Non-Equilibrium Gaseous Plasma, December 9th December 13th 2011, Crklje na Gorenjeskem, Slovenia.
2. N. Selaković, D. Maletić, N. Puač, S. Lazović, G. Malović, A. Dorđević and Zoran Lj. Petrović, "Axial Profiles Of Plasma Bullet", 26th Summer School And International Symposium On The Physics Of Ionized Gases, August 27th - 31st, Zrenjanin, Serbia.
3. N. Selaković, N. Puač, M. Miletić, I. Živanović, I. Dakić, G. Malović, D. Vuković and Z. Lj. Petrović, "Methicilin resistant staphylococcus aureus inhibition areas obtained by a plasma needle treatment", 27th Summer School and International Symposium on the Physics of Ionized Gases (SPIG), August 26th - 29th 2014., Belgrade, Serbia.

4. N. Selaković, N. Puač, N. Gligorijević,M. Čavić, G. Malović, R. Janković, S. Radulović and Z. Lj. Petrović, "*Low temperatura plasma needle reduces the survival of cáncer cells",* 28th Summer School and International Symposium on the Physics of Ionized Gases (SPIG), August 29th - September 2nd 2016, Belgrade, Serbia.

SAOPŠTENJE SA MEĐUNARODNOG SKUPA ŠTAMPANO U IZVODU M34

5. D. Maletić, N. Puač, N. Selaković, S. Lazović, G. Malović, A. Đorđević and Z. Lj. Petrović, *" Time-resolved images of plasma bullet for different electrode geometries"* ESCAMPIG XXI, , July 10th-14th 2012. Viana do Castelo, Portugal.
6. D. Maletić, M. Miletić, N. Puač, N. Selaković, S. Lazović, D. Vuković, P. Milenković, G. Malović and Z. Lj. Petrović, *"Plasma needle treatment of Staphylococcus Aureus (ATCC 25923) biofilms"*, 4th International Conference on Plasma Medicine, June 17th - 21th, 2012., Orléans, France.
7. N. Selaković, D. Maletić, S. Lazović, N. Puač, , G. Malović, Z. Lj. Petrović *Mass spectroscopy investigation of an atmospheric pressure plasma bullet, CESPC,* August 25th-29th, 2013., Balatonalmadi, Hungary.
8. N. Selaković, N. Puač, D. Maletić, G. Malović, Z. Lj. *Petrović, "Time resolved mass spectrometry of positive ions originated from atmospheric-pressure plasma jet"* Bulletin of the American Physical Society, 2013. Princeton, USA.
9. N. Puač, S. Živković, N. Selaković, M. Milutinović, J. Boljević, G. Malović, and Z. Lj. Petrović, "*Application of atmospheric plasma sources in growth and differentiation of plant and mammalian stem cells*", 67th Annual Gaseous Electronics Conference, November 2nd - 7th, 2014. Raleigh, North Carolina, USA. (predavanje po pozivu)
10. A. Stancampiano, M. Gherardi, V. Colombo, N. Selaković, N. Puač and Z. Lj. Petrović, "*Mass spectroscopy and ICCD analysis of coupled and uncoupled mode in a Gatling-gun like plasma source*", The 42nd IEEE International Conference on Plasma Science (ICOPS), May 24th - 28th, 2015., Antalya, Turkey.
11. N. Selaković, J. Stašić, N. Puač, M. Miletić, V. Miletić, G. Malović and Z. Lj. Petrović, "*Modification of the dentin surface of human teeth by atmospheric pressure plasma needle",* XXIII Escampig, July 12th-16th, 2016, Bratislava, Slovakia.
12. N. Selaković, J. Voráč, N. Puač, G. Malović, P. Dvořák and Z. Lj. Petrović, "*Influence of humidity on formation of pulsed atmospheric pressure plasma streamers*", XXXIII International Conference on Phenomena in Ionized Gases, ICPIG, July 9th - 14th 2017., Estoril, Portugal.

Република Србија
Универзитет у Београду
Физички факултет
Д.Бр.2011/8034
Датум: 02.02.2017. године

На основу члана 161 Закона о општем управном поступку и службене евиденције издаје се

УВЕРЕЊЕ

Селаковић (Бранислав) Ненад, бр. индекса 2011/8034, рођен 14.11.1981. године, Београд, Београд-Земун, Република Србија, уписан школске 2016/2017. године, у статусу: самофинансирање; тип студија: докторске академске студије; студијски програм: Физика.

Према Статуту факултета студије трају (број година): три.
Рок за завршетак студија: у двоструком трајању студија.

Ово се уверење може употребити за регулисање војне обавезе, издавање визе, права на дечији додатак, породичне пензије, инвалидског додатка, добијања здравствене књижице, легитимације за повлашћену вожњу и стипендије.

Овлашћено лице факултета

_____

Република Србија
Универзитет у Београду
Физички факултет
Број индекса: 2011/8034
Датум: 02.02.2017.

На основу члана 161 Закона о општем управном поступку и службене евиденције издаје се

УВЕРЕЊЕ О ПОЛОЖЕНИМ ИСПИТИМА

Ненад Селаковић, име једног родитеља Бранислав, рођен 14.11.1981.године, Београд, Београд-Земун, Република Србија, уписан школске 2011/2012. године на докторске академске студије, школске 2016/2017. године уписан на статус самофинансирање, студијски програм Физика, током студија положио је испите из следећих предмета:

Р.бр.	Шифра	Назив предмета	Оцена	ЕСПБ	Фонд часова**	Датум
1.	ДС09ЈП1	Извори јонизованог гаса	10 (десет)	15	I:(5+0+0)	10.09.2011.
2.	ДС09ЈП3	Дијагностика плазме	10 (десет)	15	II:(5+0+0)	24.10.2012.
3.	ДС09ФРНД1	Рад на докторату 1. део	П.	30	I:(0+0+15) II:(0+0+15)	10.09.2012.
4.	ДС09ЈП5	Физика електричних гасних пражњења	10 (десет)	15	III:(5+0+0)	22.05.2013.
5.	ДС09ЈП8	Одабрана поглавља физике јонизованих гасова	10 (десет)	15	IV:(5+0+0)	12.06.2013.
6.	ДС09ФРНД2	Рад на докторату 2. део	П.	30	III:(0+0+15) IV:(0+0+15)	

* - еквивалентиран/признат испит.
** - Фонд часова је у формату (предавања+вежбе+остало).

Укупно остварено 120 ЕСПБ.
Општи успех: 10,00 (десет и 00/100) , по годинама студија (10,00, 10,00, /).

Овлашћено лице факултета

Naučna aktivnost kandidata

Nenad Selaković je angažovan na projektu III41011 "Primene niskotemperaturnih plazmi u biomedicini, zaštiti čovekove okoline i nanotehnologijama", pod rukovodstvom dr Nevene Puač, finansiranim od strane Ministarstva za prosvetu, nauku i tehnološki razvoj Republike Srbije.

Naučna delatnost i doprinos kandidata vezana su za proučavanje i primenu pražnjenja koja rade na atmosferskom pritisku. Njegov diplomski rad bio je posvećen električnoj karakterizaciji i prostorno-vremenski razloženim snimcima atmosferskog plazma džeta. Kandidat Selaković je u okviru svog diplomskog rada određivao strujno-naponske karakteristike plazma džeta, kao i snagu predatu plazmi. Optička emisiona spektroskopija ovog sistema je urađena pomoću brze ICCD kamere. Dobijeni su prostorno-vremenski razloženi snimci iz kojih se vidi da plazma nije kontinualna već da se sastoji iz paketa plazme. Cilj diplomskog rada je bio da se pomoću sistematskih, dobro definisanih merenja precizno odrede parametri plazme i njene karakteristike za što lakšu primenu u tretmanima.

Nakon diplomiranja nastavio je rad na proučavanju plazma džeta i pored već pomenutih dijagnostika proširio je aktivnost na maseno-energijsku analizu plazma izvora pomoću masenog spektrometra HIDEN HPR60. Ovaj maseni spektrometar je karakterističan po tome što radi na atmosferskom pritisku i omogućava karakterizaciju atmosferskih plazmi. Merenja obuhvataju snimanje masenih spektara neutrala i jona kao i spektara dobijenih menjanjem energije elektrona u jonizacionom izvoru samog uređaja. Takođe, pošto je ustanovljeno da se plazma ne prostire kontinualno već u obliku plazma paketa radiće se i vremenski razloženo snimanje neutrala i jona iz plazme. Ova analiza se vrši sa ciljem nalaženja optimalnih parametara pogodnih za tretman različitih vrsta uzoraka. Jedan od ključnih parametara svakako jesu koncentracije radikala i molekula formiranih u samoj plazmi. Merenja će da se vrše za različite uslove rada ovog plazma izvora. Očekujemo da će dalja istraživanja u ovom smeru dovesti do boljeg razumevanja veze između električnih karakteristika pražnjenja i hemijskih procesa u plazmi, a samim tim će se otvoriti nove mogućnosti primena atmosferskih niskotemperaturnih neravnotežnih plazmi.

Pored dijagnostike plazma džeta kandidat učestvuje i u istraživanjima uticaja plazme na: meristemske ćelije biljaka - *kalusa* (u saradnji sa Biološkim institutom “Siniša Stanković”); gram pozitivnih i gram negativnih bakterija (u saradnji sa Institutom za Mikrobiologiju i imunologiju i Stomatološkim fakultetom u Beogradu) korišćenjem plazma igle.

U daljem radu kandidat je proširio delatnost primene plazma igle gde se pomenuti izvor atmosferskog pražnjenja koristi za modifikaciju strukture ljudskog dentina (u saradnji s kolegama sa Stomatološkog fakulteta) i u redukciji rezistivnih kancerogenih ćelija pluća i grlića materice (u saradnji s kolegama sa Instituta za onkologiju i radiologiju). U proteklom periodu kolega Nenad Selaković je zajedno s kolegama iz Laboratorije za gasnu elektroniku ostvario saradnju sa kolegama iz inostranstva (Grčka, Češka i Italija). Iz tih saradnji proisteklo je nekoliko publikacija u međunarodnim časopisima i na međunarodnim konferencijama. U toku je finalizovanje još nekoliko radova koji će biti objavljeni u međunarodnim časopisima a proistekli su iz ovih saradnji. Takođe, kandidat je učestvovao u radu COST akcije TD1208 Plasmas in Lyquids i u okviru nje je posetio Masaryk Univeryitet u Brnu gde su izvršena merenja koncentracije OH radikala u pražnjenju plamza džeta.

РЕПУБЛИКА СРБИЈА
УНИВЕРЗИТЕТ У БЕОГРАДУ
ИНСТИТУТ ЗА ФИЗИКУ
080 Бр. 1207/17
24 -09- 2014 год

На основу члана 82. Закона о научноистраживачкој делатности ("Службени гласник Републике Србије", број 110/2005, 50/2006 - испр. и 18/2010), члана 33. тачка 5. Статута Института за физику и захтева који је поднео

НЕНАД СЕЛАКОВИЋ
на седници Научног већа Института за физику одржаној 23.09.2014. године, донета је

ОДЛУКА
О СТИЦАЊУ ИСТРАЖИВАЧКОГ ЗВАЊА

НЕНАД СЕЛАКОВИЋ
стиче истраживачко звање
Истраживач сарадник

ОБРАЗЛОЖЕЊЕ

Ненад Селаковић је 16.06.2014. године поднео захтев за стицање истраживачког звања истраживач сарадник. Научно веће Института за физику је на седници одржаној 17.06.2014. године образовало Комисију за спровођење поступка у саставу др Невена Пуач, виши научни сарадник у Институту за физику, др Гордана Маловић, научни саветник у Институту за физику и др Срђан Буквић, редовни професор Физичког факултета у Београду. Научно веће је на седници од 23.09.2014. године утврдило да именовани испуњава услове из члана 70. став 3. Закона о научноистраживачкој делатности за стицање истраживачког звања **истраживач сарадник,** па је одлучило као у изреци ове одлуке.

Одлуку доставити подносиоцу, архиви Института за физику, кадровској служби Института за физику и рачуноводственој служби Института за физику.

Председник Научног већа
др Љубинко Игњатовић

Директор Института за физику
др Александар Богојевић

Long and short term effects of plasma treatment on meristematic plant cells

N. Puač,[1] S. Živković,[2] N. Selaković,[1] M. Milutinović,[2] J. Boljević,[2] G. Malović,[1] and Z. Lj. Petrović[1]
[1]*Institute of Physics, University of Belgrade, Pregrevica 118, 11080 Belgrade, Serbia*
[2]*Institute for Biological Research "Siniša Stanković," University of Belgrade, Bulevar despota Stefana 142, 11060 Belgrade, Serbia*

(Received 23 February 2014; accepted 16 May 2014; published online 30 May 2014)

In this paper, we will present results of plasma treatments of meristematic cells of *Daucus carota*. Plasma needle was used as an atmospheric pressure/gas composition source of non-equilibrium plasma in all treatments. Activity of antioxidant enzymes superoxide dismutase and catalase was measured immediately after plasma treatment and after two weeks following the treatment. Superoxide dismutase activity was increased in samples immediately after the plasma treatment. On the other hand, catalase activity was much higher in treated samples when measured two weeks after plasma treatment. These results show that there is a direct proof of the triggering of signal transduction in the cells by two reactive oxygen species H_2O_2 and O_2^-, causing enzyme activity and short and long term effects even during the growth of calli, where the information is passed to newborn cells over the period of two weeks. © *2014 AIP Publishing LLC*.
[http://dx.doi.org/10.1063/1.4880360]

In the last decade, the expansion of the plasma medicine and its demand for *in-vivo* treatments resulted in fast development of various plasma devices that operate at atmospheric pressure. It is much more difficult to achieve non-equilibrium (non-thermal) mode of operation (as opposed to the thermal mode) at atmospheric pressures. Nevertheless, nonequilibrium operation is essential for treatment of biological samples for a number of reasons. For example, temperature of the tissue treated by plasma has to be kept below the threshold for the denaturation of the proteins. Another demand is that atmospheric plasma sources have to be able to do precise and localized treatments. This is so since some of the reactive species which have beneficial effects in small doses (as low as a single molecule serving as a trigger) may have very harmful effect in larger quantities.

In spite of difficulties to achieve nonequilibrium operation, numerous atmospheric pressure plasma sources fulfill all demands for application on biological samples. So far, atmospheric pressure discharges (APPD) were used for sterilization,[1] treatment of wounds,[2] improved blood coagulation,[3] treatments of skin,[4] treatment of cancer,[5] etc.

One of the sources that meet all the requirements needed for treatment of biological material is plasma needle. This device was first described by Stoffels and coworkers,[6] and it has been used to induce apoptosis and necrosis of cultured eukaryotic cells,[7] bovine aortic endothelial cells,[6] or human (epithelial cells—MR65 cells originating from non-small cell lung carcinoma (NSCLC)[8]) tissues.

We have developed a somewhat improved version of this device and used it for sterilization of planctonic samples of bacteria, MRSA biofilm, for improved differentiation of human periodontal stem cells into osteogenic line and for treatment of plant meristematic cells.[9,10] The derivative probe measurements of power delivered to the plasma and mass spectrometry of the plasma generated by the needle have already been presented in our previous work.[11,12] Plasma needle generates reactive oxygen species (ROS) and reactive nitrogen species (RNS) radicals like N, O, O_3, OH, and NO that strongly affect metabolism of living cells. One of the open issues is to correlate external plasma products (electrons, ions, RNS, ROS, photons, strong fields, etc.) with the immediate internal response which triggers or induces effects in the living cell. For that purpose, we study the kinetics of two enzymes which are typical indicators of the identity of reactive species from the plasma created environment that can trigger signal transduction in the cell and ensue cell activity.

In plants, ROS are always formed by the inevitable attachment of electrons to O_2 from the electron transport activities of chloroplasts, mitochondria, and plasma membranes or as a byproduct of various metabolic pathways localized in different cellular compartments.[13–15] All ROS are extremely harmful to organisms at high concentrations. When the level of ROS exceeds the defense mechanisms, a cell is said to be in a state of "oxidative stress." In order to avoid the damage caused by ROS, plants have evolved molecular defense systems that both limit the formation of ROS and promote its removal.[16] The plant enzymatic defenses include antioxidant enzymes, such as the phenol peroxidase (POX), ascorbate peroxidase (APX), glutathione peroxidase, (GPX), superoxide dismutase (SOD), and catalase (CAT), which together with other enzymes of the ascorbate–glutathione cycle promote the scavenging of ROS.[17]

In this paper, we will show results for the SOD and CAT activity in the *Daucus carota* calli cells immediately after the plasma treatment and two weeks after the treatment. SOD is considered to be the first line of defense against ROS.[18] It catalyzes the dismutation of O_2^- to H_2O_2 and molecular oxygen. CAT is present in the peroxisomes of nearly all aerobic cells, and, to a lesser extent, in mitochondria.[19] It serves as protection of the cell from H_2O_2 by catalyzing its decomposition into O_2 and H_2O.[20] Thus, both serve as good markers of internal chemical effects of the external plasma products and may also inspire similar procedures in animal and in human cells as well as for the bacteria.

 © 2014 AIP Publishing LLC

This article is copyrighted as indicated in the article. Reuse of AIP content is subject to the terms at: http://scitation.aip.org/termsconditions. Downloaded to IP: 109.121.73.231 On: Fri, 30 May 2014 20:30:40

For plasma treatment of calli, we have used plasma needle which is powered by sinusoidal signal at 13.56 MHz radio-frequency (RF). Construction and diagnostics of this device are described in more detail in Refs. 11 and 12. We have used helium as the working gas and the flow was 1 standard liter per minute (slm). As the working gas mixes with the air from the surrounding atmosphere, free radicals are generated within the plasma, such as reactive oxygen, nitrogen, nitrogen oxides, and ozone. The yields that were obtained for H_2O_2 and O_2 were 0.03% and 7.2%, respectively, in the helium flow of 1 slm while O_2^- was detected but no quantitative measurements could be made so far. Electrical circuit that supplies plasma needle consisted of signal generator which provided sine wave signal at RF frequency. This signal was amplified through a linear amplifier. We have used home-made derivative probes for measurement of the mean power transmitted to the plasma.

The embryogenic calli cultures of carrot (*Daucus carota*) were established from storage root explants and maintained on solid MS medium[21] supplemented with 2, 4-dichlorphenoxyacetic acid (2.4-D, 1.0 mg l^{-1}). Calli samples (10–30 mg) were placed in 96 wells micro-titer plate. The distance between the edge of the well and glass tube was 0.5 mm in all treatments. Well diameter was larger than diameter of the glass tube by 0.5 mm. Also, tip of the needle is located 1.5 mm outside the glass tube thus created plasma was in a mixture of helium and ambient air. During all experiments, plasma was covering whole surface of the samples and average distance between the needle and the culture surface was 4 mm. Culture was attached to the gel environment placed at the bottom of the micro titter plates. The treatment times were 10, 30, 60, and 120 s at two powers of 0.4 W and 1.6 W. Control calli samples were kept in micro-titer plate during the experimental procedure to ensure equal treatment conditions. Samples were also subjected to the treatment of only helium flow without the discharge with the exposure time of 120 s in order to determine whether helium flow affects the samples. After the treatment, calli were immediately frozen in liquid nitrogen and kept at −70 °C until use, or continuously cultured on fresh basal MS medium without plant growth regulators for 2 weeks before use. Plant tissue was grinded to a fine powder, and proteins were extracted in 100 mM potassium-phosphate buffer (pH = 6.5) supplemented with protease inhibitor cocktail for plant tissue extracts and 5 mM ascorbate. Protein content was determined according to Bradford (1976) using bovine serum albumin as a standard[22] and separated by native PAGE. The protein amounts applied to each well for the measurements of enzyme activity were 30 μg. Gels were stained for CAT activity as in Ref. 23. SOD activity (in units of enzyme activity mg^{-1}soluble protein) was determined as in Ref. 24.

ROS that include hydroxyl radicals (OH·), superoxide anion (O_2^-), and hydrogen peroxide (H_2O_2) are produced during normal cellular functioning. Under standard conditions antioxidant systems of the cell minimize the perturbations caused by ROS. If ROS generation is increased either externally outside the cell or internally, the result of this imbalance is oxidative stress.[25–27] Aerobic organisms evolved defenses that include both non-enzymatic and enzymatic antioxidants in order to minimize the damaging effects of ROS.[25,28] Because ROS are toxic, but also participate in signaling events, plant cell requires at least two different mechanisms to regulate their intracellular concentration by scavenging the ROS: one that will enable the fine modulation of low levels of ROS for signaling purposes and one that will enable the detoxification of excess ROS, especially during stress.[29] Major ROS scavenging mechanisms of plants include SOD, CAT, and different types of peroxidases. Their role is to directly scavenge superfluous amounts of the ROS created inside the cell or coming into the cell from the outside source. The SOD scavenges super oxide anion catalyzing its dismutation to hydrogen peroxide, while CAT reduces hydrogen peroxide to water.[30] Figure 1 shows the reaction paths inside the cell for the SOD and CAT.

We can see that the first enzyme that is usually employed in the cell defense is SOD followed then by the catalase that is responsible for the destruction of the products coming from the reactions involving SOD enzyme. We have measured activity of the SOD and CAT immediately after the plasma treatment and two weeks after the treatment. The analysis for the SOD activity performed immediately after the plasma treatment (Figure 2(a)) showed that enzyme activity of the carrot calli for the treatments with 0.4 W plasma did not alter significantly compared to the control samples. On the other hand, enzyme activity increased gradually with the treatment time for the higher power of 1.6 W. The highest SOD activity was observed for the treatment time of 120 s. Increase in the enzyme activity implies that more superoxide anions are present inside the cell and that calli cells are under oxidative stress. In order to cope with the elevated level of ROS antioxidants mechanisms in carrot calli had been triggered and enzyme activity was correlated with the stress level.

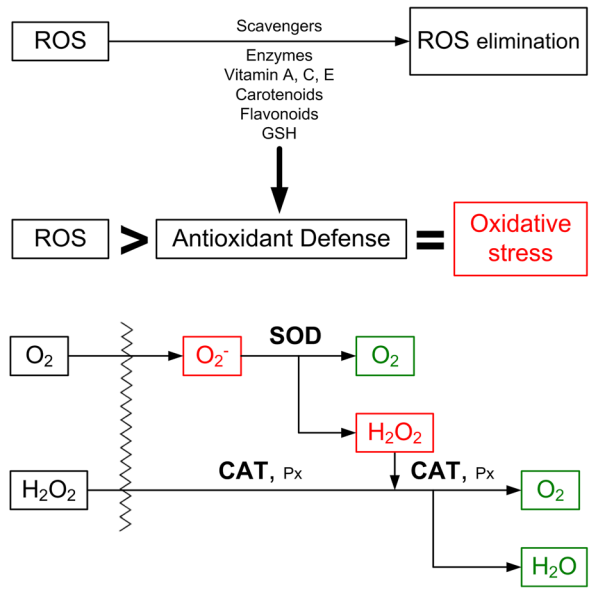

FIG. 1. The sources and cellular responses to ROS. Oxidants are generated as a result of normal intracellular metabolism in mitochondria and chloroplast, as well as from enzyme systems. A sophisticated enzymatic and non-enzymatic antioxidant defense system, including CAT, SOD, peroxidases (Px), and glutathione (GSH), counteracts and regulates overall ROS levels to maintain physiological homeostasis. When ROS production exceeds antioxidant defenses, oxidative stress occurs.

This article is copyrighted as indicated in the article. Reuse of AIP content is subject to the terms at: http://scitation.aip.org/termsconditions. Downloaded to IP: 109.121.73.231 On: Fri, 30 May 2014 20:30:40

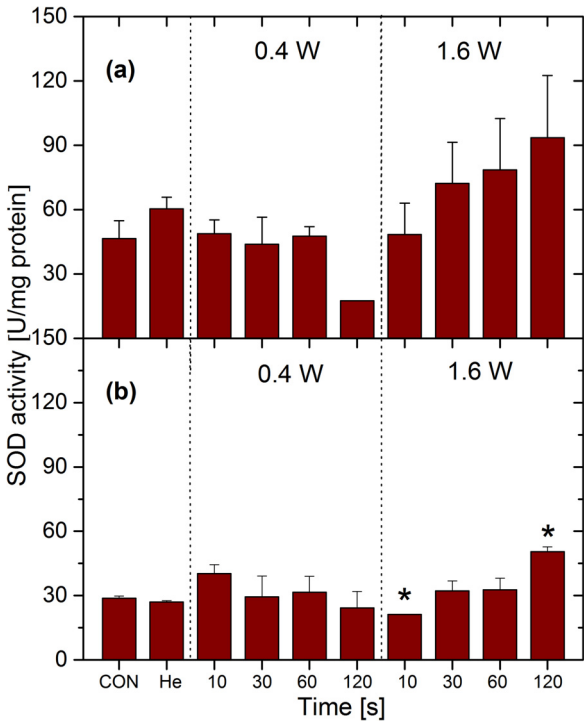

FIG. 2. SOD activity of carrot calli measured immediately (a) or two weeks after plasma treatment (b). Values are means ± SE obtained from two independent experiments. The asterisk represents statistical significance in comparison with control value (*$p < 0.05$ and **$p < 0.01$).

SOD activity in carrot calli after continuous two weeks growth showed much lower values (~2 fold), confirming that under non-stressful conditions the antioxidant defense system provides adequate protection against ROS (Figure 2(b)). Nevertheless, in two weeks grown calli SOD activity retained higher levels in comparison to control with a clear plasma power dependence. Comparison of SOD activity in calli cells immediately after the plasma treatment and two weeks after the treatment illustrates the importance of SOD for antioxidant defense of plants under excessive stress conditions.

The explanation for elevated levels of the SOD activity immediately after the plasma treatment can be found in the presence of the radicals and ions delivered by the plasma to the cell membrane. The oxygenation of the tissue was already observed in treatment of cancer cell.[31] The triplet state of molecular oxygen is not a highly reactive species when it comes to chemical pathways inside the cells. On the other hand, singlet oxygen molecule ($^1\Delta_g O_2$) more easily reacts with other species forming superoxide anion. In case when plasma is present, the concentration of the singlet delta oxygen (SDO) molecules is especially increased. Atmospheric plasmas are known as a good source of the singlet delta oxygen species.[32] When comparing atmospheric sources, it is shown that those operating at RF frequencies, like plasma needle, are much more efficient in production of SDO than the kHz sources.[33] The production of the singlet delta oxygen molecules is also more efficient with an increase of the power transmitted to the discharge.[33] This coincides with an increased activity of SOD for the higher power of 1.6 W. Apart from the singlet oxygen molecules in plasma, we have negative ions present including the superoxide ion. Its contribution should not be neglected even though concentration of O_2^- reaching the surface of the sample is quite low. The reader has to have in mind that we are here neglecting whole cocktail of species created in plasma and concentrating only on these two types of species since SOD is involved only in the reactions including O_2^-.

The product of the SOD catalytic reaction inside the cells is hydrogen peroxide. This molecule is lately recognized as signaling molecule in the chemical pathways of the cell,[28] but mainly, in higher concentration, it is highly dangerous and leads to cell damage and consequently in cell death. The reactivity of H_2O_2 is the result of its reduction by metal ions to form the highly reactive hydroxyl radical.[34] Hydrogen peroxide is a participant in a number of reactions, and it is capable of diffusing across membranes.[35] This means that H_2O_2 created in the plasma also has significant influence on the hydrogen peroxide balance inside the calli cells. CAT is one of the most active enzymes which decompose hydrogen peroxide molecules at extremely rapid rate. Another important point is that, depending on the concentration of H_2O_2, different reactions are activated. Hydrogen peroxide is decomposed by oxidizing some of the hydrogen donors inside the cell (e.g., ethanol, ascorbic acid) at lower concentrations. This is done through the reaction: $RH_2 + H_2O_2 \rightarrow R + 2H_2O_2$. In case of higher concentrations of H_2O_2 molecules, CAT decomposes it in a pure catalytic reaction: $2H_2O_2 \rightarrow O_2 + 2H_2O$. Catalase is unique among H_2O_2-degrading enzymes in that it can degrade H_2O_2 without consuming cellular reducing equivalents. Hence, catalase provides the cell with a very energy-efficient mechanism to remove H_2O_2. Therefore, when cells are stressed for energy and are rapidly generating H_2O_2 through "emergency" catabolic processes, H_2O_2 is degraded by catalase in an energy-efficient manner.[36]

In this study, CAT activity was measured immediately after the plasma treatment (see Figure 3(a)) and in the carrot calli that were grown within two weeks after the treatment (Figure 3(b)). The CAT activity increased when compared to the control samples, but we could not obtain a clear picture about its dependence on the applied power or treatment time. In our experiments, we have measured enzyme activity shortly after plasma treatment. 1–2 min after the treatment samples were frozen in liquid nitrogen and prepared for measurements. We assume that this time was not enough for the enzyme to react adequately. Especially in the case of the CAT which is the second in line and it is activated after the SOD enzyme. Evidently, it is necessary to evaluate the activity of these enzymes in a period of few hours after the plasma treatment.

However, CAT activity in calli samples that were grown for two weeks increased gradually with the increment of plasma power and time of treatment exhibiting 1.5 fold higher values in comparison with CAT activity measured in calli samples immediately after the plasma treatment. This means that in the treated cells, even two weeks later, the levels of H_2O_2 are elevated compared to the control samples. This long term effect of plasma could be explained by the increase in the morphogenic potential of the directly treated cells.[37–39] The increase in the morphogenic potential may be through the activation of some section in the DNA

This article is copyrighted as indicated in the article. Reuse of AIP content is subject to the terms at: http://scitation.aip.org/termsconditions. Downloaded to IP: 109.121.73.231 On: Fri, 30 May 2014 20:30:40

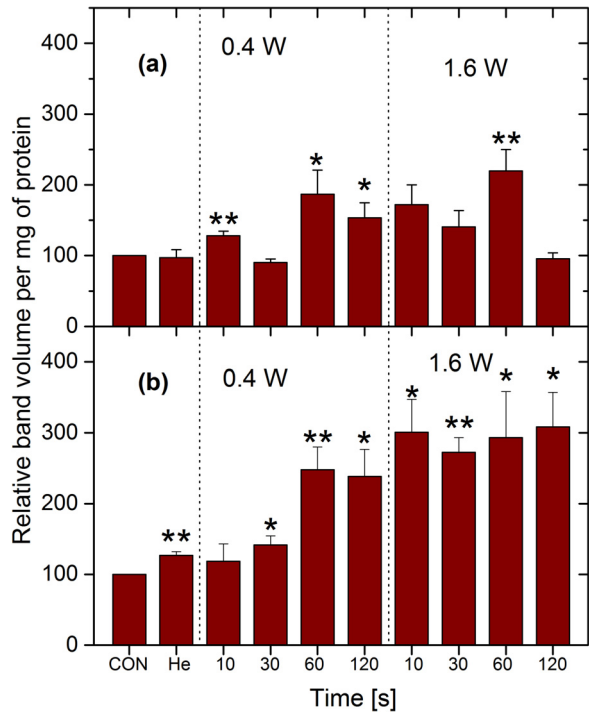

FIG. 3. Catalase activity of carrot calli measured immediately (a) or two weeks after plasma treatment (b). The band volume was recorded using densitometric analysis. Data were normalized using control signal. Values are means ± SE obtained from three independent experiments. The asterisk represents statistical significance in comparison with control (*$p < 0.05$ and **$p < 0.01$).

responsible for the proliferation and/or somatic embryogenesis (SE) of the cells. An increasing number of publications correlate ROS and SE. Kairong and coworkers suggested that plant SE is a special cell differentiation process and established a link or "partial overlapping" of ROS and cell differentiation.[40]

Until now, we have shown that plasma has significant influence on several types of cells and bacteria. The effect of the treatment was investigated up to few days after the plasma treatment. This was the case for all studies: stem cell differentiation potential[10] and sterilization.[9] So far, the only long term effects were the increase of the fresh weight of the treated *Fritillaria imperialis* calli.[11] At the same time, the whole field in general is seeking means to connect the external agents produced by plasma to the intracellular events, agents, and triggering mechanisms. In this paper, we have presented results of enzyme activity that provides direct link between the external ROS and the activity of enzymes inside the cell.

The observable effects on enzymes were obtained immediately after the plasma treatment and also after a delay of two weeks. The SOD activity, while still being considerably greater than the activity in untreated cells, decreased after two weeks compared to the activity immediately after the treatment. The presence of increased densities of ROS may lead both to an increase or decrease of the enzymes. A decrease happens when the response of the living cell cannot keep up with an increased intake of ROS and in that case the survival of the cell is endangered. On the other hand, an increase may mean that, triggered by the ROS, production of enzymes is increased and final concentration is not under control of enzymes.

CAT activity was significantly increased in the samples in the period of two weeks following the treatment. This long term plasma effect due to exposure to the ROS and RNS generated by plasma on the treated meristematic cells is consistent with the previously observed increase of the morphogenic potential of cells.[41,42] One should bear in mind that the observed increases over long term period are significant as the recorded values are always normalized to the mass of the growing calli (per mg of the protein isolated from the samples).

This paper provides a clear indication of the two facts: it is possible to associate increased activities inside the cell to the external plasma and one may claim a proof that at least H_2O_2 and O_2^- may pass through the cell membrane and induce a chain of events inside. In addition, some long term effects of plasma treatment on the cells in growing cultures have been observed where most likely triggering by ROS induces cell response and higher enzyme activity.

This study was supported by Grant Nos. III41011, ON171037, and ON173024, Ministry of Education, Science and Technological Development, Republic of Serbia.

[1]G. Fridman, L. Peddinghaus, T. Vinovrski, A. Jah, A. Fridman, M. Balasubramanian, A. Gutsol, and G. Friedman, *Use of Non-Thermal Atmospheric Pressure Plasma Discharge for Coagulation and Sterilization of Surface Wounds* (IEEE, 2005), pp. 257–257.
[2]T. Nosenko, T. Shimizu, and G. E. Morfill, New J. Phys. **11**, 115013 (2009).
[3]G. Fridman, G. Friedman, A. Gutsol, A. B. Shekhter, V. N. Vasilets, and A. Fridman, Plasma Processes Polym. **5**, 503 (2008).
[4]S. Y. Moon, D. B. Kim, B. Gweon, W. Choe, H. P. Song, and C. Jo, Thin Solid Films **517**, 4272 (2009).
[5]B. Gweon, M. Kim, D. Bee Kim, D. Kim, H. Kim, H. Jung, J. H. Shin, and W. Choe, Appl. Phys. Lett. **99**, 63701 (2011).
[6]E. Stoffels, I. E. Kieft, R. E. J. Sladek, L. J. M. Van Den Bedem, E. P. Van Der Laan, and M. Steinbuch, Plasma Sources Sci. Technol. **15**, S169 (2006).
[7]I. E. Kieft, M. Kurdi, and E. Stoffels, IEEE Trans. Plasma Sci. **34**, 1331 (2006).
[8]I. E. Kieft, N. A. Dvinskikh, J. L. V. Broers, D. W. Slaaf, and E. Stoffels, Proc. SPIE **5483**, 247 (2004).
[9]S. Lazović, N. Puač, M. Miletić, D. Pavlica, M. Jovanović, D. Bugarski, S. Mojsilović, D. Maletić, G. Malović, P. Milenković, and Z. Petrović, New J. Phys. **12**, 083037 (2010).
[10]M. Miletić, S. Mojsilović, I. Okić Đorđević, D. Maletić, N. Puač, S. Lazović, G. Malović, P. Milenković, Z. Lj Petrović, and D. Bugarski, J. Phys. D. Appl. Phys. **46**, 345401 (2013).
[11]N. Puač, Z. L. Petrović, G. Malović, A. Dordević, S. Živković, Z. Giba, and D. Grubišić, J. Phys. D. Appl. Phys. **39**, 3514 (2006).
[12]G. Malović, N. Puač, S. Lazović, and Z. Petrović, Plasma Sources Sci. Technol. **19**, 034014 (2010).
[13]C. Signaling, L. M. Sandalio, F. J. Corpas, M. Palma, J. B. Barroso, and L. A. Rı, Plant Physiol. **141**, 330 (2006).
[14]O. Blokhina and K. V. Fagerstedt, Physiol. Plant. **138**, 447 (2010).
[15]E. Heyno, V. Mary, P. Schopfer, and A. Krieger-Liszkay, Planta **234**, 35 (2011).
[16]R. G. Alscher, N. Erturk, and L. S. Heath, J. Exp. Bot. **53**, 1331 (2002).
[17]F. R. Cavalcanti, J. Tadeu, A. Oliveira, A. S. Martins-Miranda, and R. A. Viégas, New Phytol. **163**, 563 (2004).
[18]J. M. Gomez, A. Jimenez, E. Olmos, and F. Sevilla, J. Exp. Bot. **55**, 119 (2004).
[19]S. Shigeoka, T. Ishikawa, M. Tamoi, Y. Miyagawa, T. Takeda, Y. Yabuta, and K. Yoshimura, J. Exp. Bot. **53**, 1305 (2002).
[20]C. H. Foyer and N. Graham, New Phytol. **146**, 359 (2000).
[21]T. Murashige and F. Skoog, Physiol. Plant. **15**, 473 (1962).
[22]M. M. Bradford, Anal. Biochem. **72**, 248 (1976).
[23]W. Woodbury, A. Spencer, and M. Stahmann, Anal. Biochem. **44**, 301 (1971).

This article is copyrighted as indicated in the article. Reuse of AIP content is subject to the terms at: http://scitation.aip.org/termsconditions. Downloaded to IP: 109.121.73.231 On: Fri, 30 May 2014 20:30:40

[24]W. F. Beyer and I. Fridovich, Anal. Biochem. **161**, 559 (1987).
[25]J. M. Matés, Toxicology **153**, 83 (2000).
[26]D. B. Graves, J. Phys. D. Appl. Phys. **45**, 263001 (2012).
[27]M. B. França, A. D. Panek, and E. C. A. Eleutherio, Comp. Biochem. Physiol. A. Mol. Integr. Physiol. **146**, 621 (2007).
[28]J. G. Scandalios, Brazilian J. Med. Biol. Res. **38**, 995 (2005).
[29]R. Mittler, Trends Plant Sci. **7**, 405 (2002).
[30]H. Willekens, S. Chamnongpol, M. Davey, M. Schraudner, C. Langebartels, M. Van Montagu, D. Inzé, and W. Van Camp, EMBO J. **16**, 4806 (1997).
[31]G. Collet, E. Robert, A. Lenoir, M. Vandamme, T. Darny, S. Dozias, C. Kieda, and J. M. Pouvesle, Plasma Sources Sci. Technol. **23**, 012005 (2014).
[32]J. S. Sousa, G. Bauville, B. Lacour, V. Puech, M. Touzeau, and L. C. Pitchford, Appl. Phys. Lett. **93**, 011502 (2008).
[33]J. S. Sousa, K. Niemi, L. J. Cox, Q. T. Algwari, T. Gans, and D. O'Connell, J. Appl. Phys. **109**, 123302 (2011).
[34]A. Slater, N. W. Scott, and M. R. Fowler, *Superoxide dismutase, catalase and peroxidase activities do not confer protection against oxidative damage in salt-stressed cowpea leaves* (Oxford University Press, 2008), p. 212.
[35]P. Mullineaux, L. Ball, C. Escobar, B. Karpinska, G. Creissen, and S. Karpinski, Philos Trans R Soc Lond B. Biol. Sci. **355**, 1531 (2000).
[36]J. G. Scandalios, *Oxidative Stress and the Molecular Biology of Antioxidant Defenses* (Cold Spring Harbor Laboratory, 1997), p. 349.
[37]S. Bajaj, M. V. Rajam, S. Campus, and B. J. Road, Plant Physiol. **112**(3), 1343 (1996).
[38]R. Mihai, A. Brezeanu, and G. Cogalniceanu, "Aspects of some elicitors influence on non-morphogenic callus of Vitis vinifera var. Isabelle," Rom. Biotechnol. Lett. V **14**, 4511–4518 (2009).
[39]S. H. Tan, R. Musa, A. Ariff, and M. Maziah, Am. J. Biochem. Biotechnol. **6**, 284 (2010).
[40]C. Kairong, L. Ji, X. Gengmei, L. Jianlong, W. Lihong, and W. Yafu, Plant Cell. Tissue Organ Cult. **68**, 187 (2002).
[41]A. Adamczuk, I. Siegie, and I. Ciereszko, *Morphogenesis of Plants in Vitro under Stress Conditions in Biological Diversity—From Cell to Ecosystem* (Polish Botanical Society, Bialystok, Poland, 2012), pp. 25–40.
[42]L. Jo, A. L. W. Dos Santos, C. A. Bueno, H. R. Barbosa, and E. I. S. Floh, Tree Physiol. **34**, 94 (2014).

This article is copyrighted as indicated in the article. Reuse of AIP content is subject to the terms at: http://scitation.aip.org/termsconditions. Downloaded to IP: 109.121.73.231 On: Fri, 30 May 2014 20:30:40

IOP Publishing Plasma Sources Science and Technology

Plasma Sources Sci. Technol. **24** (2015) 025006 (9pp) doi:10.1088/0963-0252/24/2/025006

Time-resolved optical emission imaging of an atmospheric plasma jet for different electrode positions with a constant electrode gap

D Maletić[1], N Puač[1], N Selaković[1], S Lazović[1], G Malović[1], A Đorđević[2,3] and Z Lj Petrović[1,2,3]

[1] Institute of Physics, University of Belgrade, Pregrevica 118, 11080 Belgrade, Serbia
[2] School of Electrical Engineering, University of Belgrade, Bul. kralja Aleksandra 73, 11000 Belgrade, Serbia
[3] Serbian Academy of Sciences and Arts, Knez Mihajlova 35, 11001 Belgrade, Serbia

E-mail: dejan_maletic@ipb.ac.rs

Received 13 August 2014, revised 4 November 2014
Accepted for publication 5 January 2015
Published 3 February 2015

Abstract

The aim of this paper is to determine the influence of the position of the electrodes on the range of a plasma jet, for specific experimental conditions, by using time-resolved optical emission spectroscopy. The optimal position of the electrodes is determined for a fixed gas flow rate and applied excitation voltage. We characterize the helium plasma jet for different distances from the end of the glass tube, showing detailed results for four different electrode positions from the jet nozzle (7, 15, 30 and 50 mm). It was found that at the distance of 15 mm, the length of the plasma jet is at its maximum. The highest speeds of the plasma package travelling outside the glass tube of the atmospheric plasma jet are obtained for the same electrode configuration (15 mm from the jet nozzle). With the electrodes positioned at smaller distances from the nozzle, the plasma plume was much shorter, and at the larger distances the plasma did not even leave the glass tube.

Keywords: plasma jet, ICCD, time resolved, optical emission spectroscopy

(Some figures may appear in colour only in the online journal)

1. Introduction

Interest in plasma jets that operate at atmospheric pressure has been increasing in research literature in the last decade because of possible applications and also because of their unique characteristics and interesting physics. The most important characteristic of these atmospheric pressure plasma jets (APPJs) is low gas and ion temperature and abundant plasma chemistry. Atmospheric plasma jets produce relatively high concentrations of reactive chemical species, such as atomic oxygen and nitrogen, OH radicals, NO_x and ozone [1].

It is important to understand plasma jets because of their wide range of possible application in the new, fast developing field of plasma medicine [2] and treatment of organic materials [3]. In stomatology, plasma was used in the removal of biofilms of bacteria responsible for the formation of dental plaque and caries [4–7] and also for the sterilization of bacteria responsible for periodontitis [8, 9]. Plasma sterilization of surgical instruments and heat sensitive implants [10, 11] is more efficient than using classical methods such as thermal and chemical sterilization. It is shown that the plasma can also accelerate blood coagulation, speeding up wound healing. It can also kill and remove cancer cells [2, 12–14]. Because of the fungicidal and antimicrobial properties of plasmas, low temperature plasmas may be used in dermatology for healing some chronic skin diseases that are non-sensitive to standard drugs [15].

Some of the pioneering work in the field has been done using a plasma needle, which, although it appears to be similar to plasma jets, has a different electrode configuration [3] and

 © 2015 IOP Publishing Ltd Printed in the UK

regime of operation. Still, a large, perhaps even the largest, percentage of activities in plasma medicine are currently based on plasma jets. Many authors have reported results obtained by using various types of plasma jets. These jets can be divided into several groups using several criteria: operating gas, excitation frequency, type of excitation signal, electrode type and geometry. A noble gas, such as helium or argon, is usually used as the operating gas [16, 17] to reduce the breakdown voltage. Gas mixtures were used in order to control the concentration of desirable active species. Usually a small amount (∼1%) of oxygen or nitrogen is added to pure argon or helium. Multiple bullets can appear in a single tube configuration too, by adding small amounts of nitrogen to helium feed gas. In this case, up to eight bullets are reported [18]. Air impurities such as water vapour can also affect plasma propagation and the production of reactive species [19, 20]. The operating frequency can be in the kilohertz, megahertz (13.56 or 27.12 MHz) or gigahertz domain, while the driving signal can be pulsed or sine wave [21, 22]. There are three main groups of electrodes that are typically used in plasma jet devices. The first type is with the electrodes separated from the buffer gas by an insulator, usually a glass tube [23] or capillary [24]; the second type is when they are in contact with the buffer gas [25]; and the third type is when the powered electrode is in contact with the buffer gas and the grounded electrode is isolated from the gas [26]. The electrodes can be cylindrical [27], flat [28], ring shaped [29], needle like [30], etc. Apart from results on systems with different electrode geometries, in the literature results obtained using different geometries of the glass tubes/gas flow may be found. While it has not been reported in most papers that a discharge may go beyond the grounded electrode (as observed by us), in [31] it is reported that in a T-shaped configuration, bullets appear at two ends of the tube asynchronously. This is, however, in both cases, motion of the bullet downstream. The electrode gap, geometry, frequency and type of gas used determine the behaviour of the plasma jet. These parameters have a large impact on the breakdown voltage, operating mode (chaotic, bullet or continuous [26]), voltage–current characteristics, dissipated power in plasma and the effluent length.

Several well-known techniques, such as optical emission spectroscopy, absorption spectroscopy, mass spectrometry, laser spectroscopy and electrical probes, can be used for the characterization and diagnostics of plasma jets. Fast time resolved ICCD imaging is the easiest way to investigate time/space development of plasma. From these high-speed images, it can be seen that plasmas in plasma jets are not always continuous. They sometimes appear to travel in a form of small plasmas that propagate from the glass tube filled with a flow of helium into the surrounding atmosphere [23]. These plasma packages, the so-called 'plasma bullets' or PAPS (pulsed atmospheric pressure streamers) [32], are not yet fully understood. Several theories explaining the formation of these fast travelling plasma packages have been proposed [23, 29, 33]. There have been some attempts to simulate the 'plasma bullets' as positive streamers [34], but there is some discrepancy between the simulation and experimental data [35–38]. It is assumed that photons and Penning ionization [39, 40] play the main role in the propagation of 'plasma bullets'.

In our previous paper, we have presented formation and time/space development of 'plasma bullets'. The powered electrode was 5 mm from the edge of the glass tube and the electrode gap was 15 mm [40]. The point of that paper was to show the operation of a plasma jet with transparent electrodes, so that the development of the plasma could be followed at all times. The aim of this study is to take advantage of the technique presented earlier and provide systematic experimental data over a wider range of configurations and operating conditions. Apart from providing such data in order to provide theory with well-defined data that may be used for qualitative and even quantitative comparisons, we also try to determine the optimal distance of the electrodes from the edge of the glass tube at a constant electrode gap in order to obtain the largest plasma range for the conditions of our plasma source.

2. Experimental setup

A low temperature atmospheric plasma jet that can operate in the 'bullet mode' has been briefly described in [40]. The plasma jet consists of a Pyrex glass tube (inner diameter 4 mm and outer diameter 6 mm) and two transparent electrodes that allow the observation of plasma development inside the electrodes. The electrodes were made of polyethylene terephthalate (PET) covered with a thin conducting film of indium tin oxide. The electrodes were 15 mm wide with the inter-electrode gap of 15 mm. These dimensions were kept constant in the measurements. The electrode closer to the end of the glass tube was connected to the power source (powered electrode). The second electrode was connected through a resistor of 100 kΩ to the ground. Figure 1 shows an ignited plasma jet with the instruments used in the experiment. The parameter that was varied was the distance between the powered electrode and the external edge of the glass tube. We have followed the development of the plasma plume by varying the geometry for many geometries with 1 mm steps; we chose to only present the data for the four dimensions as selected in the text. Above 30 mm, the plasma did not leave the glass tube. Below 30 mm it did, and the maximum range occurred at 15 mm. Here we will show results for distances of 7, 15, 30 and 50 mm.

The operating frequency of the plasma jet was 80 kHz, adjusted by a signal generator. In order to power the plasma jet, the signal generator was connected to a custom built amplifier. The amplifier can produce voltages up to 1 kVpp, which is insufficient for plasma ignition. Therefore, an additional HV transformer was connected after the amplifier so that the voltage was increased up to more than 7 kVpp. Two commercial voltage probes were used for the current and voltage characterization of the system. The average power was calculated from the current and voltage signals obtained by these two probes. In all measurements, the amplifier power was kept at the constant value of 4 W. A very important note is that using a sinusoidal voltage simplifies the electrical power

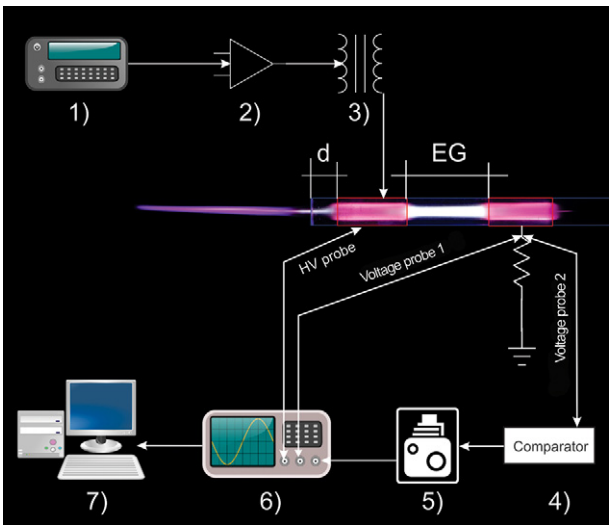

Figure 1. Experimental setup: (1) signal generator; (2) amplifier; (3) high-voltage transformer; (4) voltage comparator; (5) ICCD camera; (6) oscilloscope; (7) computer. EG = electrode gap (15 mm) and d = distance between the powered electrode and the edge of the glass tube (d = 7, 15, 30 and 50 mm).

supply and most measurements, but it also limits the range of plasma bullets (ionization fronts).

We had to introduce the third voltage probe in order to synchronize the ICCD camera (Andor iStar DH734I) with the driving signal of the plasma jet. This probe was connected at the same point in the electrical circuit as the probe for measuring the voltage on the 100 kΩ resistor (voltage probe 2 in figure 1). The signal taken from this probe was introduced in a custom built voltage comparator. The voltage comparator enables triggering of the camera in each cycle (12.5 μs) of the signal while keeping the relative time within the cycle. The stability of the voltage comparator is important since the ICCD camera has to record 160 images during the adjusted exposure time of 2 ms, while keeping the 25 ns gate width. All these single images were then integrated at the chip of the ICCD camera and transferred to the computer by Andor software. The position of the gate was scanned over the whole period of 12.5 μs using the camera's internal delay generator. Thus, the emission over the duration of the entire period was recorded. We have checked our integration and timing jitter by comparing the single shot and the averaged recordings and looked for a change in shape or timing, which turned out to be negligible. In our experimental conditions presented in this paper we have always had only one PAPS formed during one cycle. The moment of formation corresponded to the voltage maximum. The results were experimentally reproducible and there was no evidence of the formation of multiple bullets. In all experiments, helium was flowing through the glass tube at the constant rate of 4 slm (standard litre per minute).

3. Results and discussion

3.1. Images for different distances between the electrodes and the edge of the tube

In this section, we show ICCD images for four different distances between the electrodes and the edge of the glass tube,

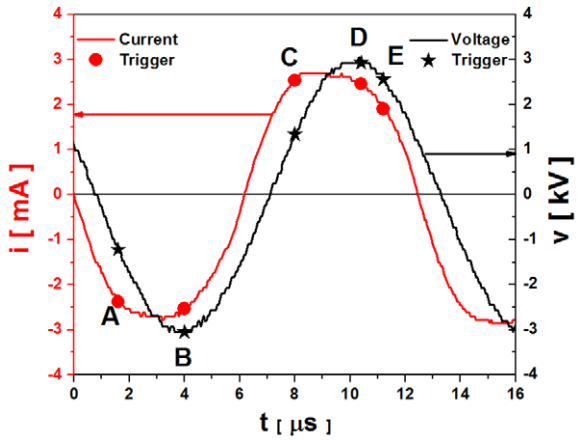

Figure 2. Current–voltage signals with trigger positions (for the distance of 15 mm). One period is 12.5 μs.

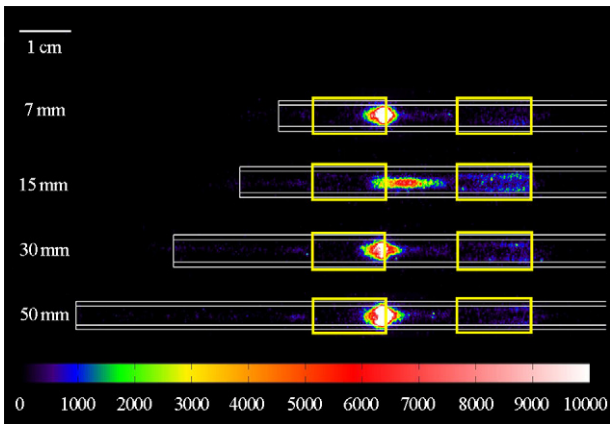

Figure 3. Time-resolved ICCD images at A (1.6 μs).

along with the current and voltage signals with the triggering positions marked that correspond to the timing of those images. The current and voltage signals with the triggering positions A (1.6 μs), B (4.0 μs), C (8.0 μs), D (10.4 μs) and E (11.2 μs) for the gap of 15 mm are shown in figure 2. The beginning of the period is chosen to be in the downward slope of the current and the voltage, when current is close to zero and the voltage is about 1 kV. The voltage signal is a pure sine wave, while the current signal is slightly deformed due to the superimposing of the plasma jet current on the displacement current. (The displacement current is observed directly when there is no plasma.) The peak-to-peak values of the voltage and current are 7 kV and 6 mA, respectively.

In figure 3 we show the emission intensities taken for the triggering time of 1.6 μs after the beginning of the period (point A in figure 2). For this trigger time, the voltage signal is negative and at about one half of its amplitude, while the current signal reaches its maximum negative value. For all cases except for the distance of 15 mm, plasma is formed at the right edge of the powered electrode and fills the tubes almost uniformly. For the distance of 15 mm, however, plasma is somewhat shifted towards the grounded electrode and the main emission originates between the electrodes. It almost appears that the development at 15 mm is slightly ahead of those for other distances.

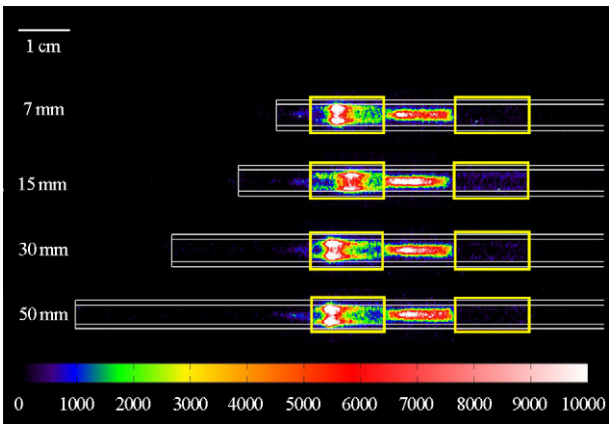

Figure 4. Time-resolved ICCD images at B (4.0 μs).

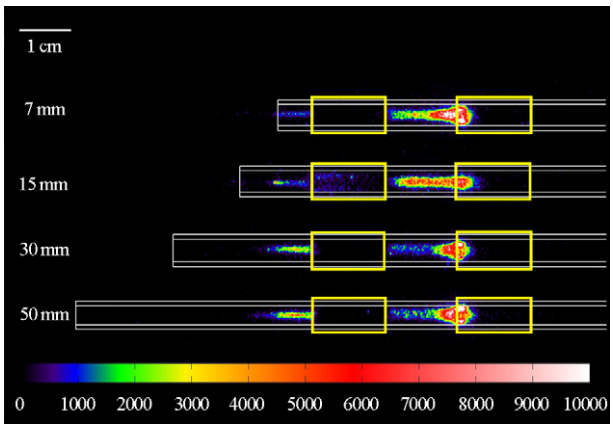

Figure 5. Time-resolved ICCD images at C (8.0 μs).

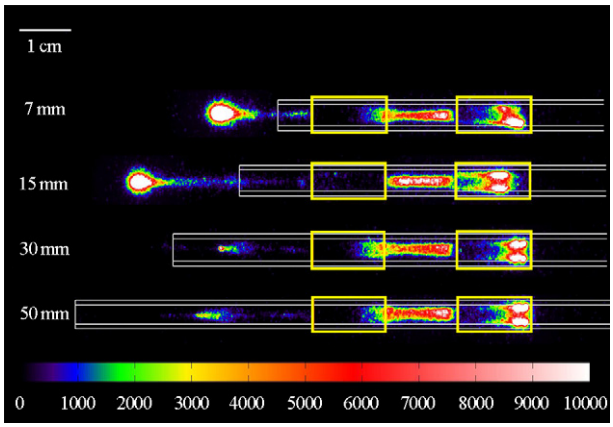

Figure 6. Time-resolved ICCD images at D (10.4 μs).

If we move further along the voltage/current cycle, the ionization wave indicated by the light emission starts propagating inside the powered electrode from its right edge to the left one (downstream of the helium flow and towards the exit of the tube). These images are shown in figure 4 and correspond to the triggering point B in figure 2. For this current/voltage combination, the plasma (as indicated by light emission) inside the powered electrode peaks close to the inner surface of the glass tube and has a ring-like shape. At the same time, the emission intensities originated from between the electrodes indicate that the plasma (emission) is confined at the axis of the glass tube. Comparing the images shown in figure 4, we can see that the plasma behaviour is again similar for all distances except for 15 mm. In the latter case, the position of the maximum emission inside the powered electrode is lagging compared to the results for the distances of 7, 30 and 50 mm. At the same time, the discharge for 15 mm appears to be ahead of other discharges in between the electrodes.

At 8.0 μs (C in figure 2), the voltage is at one half of its amplitude and the current is almost at the maximum in the positive half-cycle. Plasma in the inter-electrode gap reaches the left edge of the grounded electrode (see figure 5) and extends inside. At the same time, inside the powered electrode there is almost no light emission (for 7, 30 and 50 mm) except for the distance of 15 mm, where emission is detected inside the powered electrode. At this point, a PAPS precursor is being formed. We can see that there is a plasma channel connecting the tip of the plasma with the powered electrode. This channel is much stronger when the electrodes are further away from the edge of the glass tube and the ambient air. For the two smaller distances (7 and 15 mm), this channel produces weaker emission, but we can see that plasma is already in contact with ambient air, and PAPS are being formed. At the same time, for the distance of 15 mm, one can see a transition from a hollow emission distribution (peaking close to the wall–wall hugging) to the single peak on the axis in the transition when plasma leaves the electrode. In other words, the wall-hugging emission profile occurs when there is a conducting electrode on the other side of the glass.

When the voltage signal reaches its maximum, the PAPS is already formed and for the distances of 7 and 15 mm it is already travelling outside of the glass tube (see figure 6). For longer distances (30 and 50 mm), we only see the precursor inside the tube travelling downstream of the helium flow. It is also obvious that at the moment of departure of the plasma from the tube, it starts moving faster and becomes brighter. Whatever the explanation for the brighter glow of the plasma (Penning ionization mentioned in [40] and elaborated on in [39] or field distribution [41, 42]), the formation of the brighter region requires some time after the departure from the tube and it appears to be connected to the origin of plasma, thus supporting the streamer-like explanation. In the grounded electrode, the wall-hugging plasma propagates with varying velocities and a possible breakdown of symmetry occurs in one case.

Finally, the plasma reaches its maximum range when the voltage and current start to drop. This case is denoted by the point E (11.2 μs) in figure 2. ICCD images for this triggering time are presented in figure 7. The two bullets formed for shorter distances are progressing further away and dimming. We can see that for a distance of 30 mm, the plasma reached the edge of the glass tube with an indication of growth in brightness, whereas for 50 mm it is still inside the tube. For both these distances, the bright plasma ball (bullet) did not form as a separate plasma package outside the glass tube at any moment during the whole period of 12.5 μs, although a continuous development inside the tube is observable. As for the grounded electrode, the discharge has reached its end, but it does not seem to penetrate any further.

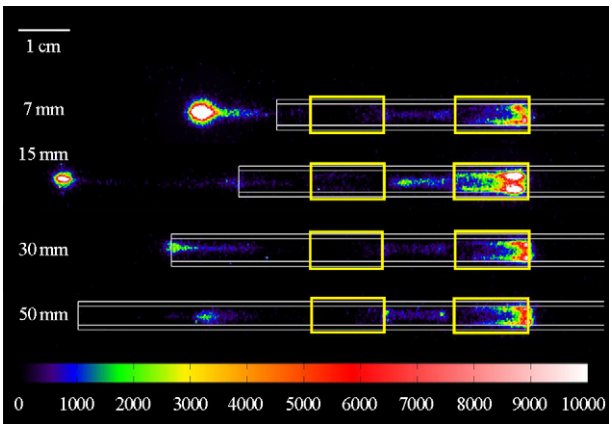

Figure 7. Time-resolved ICCD images at E (11.2 μs).

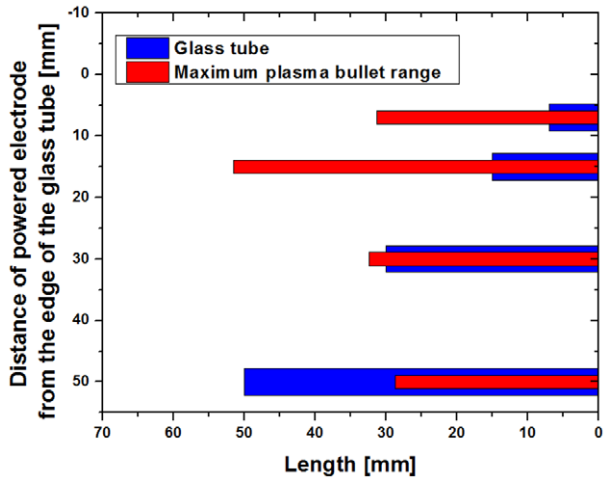

Figure 8. Maximum plasma bullet range.

The maximum ranges that plasma packages can reach are shown in figure 8. We repeat that the development of the bullet may be extended further by a pulsed dc power supply that would allow the existence of the potential gradient at the edge for a longer time. For clearer presentation, we present a histogram graph showing the maximum ranges of the plasma package and the positions of the glass tube. The maximum ranges are obtained from the corresponding ICCD images at 11.2 μs (point E in figure 2). The range is measured as the distance from the left edge of the powered electrode to the left edge of the plasma bullet. The left edge of the bullet was determined in such a way that the intensity of the measured points was not below 2000 a.u. The maximum range reached by the plasma bullet is almost the same when the distances are 7, 30 and 50 mm, and it is about 30 mm. For the distance of 15 mm, the plasma reaches a radically larger range of approximately 50 mm.

The main difference in results among all presented configurations is the maximum travelling range of PAPS. As can be seen from figure 8, the optimal distance of the powered electrode for the maximal plasma range is at 15 mm from the edge of the glass tube. Hence, this particular case will be presented in more detail.

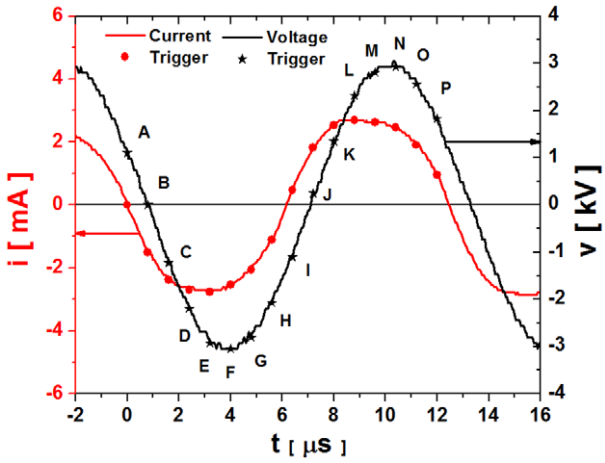

Figure 9. Current–voltage signals with trigger positions.

3.2. The optimal position of the electrodes

Current and voltage waveforms with marked triggering positions of the ICCD camera are shown in figure 9. The ICCD images (figure 10, left column) were taken for the delays from 0.0 to 12.0 μs, with a step of 0.8 μs, to provide detailed time development of the plasma jet. Each image and profile correspond to the letters (A–P) on the current–voltage signal. Axial profiles (figure 10, right column) of the plasma light emission along the glass tube axis were calculated from the obtained ICCD images. The presented profiles are calculated as a sum of the light emission coming from the plasma along the axis of the glass tube. The right edge of the grounded electrode was used as the zero distance. The position of the edge of the glass tube was at 6 cm.

In the downward slope of the current and voltage signal (A–E in figures 9 and 10), the plasma emission is mainly originating from within the electrode gap. As current reaches its maximum negative value, the discharge enters the powered electrode, taking the form of a ring shape. From the emission intensity profiles (figure 10, axial profiles A–E), we can see that the highest intensity inside the powered electrode is at the moment when the plasma is forming at the right edge of the electrode ($D = 2.4\,\mu$s in figure 10). After that moment, the plasma starts to move inside the powered electrode along the surface of the glass tube in the same direction as the helium gas flow. One should bear in mind that the transparency of the electrode film is less than 100%. With the movement of the plasma inside the powered electrode, the emission intensity is decreasing both inside the electrode and in the electrode gap (figure 10, $E = 3.2\,\mu$s to $I = 6.4\,\mu$s). This coincides with the increase of the current and voltage in the negative part of the period (see figure 9).

The positive part of the period of the voltage starts with the point J in figure 9. Now the discharge is almost extinguished inside the powered electrode and the main emission originates from the electrode gap. With the increase in the voltage signal, the discharge is formed at the left edge of the grounded electrode (figure 10, $K = 8.0\,\mu$s). The discharge inside the grounded electrode behaves similarly at some points as in the powered electrode. It is ring-shaped and travels through the

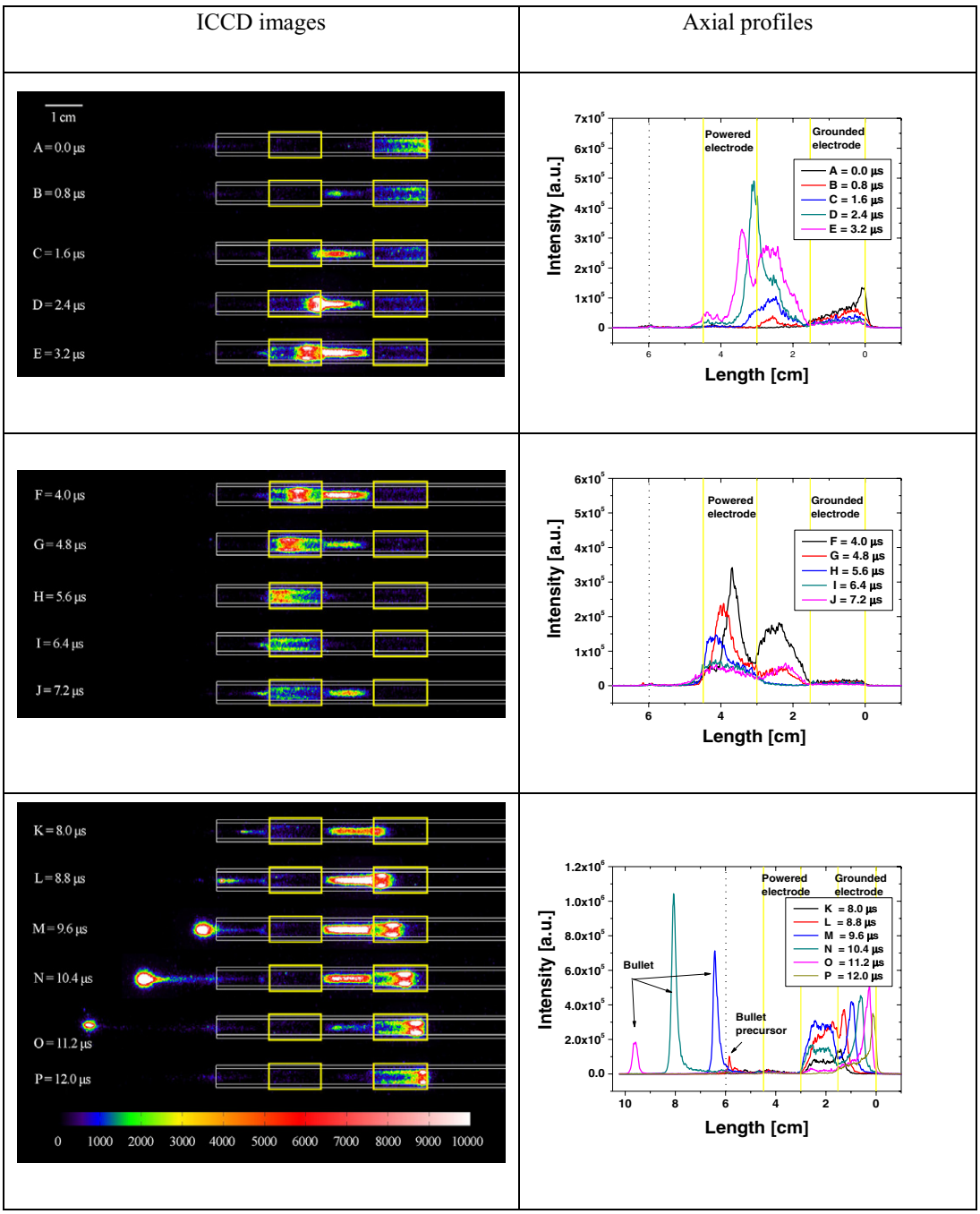

Figure 10. Time-resolved ICCD images for delays 0–12.0 μs (left) and axial light emission profiles for delays 0.0–12.0 μs (right), for 4 slm and power of 4 W.

electrode along the wall of the glass tube. The differences are that in the case of the grounded electrode, the discharge moves contrary to the gas flow and the maximal intensity of the discharge profile increases with the movement (figure 10, K–P axial profiles). In the case of both electrodes, the maximum emission intensity is always at the edge that is further away from the edge of the glass tube. At the same time, when the discharge enters the grounded electrode, a part of the discharge starts to travel away from the powered electrode and towards the exit of the tube (figure 10, $K = 8\,\mu$s). While it travels through the glass tube, we can see that the highest emission is originating from the head of the formed plasma with a low-intensity tail behind (figure 10, K, L images and profiles). We could say that a precursor is formed which will turn into the high-speed travelling package of plasma when it leaves the glass tube. Only upon exiting the glass tube, the plasma significantly expands in volume and the light intensity rises by several orders of magnitude. It appears that the main reason for a fast increase in the emission and volume of the plasma is the contact of excited helium atoms and metastables with molecules of nitrogen and oxygen from the ambient air [38, 39]. However, it appears that the field distribution outside the tube provides a greater potential drop at the front and thus increases ionization considerably.

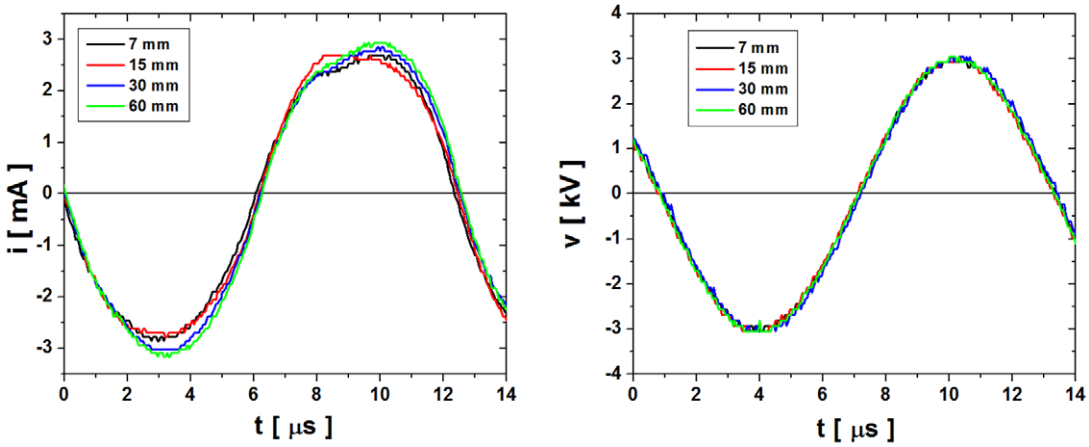

Figure 11. Comparison of current (left) and voltage (right) waveforms for different distances between the electrode and the edge for the glass tube. The flow of the helium was 4 slm.

The propagation of the plasma package in the open air can be explained as propagation of a positive streamer [19, 34]. The peak emission intensity of the propagating streamer is obtained for the delay of $N = 10.4\,\mu$s. We can see that the highest intensity position corresponds to one half of the maximum distance travelled by the plasma. At this point, it is clearly seen that the ionization front is still connected to the main discharge inside the jet tube with a thin, hardly visible and apparently conductive, tail (figure 10, N). With further movement of the ionization front, this conductive tail is diminishing, accompanied by the diminishing intensity of the emission coming from the travelling plasma package. When the ionization front is at the maximal distance from the tube, the emission intensity is low and the plasma tail is thin. We have to point out that from the moment when the plasma package leaves the glass tube and enters surrounding air until the extinguishing of the package, the package appears to be constantly connected to the main discharge inside the tube with a long, streamer-like plasma tail.

The main difference that we have observed between the 15 mm configuration and other configurations is in the current waveform. It is smaller in amplitude during the negative part of the waveform compared to the signal for the other three configurations (see figure 11). Also, the positive peak of this waveform leads the other peaks (obtained for 7, 30 and 50 mm). This difference can be seen in more detail in the frequency domain. For the case of 15 mm, the 2nd and 4th harmonics are smaller in intensity compared to the same harmonics for other configurations. We can see that there is no significant difference between the voltage signals for different configurations. The main conclusion that can be drawn here is that the characteristics of the plasma jet and the plasma packages are influenced by the configuration of the electrodes, i.e., their dimensions and the distance from the mixing point of working noble gas with air. Also, the same system can be tuned by adjusting the electrode configuration with no need to change any component in the power supply system.

3.3. Velocities

The velocities of the emission peaks were determined (calculated from the ICCD spatial emission profiles at different times) for the propagation of plasma through the powered, grounded electrode and outside the glass tube (figure 12). The velocity of the ionization front in the powered electrode starts to rise from the right edge of the electrode. At about 4 mm from the edge it reaches the speed of 4 km s^{-1}. The velocity is almost constant until the ionization front reaches the left edge of the electrode. The propagation direction of the ionization wave is downstream of the helium flow. When the electrode is grounded, the ionization wave starts to accelerate from the left edge of the electrode and reaches the speed of 4 km s^{-1} at 2 mm from the edge of the electrode. The velocity is almost constant until the plasma reaches the centre of the electrode. Thereafter, it starts to accelerate again and reaches the maximal speed of 5 km s^{-1}. Near the edge of the grounded electrode, the ionization front starts to rapidly slow down. The propagation of the ionization wave inside the grounded electrode is upstream of the helium flow. We have performed several experiments where we varied the helium flow while keeping the electrode geometry constant. These results are not in the scope of this paper. We have seen that helium flow does not influence the propagation velocity of PAPS outside the glass tube, but greatly influences its range.

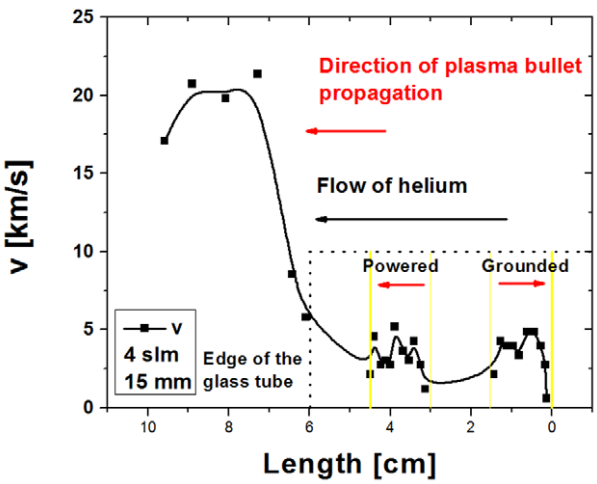

Figure 12. Plasma velocity inside and outside glass tube.

Velocity outside the glass tube rises from the edge of the glass tube and reaches its maximum of approximately 20 km s^{-1} at the distance approximately 15 mm from the edge of the glass tube. The velocity is constant from 15 to 30 mm and thereafter it starts decreasing. The larger velocities outside the glass tube than inside may be due to the changes in the composition of the medium through which the plasma propagates. In the tube, we have pure helium, and outside the tube components of air diffuse into the stream of helium that leads to new and complex reactions in the plasma. Nevertheless, studies like this one, and quantitative comparison of models with the experimental data may be the best way to investigate these plasmas.

4. Conclusion

In this paper, we have shown results of optical emission spectroscopy for four different configurations of a plasma jet. In all configurations, the distance between the powered and grounded electrode was kept constant, while the distance of the electrodes from the edge of the glass tube was varied. Measurements were taken for distances of 7, 15, 30 and 50 mm from the edge of the glass tube.

Several conclusions can be drawn from the presented data that can be applied to all electrode configurations:

- while inside the electrodes, the plasma has a ring-like shape and it is mainly travelling along the walls of the glass tube;
- inside the glass tube (not in the electrode region) plasma is confined to the central axis of the tube and the main emission originates from that volume;
- only when the plasma comes into contact with the ambient air does the volume of discharge increase and the plasma form a sphere-like shape before it starts to travel in the open air;
- in all cases when PAPS is formed, we have seen that it has a trail of very small emission that 'connects' it with the main discharge inside the tube; the connection through the weakly lit plasma to the point of origin resembles streamer-like propagation and is consistent with proposed theoretical explanations.

The main difference between the configurations used in these experiments occurred in the maximum range that PAPS can reach before extinction. For the distances of 7 and 15 mm, PAPS is formed and it starts travelling outside the glass tube. In the case of 30 mm, the plasma reaches the edge of the tube, starts to increase in volume, but does not detach from the tube in order to start travelling in the open air. For 50 mm, the plasma stays inside the tube throughout the whole period of 12.5 μs. Nevertheless, even if plasma does not leave the glass tube, the maximum distance that it can reach is around 30 mm, which corresponds to the ranges obtained for 7 and 30 mm. Only in the case when electrodes are 15 mm away from the edge of the glass tube, is the maximum travelling range of PAPS 50 mm. However, the travelling speed of PAPS for all configurations is almost the same and in open air it reaches about 20 km s^{-1} (for the 15 mm case, and 17 km s^{-1} for the 7 mm case). One should bear in mind that we can measure the velocity only when the PAPS departs from the edge of the tube. It appears that the propagation of the plasma PAPS for the 7 mm case is slow when the plasma leaves the tube and forms the bullet, which could be related to the distribution of the electric field beyond the edge of the tube.

One could argue that the distribution of the field along the glass tube beyond the powered electrode is a key consideration in establishing the range of plasma bullets. In addition, one should consider that for 15 mm the transit time allows the plasma to leave the tube just when the voltage waveform goes through the maximum at a phase of 1.5π. All of these aspects, and other considerations, may be interpreted as the basis for an explanation within some plasma model that is sufficiently detailed and comprehensive. We hope that our results will promote and support such an analysis and its conclusions.

Acknowledgments

This research has been supported by the Ministry of Education, Science and Technological Development, Republic of Serbia, under projects ON171037 and III41011. ZLjP, NP, GM and SL are also grateful for the support from the NATO SfP 984555. AĐ is grateful for the support from SASA project number F-133 for the provision of additional funds to purchase measurement equipment and generators.

References

[1] Oh J-S, Aranda-Gonzalvo Y and Bradley J W 2011 Time-resolved mass spectroscopic studies of an atmospheric-pressure helium microplasma jet *J. Phys. D: Appl. Phys.* **44** 365202
[2] Fridman G, Friedman G, Gutsol A, Shekhter A B, Vasilets V N and Fridman A 2008 Applied plasma medicine *Plasma Process. Polym.* **5** 503–33
[3] Stoffels E, Flikweert A J, Stoffels W W and Kroesen G M W 2002 Plasma needle: a non-destructive atmospheric plasma source for fine surface treatment of (bio)materials *Plasma Sources Sci. Technol.* **11** 383–8
[4] Latha S 2011 Reviews plasma therapy: an overview *J. Health Sci. Res.* **2** 33–6
[5] Sladek R E J and Stoffels E 2005 Deactivation of *Escherichia coli* by the plasma needle *J. Phys. D: Appl. Phys.* **38** 1716–21
[6] Stoffels E, Sakiyama Y and Graves D B 2008 Cold atmospheric plasma: charged species and their interactions with cells and tissues *IEEE Trans. Plasma Sci.* **36** 1441–57
[7] Kim G C, Lee H W, Byun J H, Chung J, Jeon Y C and Lee J K 2013 Dental applications of low-temperature nonthermal plasmas *Plasma Process. Polym.* **10** 199–206
[8] Lazović S *et al* 2010 The effect of a plasma needle on bacteria in planktonic samples and on peripheral blood mesenchymal stem cells *New J. Phys.* **12** 083037
[9] Miletić M, Mojsilović S, Okić Đorđević I, Maletić D, Puač N, Lazović S, Malović G, Milenković P, Petrović Z L and Bugarski D 2013 Effects of non-thermal atmospheric plasma on human periodontal ligament mesenchymal stem cells *J. Phys. D: Appl. Phys.* **46** 345401
[10] Huang H-M, Hsieh S-C, Teng N-C, Feng S-W, Ou K-L and Chang W-J 2011 Biological surface modification of titanium surfaces using glow discharge plasma *Med. Biol. Eng. Comput.* **49** 701–6

[11] Cao Z, Nie Q, Bayliss D L, Walsh J L, Ren C S, Wang D Z and Kong M G 2010 Spatially extended atmospheric plasma arrays *Plasma Sources Sci. Technol.* **19** 025003
[12] Nastuta A V, Topala I, Grigoras C, Pohoata V and Popa G 2011 Stimulation of wound healing by helium atmospheric pressure plasma treatment *J. Phys. D: Appl. Phys.* **44** 105204
[13] Dobrynin D, Wasko K, Friedman G, Fridman A A and Fridman G 2011 Fast Blood coagulation of capillary vessels by cold plasma: a rat ear bleeding model *Plasma Med.* **1** 241–7
[14] Kim C-H, Bahn J H, Lee S-H, Kim G-Y, Jun S-I, Lee K and Baek S J 2010 Induction of cell growth arrest by atmospheric non-thermal plasma in colorectal cancer cells *J. Biotechnol.* **150** 530–8
[15] Heinlin J, Morfill G, Landthaler M, Stolz W, Isbary G, Zimmermann J L, Shimizu T and Karrer S 2010 Plasma medicine: possible applications in dermatology *J. Dtsch. Dermatol. Ges.* **8** 968–76
[16] Topala I, Nastuta A V, Grigoras C and Dumitrascu N 2011 Helium atmospheric pressure plasma jet: diagnostics and application for burned wounds healing *Plasma for Bio-Decontamination, Medicine and Food Security (NATO Advanced Research Workshop, 15–18 March 2011, Slovakia)* pp 53–4
[17] Kim H, Brockhaus A and Engemann J 2009 Atmospheric pressure argon plasma jet using a cylindrical piezoelectric transformer *Appl. Phys. Lett.* **95** 211501
[18] Park S, Moon S Y and Choe W 2013 Multiple (eight) plasma bullets in helium atmospheric pressure plasma jet and the role of nitrogen *Appl. Phys. Lett.* **103** 224105
[19] Naidis G V 2013 Modelling of OH production in cold atmospheric-pressure He–H_2O plasma jets *Plasma Sources Sci. Technol.* **22** 035015
[20] Murakami T, Niemi K, Gans T, O'Connell D and Graham W G 2014 Afterglow chemistry of atmospheric-pressure helium–oxygen plasmas with humid air impurity *Plasma Sources Sci. Technol.* **23** 025005
[21] Stoffels E 2007 'Tissue processing' with atmospheric plasmas *Contrib. Plasma Phys.* **47** 40–8
[22] Xiong Q, Lu X P, Ostrikov K, Xian Y, Zou C, Xiong Z and Pan Y 2010 Pulsed dc- and sine-wave-excited cold atmospheric plasma plumes: a comparative analysis *Phys. Plasmas* **17** 043506
[23] Shi J, Zhong F, Zhang J, Liu D W and Kong M G M 2008 A hypersonic plasma bullet train traveling in an atmospheric dielectric-barrier discharge jet *Phys. Plasmas* **15** 013504
[24] Oh J, Bryant P M and Bradley J W 2011 Discharge and plasma bullet formation in a capillary DBD atmospheric-pressure microplasma jet *IEEE Trans. Plasma Sci.* **39** 2352–3
[25] Cho G, Lim H, Kim J, Jin D J, Kwon G C, Choi E and Uhm H S 2011 Cold plasma jets made of a syringe needle covered with a glass tube *IEEE Trans. Plasma Sci.* **39** 1234–8
[26] Walsh J L, Iza F, Janson N B, Law V J and Kong M G 2010 Three distinct modes in a cold atmospheric pressure plasma jet *J. Phys. D: Appl. Phys.* **43** 075201
[27] Sands B L, Ganguly B N and Tachibana K 2008 A streamer-like atmospheric pressure plasma jet *Appl. Phys. Lett.* **92** 151503
[28] Knake N, Reuter S, Niemi K, Schulz-von der Gathen V and Winter J 2008 Absolute atomic oxygen density distributions in the effluent of a microscale atmospheric pressure plasma jet *J. Phys. D: Appl. Phys.* **41** 194006
[29] Lu X and Laroussi M 2006 Dynamics of an atmospheric pressure plasma plume generated by submicrosecond voltage pulses *J. Appl. Phys.* **100** 063302
[30] Pipa a V, Bindemann T, Foest R, Kindel E, Röpcke J and Weltmann K-D 2008 Absolute production rate measurements of nitric oxide by an atmospheric pressure plasma jet (APPJ) *J. Phys. D: Appl. Phys.* **41** 194011
[31] Algwari Q Th and O'Connell D 2011 Electron dynamics and plasma jet formation in a helium atmospheric pressure dielectric barrier discharge jet *Appl. Phys. Lett.* **99** 121501
[32] Robert E, Sarron V, Riès D, Dozias S, Vandamme M and Pouvesle J-M 2012 Characterization of pulsed atmospheric-pressure plasma streams (PAPS) generated by a plasma gun *Plasma Sources Sci. Technol.* **21** 034017
[33] Shashurin A, Shneider M N, Dogariu A, Miles R B and Keidar M 2009 Temporal behavior of cold atmospheric plasma jet *Appl. Phys. Lett.* **94** 231504
[34] Naidis G V 2011 Simulation of streamers propagating along helium jets in ambient air: polarity-induced effects *Appl. Phys. Lett.* **98** 141501
[35] Naidis G V 2010 Modelling of streamer propagation in atmospheric-pressure helium plasma jets *J. Phys. D: Appl. Phys.* **43** 402001
[36] Naidis G and Walsh J 2013 The effects of an external electric field on the dynamics of cold plasma jets—experimental and computational studies *J. Phys. D: Appl. Phys.* **46** 095203
[37] Xiong Z and Kushner M J 2012 Atmospheric pressure ionization waves propagating through a flexible high aspect ratio capillary channel and impinging upon a target *Plasma Sources Sci. Technol.* **21** 034001
[38] Breden D, Miki K and Raja L L 2012 Self-consistent two-dimensional modeling of cold atmospheric-pressure plasma jets/bullets *Plasma Sources Sci. Technol.* **21** 034011
[39] Li Q, Zhu W-C, Zhu X-M and Pu Y-K 2010 Effects of Penning ionization on the discharge patterns of atmospheric pressure plasma jets *J. Phys. D: Appl. Phys.* **43** 382001
[40] Puač N, Maletić D, Lazović S, Malović G, Đorđević A and Petrović Z L 2012 Time resolved optical emission images of an atmospheric pressure plasma jet with transparent electrodes *Appl. Phys. Lett.* **101** 24103
[41] Boeuf J P 2011 personal communication
[42] Sakiyama Y, Graves D B, Jarrige J and Laroussi M 2010 Finite element analysis of ring-shaped emission profile in plasma bullet *Appl. Phys. Lett.* **96** 041501

IOP Publishing Journal of Physics D: Applied Physics

J. Phys. D: Appl. Phys. **50** (2017) 135204 (10pp) https://doi.org/10.1088/1361-6463/aa5d69

Electrical and optical characterization of an atmospheric pressure, uniform, large-area processing, dielectric barrier discharge

A Zeniou[1], N Puač[2], N Škoro[2], N Selaković[2], P Dimitrakellis[1], E Gogolides[1] and Z Lj Petrović[2,3]

[1] Institute of Nanoscience and Nanotechnology, NCSR 'Demokritos', Aghia Paraskevi, Attiki, 15310, Greece
[2] Institute of Physics, University of Belgrade, Pregrevica 118, 11080 Belgrade, Serbia
[3] Serbian Academy of Sciences and Art, Knez Mihailova 35, 11000 Belgrade, Serbia

E-mail: e.gogolides@inn.demokritos.gr

Received 4 November 2016, revised 27 January 2017
Accepted for publication 1 February 2017
Published 2 March 2017

Abstract

A printed-circuit-board (PCB) based atmospheric pressure dielectric barrier discharge (DBD) capable of uniform processing over a large area was constructed consisting of two parallel plates. The first perforated plate is comprised of four layers: a RF powered metal layer, a polymeric dielectric layer, a floating metal grid and another dielectric layer. The second, grounded, plate was fluorine doped tin oxide (FTO) glass plate with surface of $100 \times 100\,\mathrm{mm}^2$ and thickness of 2 mm. The PCB based atmospheric pressure DBD was characterized by (a) measuring electrical characteristics of the device using derivative *I*–*V* probes, (b) ICCD imaging and (c) optical emission spectroscopy (OES). Optical and electrical characteristics, as well as plasma uniformity were measured by changing He flow rate and input power, while keeping the gap between the PCB and the FTO glass plate ground electrode constant at 2 mm. The plasma uniformity strongly depends on the applied power and on the flow rate of the buffer gas. When increasing the flow rate, the intensity of the nitrogen-dominated emission drops, while emission of helium and oxygen lines increases. The source allows low temperature, uniform plasma operation over a wide area of $100 \times 100\,\mathrm{mm}^2$, which could be essential for numerous applications. Examples of etching rate and hydrophilization are demonstrated.

Keywords: optical emission spectroscopy, ICCD Imaging, plasma etching, hydrophilicity, dielectric barrier discharge, atmospheric pressure plasmas, RF plasmas

(Some figures may appear in colour only in the online journal)

1. Introduction

Atmospheric pressure plasmas have become a key emerging technology especially in the field of surface treatment of solids or liquids, both in industry and in research laboratories. One of their big advantages is their potential lower capital cost, when compared to vacuum plasma equipment, although operating (e.g. gas) costs have also to be considered. Several state of the art plasma sources have been designed for this purpose, such as atmospheric pressure plasma jets (APPJ) and dielectric barrier discharges (DBDs) [1–16]. The most broadly used DBD designs consist of two parallel metal electrodes covered by a dielectric layer. The plasma is either a stable glow discharge or a filamentary discharge depending on working conditions [18–20].

Examples of the industrial use of DBDs include particle matter (PM) removal in catalysts for the car industry [21] and material surface modification/activation [8, 17]. The latter however requires uniform processing over large areas and, in this case, filamentary type of discharges should be avoided,

 © 2017 IOP Publishing Ltd Printed in the UK

especially when soft materials are being processed. Typically, jet DBDs operating at kHz and MHz frequencies may process samples of the order of a few mm^2, which makes them useful for localized applications. Therefore, to address the need for large area processing of materials, a specific type of atmospheric plasma equipment has been designed and tested, such as roll to roll that makes use of cylindrical DBD sources, where one of the electrodes is a rotating metallic cylinder covered by a dielectric [22].

Characterization of the electrical and optical properties of generated plasma from these devices is a challenge. One technique for the electrical characterization is the use of derivative probes [23, 24], which provide crucial information regarding electrical properties such as Voltage, Current, Impendence and in general stability and discharge characteristics of the source. A further analysis can be achieved by making use of optical emission spectroscopy (OES), for detection of excited species and monitoring of plasma composition, especially regarding the role of each species in material processing [25–31].

We have recently presented a novel design of atmospheric pressure DBD that is based on printed circuit board (PCB) and is capable of large area operation [32, 33]. We have shown that the existence of a metallic grid in the PCB promotes plasma excitation uniformity, and stability and leads to higher processing rates. PCBs are used in electronics, and are a cheap and reliable source of materials for cost-effective manufacturing of the source.

In this work, we move a step further in the detailed characterization of the source in terms of electrical and optical properties of helium plasma. The aim of our work is to optimize plasma process focusing on the discharge uniformity and large-area operation and to confirm the scaling-up potential of our plasma source (from lab-scale to pilot-line). The characterization of the discharge is performed by using optical imaging via a new implementation of the PCB source with a bottom conductive glass electrode, OES and electrical measurements while varying helium flow rate and RF power. We perform measurements here with a variation of our design with respect to our first publication [32] by using a transparent ground electrode which allows us to quantify the optical characteristics of the discharge such as emission intensity, surface coverage and uniformity over areas of $80 \times 80\,mm^2$. We use OES to quantitatively measure the emission of molecular nitrogen, helium and atomic oxygen line intensities versus helium flow rate.

2. Experimental setup

A schematic of the experimental setup is presented in figure 1. In figure 1(a) we show vertical cross section of the plasma source which is composed of two plane parallel electrodes with dielectric layers facing each other. The upper powered electrode (antenna) is a square-shaped ($100 \times 100\,mm^2$) multilayer PCB with 2 mm diameter holes drilled equidistantly. The multilayer perforated PCB consists of 80 μm thick copper plate, a 1 mm thick dielectric material (FR4) and an 80 μm thick copper grid on the other side. From below, the grid is uniformly coated with an additional 1 mm thick second dielectric material (poly-dimethyl siloxane—PDMS) [32, 33]. For all measurements presented in this paper, the source configuration includes a floating grid, while the lower grounded electrode, which serves as sample holder, is fluorine doped tin oxide (FTO) coated glass.

This is different from our recently published paper with a similar source [32] where, apart from the configuration with the floating grid, we also analyzed configurations of the source with a powered grid and without the grid. Moreover, in that paper a 50 mm × 50 mm PCB plate served as grounded second electrode. Since the surface and the type of the second electrode are crucial for the *I–V* characteristics of the atmospheric DBD plasma reactor, changing these characteristics with respect to [32] will partially alter electrical properties of the source.

In figure 1(b) we show the source with schematics of electrical and detection parts of the setup. The perforated PCB is fixed at the bottom of a Plexiglas box with a hole for gas inlet at the top side. This way, uniform gas flow through all PCB holes is achieved. The powered electrode is connected through an L-type custom-made matching network to a 13.56 MHz power supply. In all experiments we had reflected power set to the minimal value and kept below 3% of the forwarded power. This was set before the measurements and we did not need to change the settings of the matching network afterwards during the measurements. Therefore, the *L–C* values of the matching network did not change. All this implies that the DBD system is well balanced and its design gives close to optimal values when it comes to matching it to the power supply. The gap between electrodes was set at 2 mm. Pure helium was used as buffer gas at flow rates from 1 to 7 standard liters per minute (slm).

For the electrical characterization of the source, derivative probes were used to obtain voltage and current waveforms at the powered electrode. The voltage probe was a capacitive T-shaped probe and the current probe was an inductive Π-shaped probe, both placed inside a stainless-steel box which was connected in-line between the plasma source and the matching network [23, 24]. The *V–I* waveforms were recorded for different helium flow rates and power values using a 3000-X series digital oscilloscope from Agilent Technologies and then fast Fourier transform (FFT) was performed to obtain the voltage and current RMS values along with the total impedance of the source and the power dissipation (P_d). Power dissipation, voltage and current values V, I and phase difference φ were calculated using the waveform analysis software of the derivative probes. Due to the probe position, calculated dissipated power is not influenced by power losses from the cable and from the passive components of matching network and therefore represents only the power delivered to the DBD source.

For plasma imaging, we used an Andor ICCD camera iStar DH734I equipped with photographic lens NIKKOR 50 mm f/1.4 AIS [34]. Since electrodes were in horizontal position, a mirror was situated under the lower transparent FTO electrode reflecting the plasma emission to the camera. In addition to the surface plasma imaging described above, side on

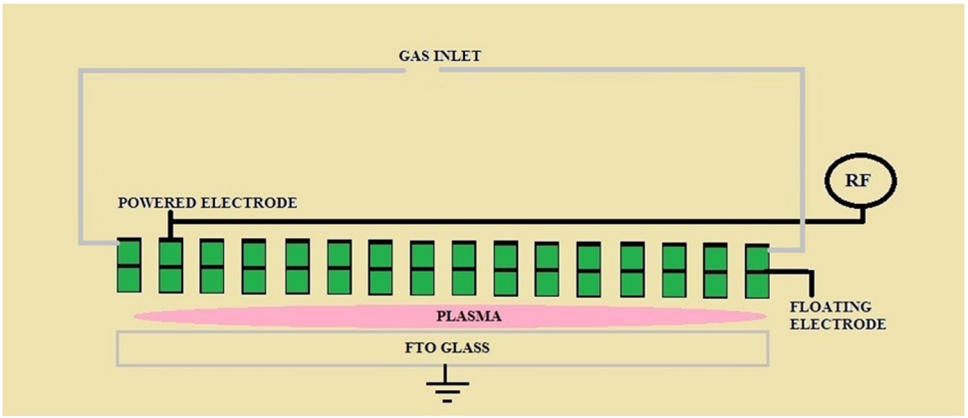

(a)

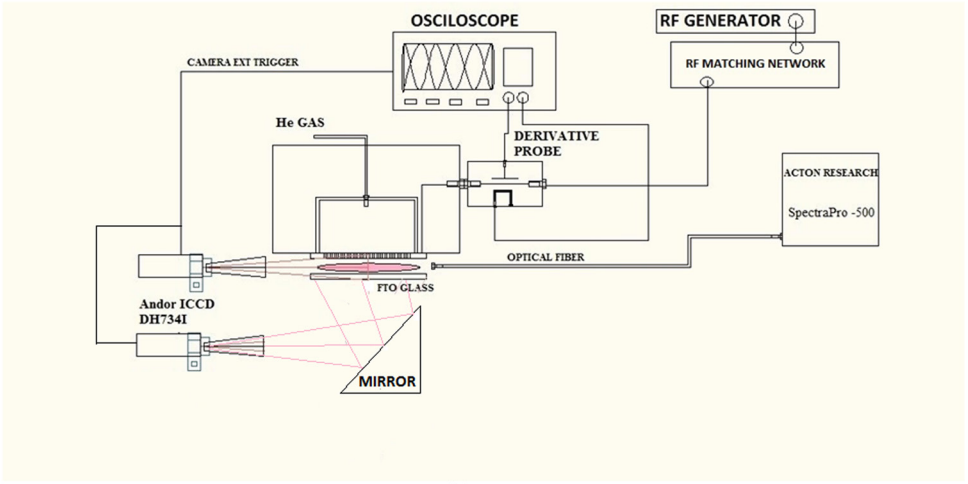

(b)

Figure 1. (a) Experimental setup of the perforated DBD source of plasma intensity and (b) vertical cross section of the perforated novel PCB source with power and ground connections.

capturing of the plasma intensity was performed. Thus, we obtained images spectrally integrated in the visible spectral range. As the exposure time was in the order of several hundred μs, obtained images were time integrated observation of discharge emission from many RF periods. The objective was transparent for the light above 375 nm.

For the OES, an Acton Research Corporation SpectraPro-500 spectrograph with a ICCD camera was used. Plasma emission was guided by a fiber, positioned in the middle of the electrode gap, to an entrance slit of the spectrograph. Thus, the fiber collected light coming from a wide angle making the observed emission integrated in space, over the whole acceptance angle. These measurements were also time-integrated since they were taken with 5 s exposure time while the spectrally resolved emission from the plasma was recorded in a wide interval of wavelengths from 300 nm up to 800 nm in steps of 10 nm. A VIS-NIR 1000 μm optical fiber with reduced emission below 360 nm and stable response above 380 nm was used.

Poly-methyl methacrylate (PMMA) films spin coated on silicon wafers, were used for plasma etching. Samples of size approximately 2 cm $\times$ 2 cm were placed on the FTO electrode, and etching was performed for 120 s. A mixture of He/Air was used as etching gas, varying He flow rates at 2, 4 and 6 slm, while keeping the power constant at 100 W using a 13.56 MHz RF generator. A Woolam M2000 Spectroscopic ellipsometer was used for the *ex situ* measurements of PMMA film thickness before and after the plasma etching in order to determine the etching rate. Our new results show the important role of He flow rate, and are consistent with our first observations [32] using a constant He flow rate, and a PCB based bottom electrode. The high etching rates of this source have been used to etch paper and subsequently render it superhydrophobic [35].

3. Results and discussion

3.1. Electrical measurements

Electrical properties of the DBD source were obtained for different power values and helium flow rates when plasma is present. For each condition, a set of *I–V* curves was recorded using derivative probes, followed by calculation of the dissipated power and the impedance in the circuit during the plasma-on period. A power range from plasma ignition up to 120 Watt was studied for He flows 1, 2, 4, 6 and 7 slm. Figures 2(a)–(d) show respectively the RMS voltage, current, impedance and impedance phase obtained versus the dissipated power. In figure 2(b), current–voltage characteristics

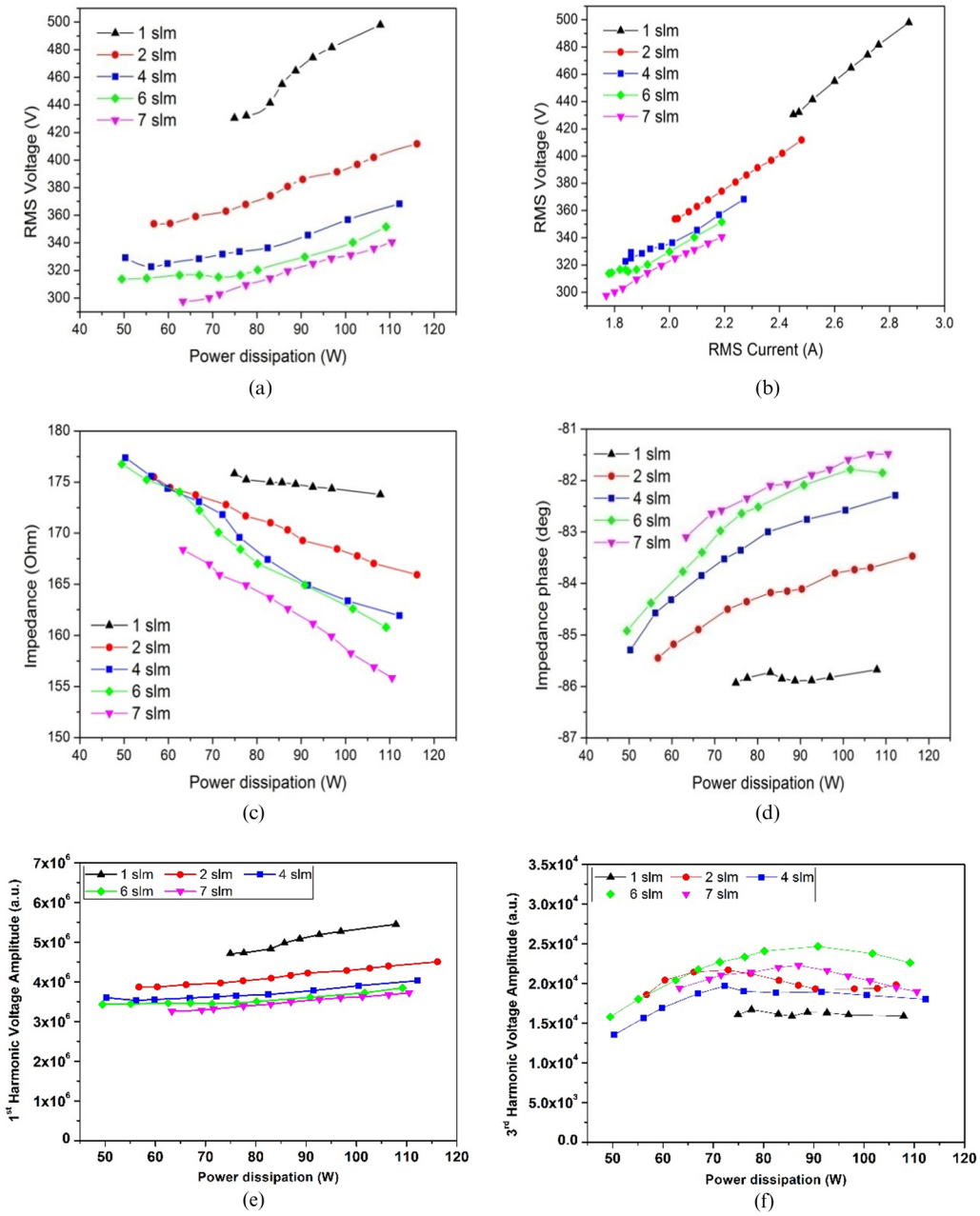

Figure 2. Electrical measurements of perforated DBD source: (a) voltage versus dissipated power and He flow, (b) current change versus dissipated power and He flow, (c) impedance behavior (source + plasma) with dissipated power and He flow change, (d) phase change with the variation of flow and power, (e) 1st harmonic (13.56 MHz) change with dissipated power and He flow and (f) 3rd harmonic (40.68 MHz) change with the variation of dissipated power and He flow.

obtained for different He flows are shown. In figures 2(e) and (f) we present changes in the voltage amplitude of the 1st and the 3rd harmonic as a function of dissipated power and different flows.

In figure 2(a) we can clearly see the effect of He flow on the ignition voltage for the same input power. Higher He flow results in lower ignition voltages. We also observe an increase of voltage with an increase of the dissipated power. Similar behavior is observed in the case of voltage variation with current, as shown in figure 2(b). From these two graphs, the amount of He has a significant effect on the discharge working point. Namely, higher He flow rate results in an increase of He percentage in-between electrodes, lowering operating voltage of the plasma at a certain power. For the highest dissipated power of 110 W the difference in operating voltages between maximum and minimum flow rate is around 170 V. Additionally, current–voltage characteristic, shown in figure 2(b), indicate that current range also decreases with an increase of the flow rate. Therefore, at certain power forwarded to the source the discharge will operate at a lower current when the gas flow rate is higher.

As expected, from the voltage and current curves and assuming that the impedance of the source is constant, in figure 2(c) we see that the absolute values of the plasma impedance decreases both with increasing He flow rate and input power as a consequence of higher efficiency of the discharge

due to the presence of He [36], indicating enhanced electron density in the plasma. In figure 2(d) we present the phase difference between the voltage and current signals (related to the imaginary component of the impedance) as a function of both He flow rate and input power. The negative sign of the phase difference indicates a capacitive behavior of the source that decreases slightly with an increasing input power. On the other hand, the increasing He flow rate has a more important effect on the impedance phase, leading to lower phase difference values, i.e. less capacitive behavior of the DBD source.

Plasmas are in general highly asymmetric systems and as a result this influences the appearance of a number of higher harmonics. The amplitudes of signals at higher harmonic frequencies, other than the main operating frequency, are indicators of the asymmetry of the system. Design of the source i.e. its construction will govern the number of harmonics that will appear. The number and intensity of harmonics are sensitive to impedance of the outer electrical circuit (matching box, cables and connectors) [37, 38]. In our case, for all He flow rates and all dissipated powers, FFT analysis showed an appearance of only the 3rd harmonic (40.68 MHz), which is two orders of magnitude smaller than the 1st harmonic (13.56 MHz). In figures 2(e) and (f) amplitudes extracted from the 1st and the 3rd harmonic after FFT analysis of the voltage signal are presented. The amplitude of the 1st harmonic increases with power. However, a decrease of the amplitude with an increase of the He flow is observed for all power levels. On the other hand, there is almost no change of the 3rd harmonic for all He flow rates and powers. This implies that asymmetry of our plasma system is not highly pronounced and that system itself is well balanced.

3.2. ICCD imaging

Recording of discharge images by ICCD camera was used to study plasma coverage of the electrode surface and it allowed us to establish optimal conditions for achieving uniform plasma operation over the entire electrode area. Measurements were performed for different He flow rates (1–7 slm) and for different dissipated power values. The end-on images obtained by using ICCD camera are presented in figures 3 and 4.

In figures 3(a)–(f) we show images taken at 7 slm of helium flow, for powers starting from ignition of the plasma at 63.3 W up to the maximum dissipated power of 110.5 W. We can clearly see that the increase of power causes the plasma to spread over the whole electrode area. The emission intensity coming from the plasma also increases. In figures 3(f)–(l) we present images obtained when the dissipated power decreases having the same values as in figures 3(a)–(f). For example, the ICCD image in figure 3(g) was obtained for the same value of dissipated power as figure 3(e). The lowest dissipated power, where we could sustain plasma discharge was 51.8 W, and with further decrease of power plasma was turned off. This power value is lower than the one needed for the discharge ignition, demonstrating a hysteresis effect of the plasma and confirming that the ignition power is always higher than the power needed to sustain plasma. As the dissipated power decreases, at certain power values, the discharge coverage shown in figures 3(g)–(l) was slightly different (compared with the images figure 3(a)–(e)) with the emission intensity decreasing more rapidly with power. The appearance of the dark patches distributed almost randomly across the electrode surface could be observed as lower power was fed to the plasma. It appears that plasma is switching off at some local channels before other even neighboring channels. This all may be due to different conditions at the surface or slightly different distance of not perfectly parallel electrodes.

In figures 4(a)–(e) we show the effect of He flow rate on uniformity and emission intensity of the plasma. The experiments were performed at 120 W input power varying He flow rate from 1 up to 7 slm. As the discharge, current varies with the flow change, dissipated power is changing for different flows. We observe that full coverage of the electrode is obtained for He flow values of 2 slm and above (figures 4(b)–(e)). Moreover, as He flow rate increases the intensity of plasma emission drops. The main reason for this drop is the reduction of the percentage of air in the air/He mixture, which is further analyzed in section 3.3.

In figures 5(a)–(c) we present side-on images of the PCB based atmospheric pressure DBD device for three different flow rates. The experiments were performed at 120 W input power by using He flow rates of 2, 4 and 7 slm. We observed that when He flow rate increases the plasma intensity across the inter-electrode gap decreases. It is also clearly seen that there is a small convergence between the plates leading to a higher distance in the right side of the board. This may be due to lack of perfect flatness of the PCB boards, or not perfectly equal spacers separating the two PCB boards. Moreover, this differentiation of distance leads to a gradual increase of the plasma intensity and an increase on the plasma variance, as one moves from the left side to the right side. The increase in the emission intensity could be explained by the higher amount of surrounding air in the admixture.

To evaluate optimum conditions when full plasma coverage of the electrodes is achieved, a more comprehensive analysis was performed. A software code was developed for automatic image processing to find the mean intensity, intensity variation (error bar of the mean intensity) and the size of plasma covered area from the discharge images. This way we performed quantification of the plasma uniformity versus RF power as well as the effect of power on the mean plasma emission intensity.

In figure 6(a) we present the percentage of the DBD surface area covered by plasma as a function of nominal power forwarded from the power supply unit for He flow rate of 2, 4, 6 and 7 slm. The electrode part is considered as covered by plasma if the intensity level of that part of the image is above 92% of the maximum intensity in the image. Then, all such areas are summed and compared to the total electrode area. Herein we consider as electrode area only the area covered by holes (showerhead) which is equal to $80 \times 80\text{mm}^2$ and not the entire electrode area ($100 \times 100\,\text{mm}^2$) as the edge effects may affect significantly the measurements. We see in the figure that for all flows, as power increases, plasma spreads over the surface of the DBD and eventually covers the whole surface. The area covered by plasma between 92%

Chromatic presentation of intensity levels in figure 4(a-e) in arbitrary units.

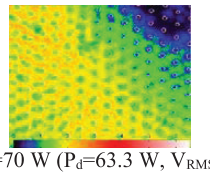

(a) P_{RF}=70 W (P_d=63.3 W, V_{RMS}=297.59 V)

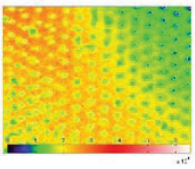

(b) P_{RF}=80 W (P_d=71.5 W V_{RMS}=302.81 V)

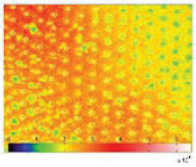

(c) P_{RF}=90 W (P_d=82.9 W V_{RMS}=314.36 V)

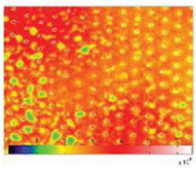

(d) P_{RF}=100 W (P_d=92.6 W V_{RMS}=324.99 V)

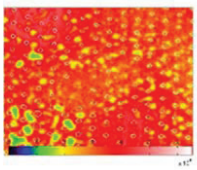

(e) P_{RF}=110 W (P_d=101.1 W V_{RMS}=331.16 V)

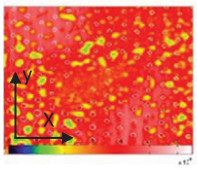

f) P_{RF}=120 W (P_d=110.5 W V_{RMS}=340.61 V)

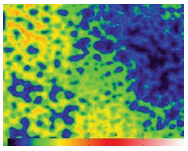

(l) P_{RF}=60 W (P_d=51.8 W V_{RMS}=278.98 V)

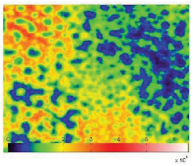

(k) P_{RF}=70 W (P_d=63.3 W V_{RMS}=290.27 V)

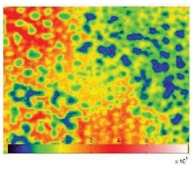

(j) P_{RF}=80 W (P_d=71.5 W V_{RMS}=301 V)

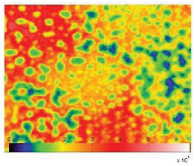

(i) P_{RF}=90 W (P_d=82.9 W V_{RMS}=310.48 V)

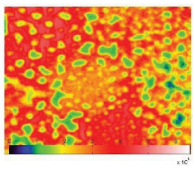

(h) P_{RF}=100 W (P_d=92.6 W V_{RMS}=321.74 V)

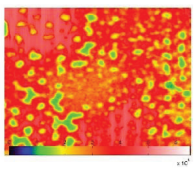

(g) P_{RF}=110 W (P_d=101.1 W V_{RMS}=331.33 V)

Figure 3. ICCD images of atmospheric pressure DBD operating with 7 slm of He for different RF input powers (P_{RF}). Calculated dissipation powers (P_d) and measured RMS voltages are shown also. Images (a)–(f) taken with power increase and (g)(l) with power decrease. Chromatic presentation of intensity levels in images is in arbitrary units.

and 100% is defined as full coverage. At higher He flow rates full coverage is reached at lower power levels. Namely, at 7 slm full coverage is reached from 75 Watts, while at 2 slm it is achieved at a power level above 110 Watts. Nevertheless, we observed that even with the lowest flow (2 slm) conditions, full plasma coverage can be achieved.

In figure 6(b) we present the mean plasma emission intensity measured at 2, 4, 6 and 7 slm as a function of the nominal power for cases when the area covered by the plasma was larger than 92% i.e. with full coverage. The mean intensity values are calculated by dividing the sum of all pixel intensities by the pixel number (240 × 240 pixels). As expected, the mean intensity increases with power for all He flow rates. The intensity for 2 slm is the highest while for higher He flow rates the intensity drops.

To quantify in more detail the uniformity of the plasma on the PCB, we calculated the mean pixel intensity and its standard deviation for each column along the *X* direction for figure 3(f), corresponding to typical operating conditions of 7 slm He and 120 W. In figure 6(c) we show the plasma variation obtained from such averaged emission intensity data

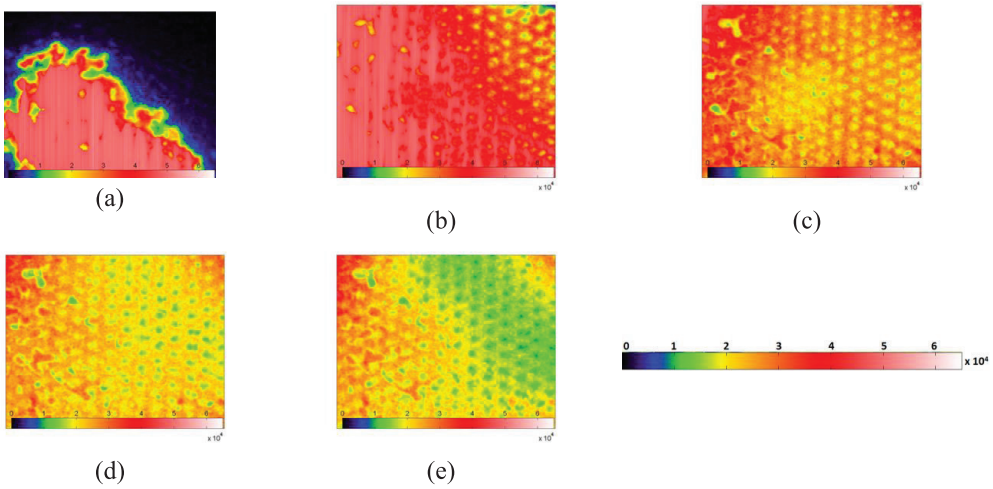

Figure 4. ICCD images of atmospheric pressure DBD for different helium flow rates at constant nominal power of the RF power 120 W. Dissipated power is indicated in parenthesis: (a) 1 slm He (109.8 W), (b) 2 slm He (108.3 W), (c) 4 slm He (110.1 W), (d) 6 slm He (111.9 W) and (e) 7 slm He (110.5 W). Chromatic presentation of intensity levels in (a)–(e) in arbitrary units.

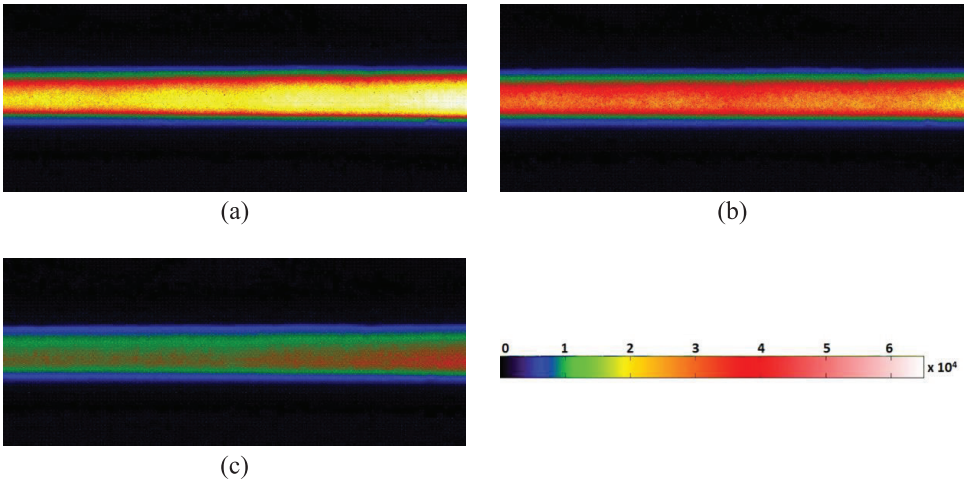

Figure 5. ICCD images of atmospheric pressure DBD for different He flow rates at constant nominal power of the RF power 120 W. Dissipated power is indicated in parenthesis: (a) 2 slm He (108.3 W), (b) 4 slm He (110.1 W) and (c) 7 slm He (110.5 W). Chromatic presentation of intensity levels in (a)–(c) in arbitrary units.

(from figure 3(f)) along the 240 columns in the *X* direction (i.e from left to right). In figure 6(d) we plot again these data to show the uniformity of the plasma along the *X* direction. The uniformity (in %) is calculated as (1 − ((|standard deviation|)/(mean Intensity))) * 100. The uniformity variation shown is due to the showerhead-type of the powered electrode. The holes on the PCB cause small local emission intensity variations, i.e. slightly lower plasma emission intensity in the position of the holes compared to the position in between the holes. Nonetheless, the level of plasma uniformity stays almost constant in a wide range of operating power, especially for higher He flow. This feature of the DBD source is very important for homogeneous treatments of large area samples.

3.3. Optical emission spectroscopy

In figure 7 we present emission spectra obtained at 100 Watt nominal power obtained for a wide range of wavelengths between 300 nm and 800 nm. The atomic O, the first negative system (FNS) of N_2 ion as well as the second positive system (SPS) of N_2 molecular transition lines are visible in the spectrum. For He there are no excitation thresholds below 19 eV, and therefore most of the excitation and ionization is due to oxygen and nitrogen. Even at 19 eV it is the metastable levels of He that would quickly transfer excitation to FNS lines of nitrogen and equivalent levels of oxygen. We also observe in figure 7 electron energy levels from He 707 line, i.e. from electrons with energy higher than 22 eV.

The results of optical emission spectrometry (OES) obtained for different power values and flow rates are presented in figure 8: we show the total emission intensity of the plasma recorded by the spectrometer in the range between 380 to 800 nm, the intensities of atomic O at 777 nm, He at 707 nm and the intensity of (0–2) SPS N2 molecular transition line (at 380 nm). We only present the 380 nm SPS N2 line due to our optical fiber limitations, which reduces the emission below 360 nm and has a stable response above 380 nm. The line intensities are corrected for the efficiency

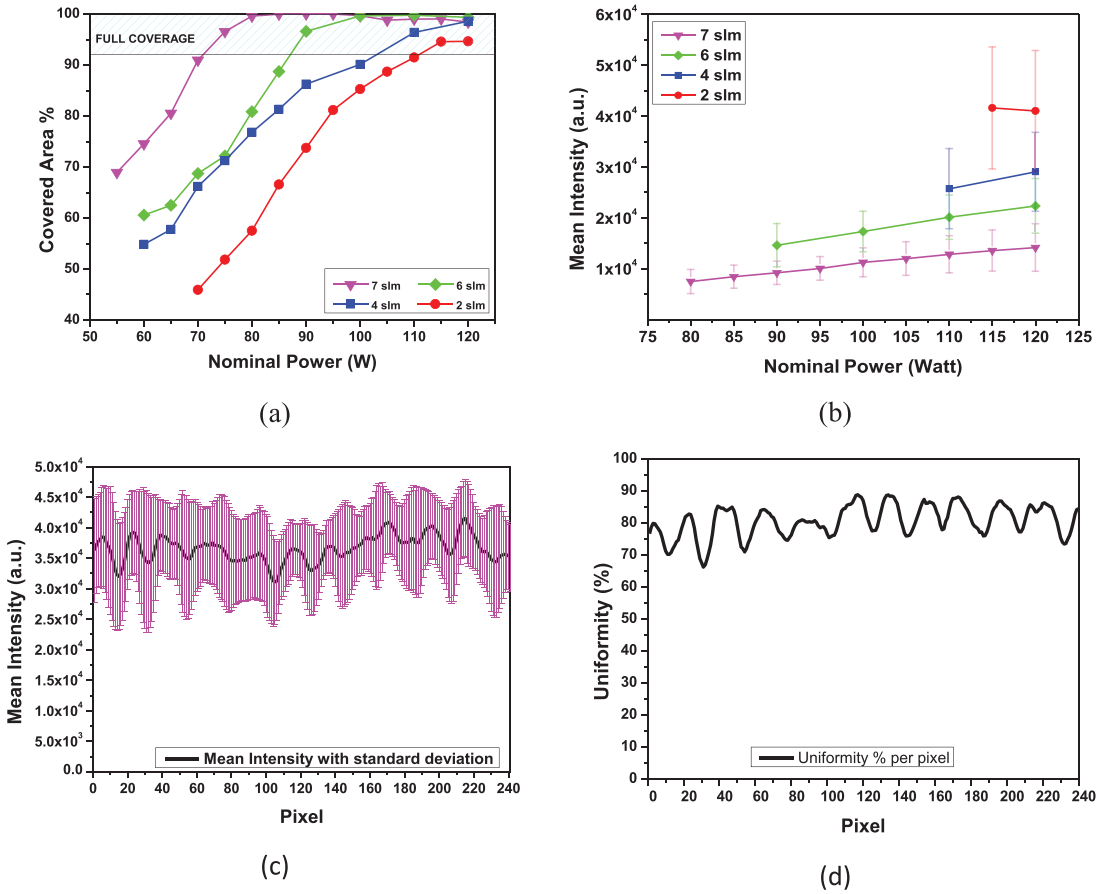

Figure 6. Results of quantitative analysis of ICCD images obtained for 2, 4, 6 and 7 slm of He. (a) Effect of power on plasma coverage of the DBD surface. (b) Effect of nominal power on the mean plasma intensity and its variation (c) column average emission intensity and its standard deviation along the *X* direction (i.e. from left to right), for figure 3(f). (d) Data of (c), plotted again as uniformity along the *X* direction.

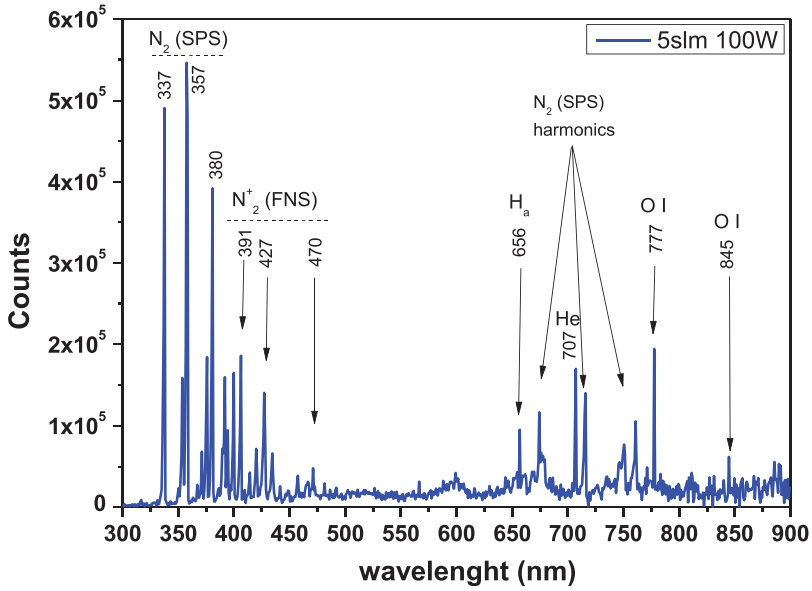

Figure 7. Optical emission spectroscopy of atmospheric pressure DBD at helium flow rate 5 slm and nominal power 100 W.

of the optical system using a curve obtained from the supplier, Princeton Instruments. However, correction due to the optical fiber limited response below 360 nm has not been applied.

In figure 8(a) left *Y* axis we can see the effect of He flow rate on the emission intensities when applying a constant 100 W input power. As expected, the He flow rate increase results in increase of the He 707 nm line intensity due to the higher

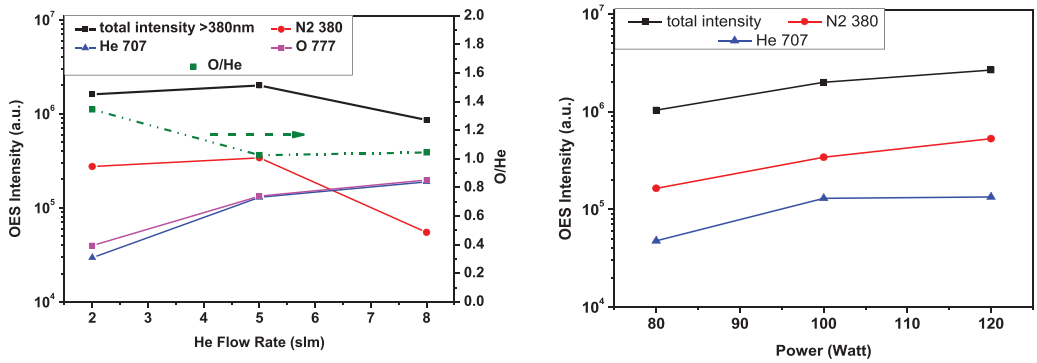

Figure 8. Effect of He flow rate and power to the total emission intensity (380–800 nm), intensity of O 777 nm, He 707 nm and SPS 380 nm N_2 band line. Atmospheric pressure DBD with (a) nominal power 100 W, (b) He flow rate 5 slm.

percentage of He in the He-surrounding air gas mixture. The emission intensity can be calculated as a function of the gas density, excitation coefficient and electron density. The emission of Oxygen also increases, although we expect a slight drop of its density at high flowrates. The increased Oxygen emission is probably due to higher electron density and/or higher excitation coefficient (due to higher electron temperature); such increases may offset any decrease of Oxygen density [39]. If we assume that the excitation coefficient ratio of He at 707 nm and O at 777.2 nm remains almost constant with flowrate, we can estimate the effect He flow rate on O density, by taking the emission intensity ratio of O/He (see figure 8(a) right *Y* axis). We observe that the ratio of intensities decreases, and this is an indication of reduced oxygen atom density at higher flowrates. Similar effects have been observed in He–O_2 mixtures [25, 40]. As we will see below this reduction of the Oxygen atom density is consistent with the reduction of the etching rate at high flowrates.

Contrary to He and Oxygen emissions, the N_2 380 nm intensity drops almost one order of magnitude as He flow changes from 2 slm to 8 slm and smaller amount of air is present between electrodes. Such behavior of total emission and N_2 380 line intensities suggests that dominant part of the spectrally integrated emission belongs to lines in N_2 SPS band.

Figure 8(b) shows the effect of input power on intensities of the same lines using 5 slm He flow rate. As expected, the power increase results in higher peak intensities of the N_2 380 nm line and He lines. Finally, in both figures 7(a) and (b) we see that the total emission intensity of the plasma follows the N_2 380 nm line intensity. Therefore, we conclude that the dominant emission is the N_2 SPS molecular transition lines, which define the total emission intensity of the plasma.

3.4. Etching and wetting properties of PMMA films

Treatment of polymeric substrates was also performed with the DBD plasma source. PMMA (Poly methyl methacrylate) thin polymeric films spin-coated on silicon were etched with the DBD source in He/air plasma. Film thickness measurements were performed using multiwavelength ellipsometry before and after plasma etching and the etch rates of polymer films were calculated. For the treatment with He/air we used 100 Watt as nominal power and He flows of 2, 4 and 6 slm. All the samples were etched for 2 min. In table 1 we can see the effect of the change of He flow rate on the etch rates, i.e. as He flow rate increases etching rate drops. This is consistent with decreased density of atomic oxygen at high flowrates, as observed by the emission intensity ratios shown above in figure 8(a) for Oxygen and Helium. At high flowrates it is also possible that the etching rate is reduced due to convective cooling of the sample from the He flow.

Table 1. PMMA etching rates and corresponding contact angle values after six weeks of ageing as a function of He flow rate at constant nominal power 100 W.

Power (Watt)	He (slm)	Etch rate (nm $min^{-1} \pm 10$)	Contact angle after 6 weeks ($\pm 3°$)
100	6	52	45
100	4	69	41
100	2	93	35

It has been shown before that plasma treatments may affect surface hydrophilicity [32]. Namely, PMMA films before treatments had contact angles approximately 70°. After the treatment surfaces became more hydrophilic, with a lower contact angle approximately 30°. We re-measured the static contact angles of the treated PMMA samples six weeks later between 40° to 50°. This result showed that aging of treated surfaces with He/air plasmas has not been significant and the surfaces remained hydrophilic, especially those treated with low He flow rates.

4. Conclusion

In this work, we present a comprehensive analysis of characteristics of the plasma generated by a novel PCB based atmospheric pressure DBD source. We performed electrical characterization, by using derivative probes, simultaneously with optical diagnostics: plasma imaging and OES. By using the data obtained from electrical measurements, we determined voltage–current characteristics and calculated power dissipation at the plasma source. We showed that behavior of

the electrical properties of the DBD are strongly affected by the He-surrounding air mixture, i.e. related to the He flow. From the analysis of higher-order harmonics we demonstrated electrical stability of operation of the source. In addition, ICCD recordings of spatially-resolved images and optical spectra of the discharge provided information about plasma structure at different operating parameters. We systematically studied the effect of He flow rate and the power forwarded to the device on the uniformity and emission intensity of the plasma, attaining the parameter range of powers and flow rates with high plasma uniformity. The high plasma uniformity makes the discharge source suitable for material processing over potentially large areas.

We also performed polymer treatment with the DBD source in terms of PMMA etching and wetting measurements. We concluded that PMMA surface aging has been significantly retarded and the surfaces remained hydrophilic even after six weeks, especially those treated with low He flow.

The source that has been built allows non-equilibrium plasma formation over a wide area. It presents high uniformity, all the benefits of DBD operating in glow regime without filamentation, and it is well controlled by adjusting the gas flow, mixture composition and power. Other modes of operation are worth exploring such as using Ar as a buffer gas, allowing a more complex chemistry and allowing pulsing and two frequency operation.

Acknowledgments

This work was financed by the NATO project SPS 984555. The COST project MP1101 funded the short-term mission of Angelos Zeniou to IOP in Belgrade for the electrical and optical measurements. Authors from the Institute of Physics acknowledge projects of MESTD of Republic of Serbia ON171037 and III41011.

References

[1] Tendero C, Tixier C, Tristant P, Desmaison J and Leprince P 2006 *Spectrochim. Acta* B **61** 2
[2] Penkov O V, Khadem M, Lim W and Kim D 2015 *J. Coat. Technol. Res.* **12** 225–35
[3] Bardos L and Barankova H 2010 *Thin Solid Films* **518** 2705
[4] Pappas D 2011 *J. Vac. Sci. Technol* A **29** 021301
[5] Larousi M and Akan T 2007 *Plasma Process. Polym.* **4** 777–8
[6] Goldman M, Goldman A and Sigmond R S 1985 *Pure Appl. Chem.* **57** 1353
[7] Schutze A, Jeong J Y, Babayan S E, Park J, Selwyn G S and Hicks R F 1998 *IEEE Trans. Plasma Sci.* **26** 6
[8] Selwyn G S, Herrmann H W, Park J and Hennins I 2001 *Contrib. Plasma Phys.* **6** 610–9
[9] Sankaran R M and Giapis K P 2002 *J. Appl. Phys.* **92** 5
[10] Laimer J and Stori H 2007 *Plasma Process Polym.* **4** 266–74
[11] Puač N, Živković S, Selaković N, Milutinović M, Boljević J, Malović G and Petrović Z L 2014 *Appl. Phys. Lett.* **104** 214106
[12] Maletić D, Puač N, Selaković N, Lazović S, Malović G, Đorđević A and Petrović Z L 2015 *Plasma Sources Sci. Technol.* **24** 025006
[13] Boselli M, Colombo V and Ghedini E 2014 *Plasma Chem. Plasma Process.* **34** 853
[14] Gherardi M, Puač N, Marić D, Stancampiano A, Malović G, Colombo V and Petrović Z L 2015 *Plasma Sources Sci. Technol.* **24** 17
[15] Iséni S, Reuter S and Weltmann K-D 2014 *J. Phys. D: Appl. Phys.* **47** 075203
[16] Voráč J, Dvořák P, Procházka V, Ehlbeck J and Reuter S 2013 *Plasma Sources Sci. Technol.* **22** 025016
[17] Kogelschatz U 2003 *Plasma Chem. Plasma Process.* **23** 1–46
[18] Morávek T, Fialová M, Kopkáně D, Ráhel J, Stahel P and Černák M 2015 *Open Chem.* **13** 236–44
[19] Kogelschatz U 2007 *Contrib. Plasma Phys.* **47** 80–8
[20] Hołub M, Kalisiak S, Borkowski T, Myśków J and Brandenburg R 2010 *Polish J. Environ. Stud.* **19** 1199–211
[21] Nehra V, Kumar A and Dwivedi H K 2008 *Int. J. Eng.* **2** 53–68
[22] Bonandini L, Barbero N, Costabello K, Pavan K, Parisi F and Viscardi G 2010 *ChemSusChem* **3** 591–6
[23] Puač N, Petrović Z L, Malović G, Dordević A, Živković S, Giba Z and Grubišić D 2006 *J. Phys. D: Appl. Phys.* **39** 3514–9
[24] Lazović S, Puač N, Spasić K, Malović G, Cvelbar U, Mozetič M, Radetić M and Petrović Z L 2013 *J. Phys. D: Appl. Phys.* **46** 075201
[25] Milosavljevic V, Donegan M, Cullen P J and Dowling D P 2014 *J. Phys. Soc. Japan* **83** 014501
[26] Sankaran R M and Giapis K P 2003 *J. Phys. D: Appl. Phys.* **36** 2914–21
[27] Staak D, Farouk B, Gutsol A and Fridman A 2005 *Plasma Sources Sci. Technol.* **14** 700–11
[28] Machala Z, Janda M, Hensel K, Jedlovsky I, Lestinska L, Foltin V, Martisovits V and Morvova M 2007 *J. Mol. Spectrosc.* **243** 194–201
[29] Thiyagarajan M, Sarani A and Nicula C 2013 *J. Appl. Phys.* **113** 233302
[30] Sarani A, Nicula C, Gonzales X F and Thiyagarajan M 2014 *IEEE Trans. Plasma Sci.* **42** 3148–60
[31] Tóth A, Szentmihályi K, Keresztes Z, Szigyártó I, Kováčik D, Černák M and Kutasi K 2015 *Open Chem.* **13** 557–63
[32] Dimitrakellis P, Zeniou A, Stratakos Y and Gogolides E 2016 *Plasma Sources Sci. Technol.* **25** 025015
[33] Gogolides E, Zeniou A and Dimitrakellis P 2015 *Greek Patent Application No* 20150100397
[34] Puac N, Maletic D, Lazovic S, Malovic G, Dordevic A and Petrovic Z L 2012 *Appl. Phys. Lett.* **101** 024103
[35] Dimitrakellis P, Travlos A, Psycharis P V and Gogolides E 2016 *Plasma Process. Polym.* at press (https://doi.org/10.1002/ppap.201600069)
[36] Moravej M, Yang X, Nowling G R, Chang J P and Hicks R F 2004 *J. Appl. Phys.* **12** 96
[37] Miller P A 1991 *Proc. SPIE* **1594** 179–88
Miller P A, Anderson H and Splichal M P 1992 *J. Appl. Phys.* **71** 1171–6
[38] Berry L, Maynard H, Miller P, Moore T, Pendley M, Resta V, Sparks D and Yang Q 2000 *J. Vac. Sci. Technol.* A **18** 2806–14
[39] Hübner S, Santos Sousa J, Puech V, Kroesen G M W and Sadeghi N 2014 *J. Phys. D: Appl. Phys.* **47** 432001
[40] Nwankire C E, Law V J, Nindrayog A, Twomey B, Niemi K, Milosavljevic V, Graham W G and Dowling D P 2010 *Plasma Chem. Plasma Process.* **30** 537–52

Eur. Phys. J. D (2017) 71: 27
DOI: 10.1140/epjd/e2016-70607-5

THE EUROPEAN PHYSICAL JOURNAL D

Regular Article

Mass spectrometry of diffuse coplanar surface barrier discharge: influence of discharge frequency and oxygen content in N_2/O_2 mixture*

Jan Čech[1], Antonín Brablec[1], Mirko Černák[1], Nevena Puač[2,a], Nenad Selaković[2], and Zoran Lj. Petrović[2,3]

[1] Masaryk University, CEPLANT – R&D Centre for Low-Cost Plasma and Nanotechnology Surface Modification, Kotlářská 2, 611 37 Brno, Czech Republic
[2] Institute of Physics, University of Belgrade, Pregrevica 118, 11080 Belgrade, Serbia
[3] Serbian Academy of Sciences and Arts, Knez Mihailova 35, 11001 Belgrade, Serbia

Received 29 September 2016 / Received in final form 7 December 2016
Published online 9 February 2017 – © EDP Sciences, Società Italiana di Fisica, Springer-Verlag 2017

Abstract. Diffuse Coplanar Surface Barrier Discharge (DCSBD) has been studied extensively for industrial applications in recent decade. So far, limited information was available on the production of ozone or nitrogen oxides important for industrial deployment of DCSBD. In this paper results of mass spectrometry of DCSBD performed at atmospheric pressure are presented. DCSBD mass spectra were studied for different oxygen contents in N_2/O_2 working gas mixture at low flow rate (estimated residence time in discharge chamber was approx. 3 s). Influence of the driving frequency (15, 30 and 50 kHz) at constant high voltage amplitude was studied as well. Ozone and NO production in DCSBD are given as typical representatives. Production of ozone decreases with the driving frequency, which could be attributed to the gas heating at higher frequencies.

1 Introduction

Dielectric barrier discharges (DBDs) have a promising potential to succeed in many industrial applications [1]. In order to better understand the DBD's properties and to control the discharge parameters, DBDs were subject of extensive research in past decades [2]. So-called Diffuse Coplanar Surface Barrier Discharge (DCSBD) is the DBD with electrodes fully embedded in the dielectrics in plane-parallel geometry [3]. The DCSBD is generated above the dielectric plate in a form of numerous micro-discharges [4]. This results in a sub-millimetre thin macroscopically diffusive layer of high power density plasma without any contact with metallic electrodes [3]. This property together with an ability to generate a macroscopically (visually) diffuse discharge in the air at atmospheric pressure provide DCSBD with a big potential for high-speed in-line industrial applications [5]. On the other hand applicability of the discharge places a high demand on thorough investigation [6] of the discharge.

In case of applications of any type of plasma, ranging from low pressure up to the atmospheric pressure, the knowledge of chemistry in the discharge and of the composition is of utmost importance. When it comes to the low pressure plasmas mass spectrometry is a well known technique that has been used for a very long time. Lately mass spectrometers that can operate at atmospheric pressure were developed[1] [7–9]. These unique systems are enabling studies of active species (molecules, atoms and ions) and their abundances even at the atmospheric pressure. So far we have used HIDEN HPR60 mass-energy analyser with several plasma sources ranging from kHz to MHz region [10–13]. In all cases it was necessary to optimize the operation of the mass-energy analyser and in some of them to overcome serious problems that can occur due to the influence of the plasma source on the HIDEN HPR60 mass-energy analyser [13].

In this paper we present the results of mass spectrometry of the DCSBD plasma source, following up the preliminary measurements realized in 2008 [12]. The measurements were made in several mixtures of nitrogen and oxygen and special attention was aimed at investigating behaviour of the reactive oxygen and nitrogen species (RONS) that are of the utmost importance in biomedical applications.

2 Experimental

2.1 DCSBD plasma source

Mass spectrometry of the DCSBD was performed on specially designed small-form-factor plasma reactor

* Contribution to the Topical Issue "Low-Energy Interactions related to Atmospheric and Extreme Conditions", edited by S. Ptasinska, M. Smialek-Telega, A. Milosavljevic and B. Sivaraman.

[a] e-mail: nevena@ipb.ac.rs

[1] http://www.hidenanalytical.com/en/.

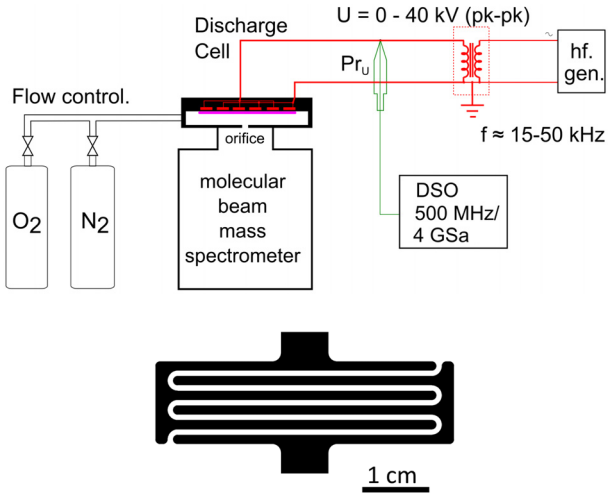

Fig. 1. Sketch of the experimental setup (top) and the details of DCSBD electrode system geometry (bottom).

of the total surface area of 7.5 cm^2 at atmospheric pressure. Firstly description of the plasma source is given followed by a more detailed description of the diagnostic technique and mass spectrometer.

A small-form-factor DCSBD plasma system studied in the presented paper consists of the discharge cell, oil cooling system and high-voltage power supply unit. The discharge cell consists of hollow polymeric cylinder cooled by the flow of oil. On top of the cylinder, DCSBD element was placed. The DCSBD consists of a ceramic plate (96% alumina) with an embedded electrode system. In Figure 1 the schematic drawing of the DCSBD discharge cell is given. The ceramic plate of the area of 80×40 mm and thickness of 0.2 mm was used. The electrode system consists of three plain-parallel (coplanar) electrode pairs of 45 mm length, 1.5 mm width and mutual distance (gap) of 1.0 mm. Plasma was generated on the top of the ceramic plate using an alternating sine-wave high-voltage of the amplitude of 11.2 kV and changeable frequency. Three frequencies were used in presented study – 15, 30 and 50 kHz. The custom-made high-voltage power supply was used. The electrical parameters were controlled using Agilent DSO 6052A oscilloscope (in Fig. 1 labelled DSO) and high-voltage probe Tektronix P6015A (in Fig. 1 labelled Pr$_U$).

The discharge was operated in the cylindrical chamber of width of 10 cm and height of 3 mm that ensures operation in defined working gas. As the working gas the mixtures of nitrogen and oxygen (purity 5.0) were used, with a constant total mass flow rate of 500 sccm. The mass flow and mixing ratios were controlled using two mass flow controllers: OMEGA FMA5518 (nitrogen) and Bronckhorst MV-302 (oxygen). The discharge chamber was attached to the face of the mass spectrometer, protected by 0.3 mm thin PET foil. In case of surface discharges that operate at atmospheric pressure sparking can occur between the powered electrode and front plate of mass spectrometer without the additional PET foil (or some other type of dielectric layer) [13]. Therefore, in order to have homogeneous discharge in the whole volume between the powered electrode of the DCSBD and the front plate of Hiden mass spectrometer we have used PET foil as dielectric layer. When measuring neutral mass spectra no observable changes were noticed with and without the PET foil.

2.2 Mass spectrometry originated radicals at atmospheric pressure conditions

In this experiment the quadrupole-based HIDEN HPR-60 molecular beam mass spectrometer (MBMS) was used for detection of radicals derived from the DCSBD plasma source. MBMS has a three stage differentially pumped inlet system that enable mass spectrometer to sample at atmospheric pressure. The pressures in all three stages ($p_1 = 1.7 \times 10^0$ Torr; $p_2 = 6.5 \times 10^{-5}$ Torr; $p_3 = 4.5 \times 10^{-7}$ Torr) were kept constant during the measurements. In all measurements DCSBD was attached to the front-side plate of MBMS with the specially designed housing and sealed with silicone rubber O-ring. This setup enabled us to operate the discharge at controlled working atmosphere and simultaneously analyse composition of the discharge. The following working gas composition/mixture ratios were used: N_2/O_2: 100/0%, 80/20%, 60/40%, 50/50%, 40/60% and 20/80%. The distance between the DCSBD's dielectric plate and inlet orifice of the MBMS was set to 2 mm to avoid arcing to the grounded front plate. The diameter of the first inlet orifice was 0.3 mm.

The mass spectrometry measurements were carried out in so-called residual gas analyser (RGA) mode. The measurements were performed in two distinct regimes: a) the mass survey spectrum recording and b) constant tracking of the selected species ('time sequence' or acquisition measurement – MID). The RGA mode uses an internal ionization source of MBMS for the detection of the neutrals derived from the analysed gas.

The mass analysis of plasma at atmospheric pressure condition is a challenging problem. In principle two approaches could be adopted to analyse the production of radicals in studied plasma system depending on the energy of electrons used for analysed gas ionization. The measurements can be carried out at a) certain fixed energy of ionizing electrons; or b) at variable energy of ionizing electrons – 'energy-resolved' measurements. Both approaches offers advantages, as well as serious drawbacks. It is worthy to note the major ones and therefore the short comments on the methods follows. If fixed energy of ionizing electrons is used, then the information on the origin of detected species is lost, unless a special attention to the measurement protocol is paid. This is because of the energy of ionizing electrons is usually as high as 70 eV, which is the level sufficient to ionize, but also dissociate the detected species, causing the detection of mass spectra signals of radicals, that are produced not only in studied plasma system, but also in the ionizer of the MBMS itself. Despite this drawback, this was the chosen regime for presented measurements, because the ionization yield can be substantially higher at this regime resulting in the sufficient

signal to noise ratio of detected species. In following text we will give the protocol of measurement and notes on the justification of the conclusions based on this approach.

The other approach is the adoption of 'energy-resolved' measurements, at which the energy of ionizing electrons is gradually increased and the signal of the particular radical is followed in the mass spectrum. The key benefit of this approach is the avoidance of parasitic mass spectrum signals, keeping the impinging electrons energy well below the dissociation threshold of species from which the particular radical could be created. Resulting energy-dependent signal course could be used to discriminate the radicals created in the instrument itself from those originating from studied plasma system. But the energy resolved measurements has also the serious drawbacks, which prevented us from the adoption of this method in our measurements and which we would like to briefly discuss.

The energy-resolved mass spectroscopy measurements were successfully used by co-authors for plasma-generated species monitoring (see e.g., [13–15]) but this technique has to be implemented unambiguously with careful consideration of the method limitations. Starting with the thresholds for dissociative ionization of N_2 and O_2 molecules which are 22 eV and 20 eV, respectively [7,16] and with the thresholds for dissociation by electron impact (that would produce neutral ground state atoms) that are 9.75 and 5.11 eV respectively [17] we see that the energy range is reasonable and yet it is rather narrow. In that energy range ionization of atoms may occur (thresholds for ionization are 14.5 and 13.6 eV respectively) but the cross section below 20 eV is still quite small thus providing a small likelihood of ionization of the fragments produced in the ionizer.

If we take into account the NO molecule that is an abundant product of the non-equilibrium atmospheric pressure plasma [18] with its thresholds for dissociative ionization (22 eV and 21 eV, respectively [7,19]) this range where we could find N and O atoms created 'only' in the discharge have to be between N and O ionization thresholds and <20 eV. By taking into account the cross sections for ionizations of N and O atoms we can see that by reducing the energy range of the ionizing electrons (for example 15–19 eV) we have low ionization efficiency. At 19 eV ionization cross section for both atoms is in the range of $0.2–0.3 \times 10^{-20}$ m^2 which is only around 10% of the cross section maximum. This indicates that in this range of energies the efficiency of detecting N and O atoms created in the plasma is quite low and prone to underestimation of the real number of neutrals in the plasma.

Here we may also mention N_2O molecule that is created in plasma ([18], see Fig. 4 of our paper). The dissociation thresholds for this molecule and creation of O and N atoms start already at around 8 eV [20,21]. This means that the signal collected for N and O atoms in energy resolved measurements in the range, for example, 15 eV to 19 eV also detects atoms created inside the instrument through dissociation of N_2O. The same issue is with CO_2 molecules with the threshold for dissociation of 11 eV [22]. These molecules are not very abundant in the atmospheric pressure discharges, but still they may contribute to the detected signal and induce some uncertainty. In addition one has to take into account the thermal decomposition of the species. Even if we are measuring in the 'safe' range of electron energies the temperature of the electron emitting filament is about 2000 K that will lead to the thermal decomposition of the molecules and contribution to the signal of neutral atoms. This is a more of an issue for O atoms than in the case of N atoms [7].

To conclude, there are several limitations of the energy profile technique. Most important, in the present case it is its poor efficiency. The discharge studied in this paper is a diffuse planar discharge with low flux of particles at any point but with a large overall production of radicals and atoms. This rendered the energy-resolved measurement approach in case of studied DCSBD plasma source unusable, as the signal during the energy-resolved experiments of DCSBD was proven to be too low to be distinguished from the background noise. On the other hand the source, with its large area and other facilities provides numerous advantages in applications and it is certainly important to provide diagnostics of different species produced by the plasma.

One can easily dismiss approach where only measurements at 70 eV (or some such energy) are made, although even in the present day literature there is no shortage of papers employing such technique. In present paper a somewhat different approach was adopted, which was called a 'time sequence measurement'. Three temporal stages were adopted in the measurement protocol, one when the plasma source is turned off, one when a valve in front of the ionization chamber is turned off and finally a stage when plasma is turned on and connected to the mass analyser. In other words the differences between the system with and without plasma were observed, allowing for the plasma products to be detected and tracked. The same type of time series measurements at 70 eV was also used by Stoffels et al. for detection of the changes in nitrogen, oxygen and nitric oxide molecules (among else) when the discharge is present and when it is extinguished [18]. It should be noted, that measurements based on both approaches ('energy-resolved' and 'time sequence') were performed on the same source and consistent results were obtained [7,18].

The measurements presented in this paper were carried out with the 70 eV electron energy used for ionization of neutrals. The background signal was measured in all experiments (molecular beam was shielded by closing the SwageLock valve) and subtracted from the total signal values in order to get the net signal of analysed gas. For whole set of experimental conditions (gas mixture and frequency of the supply voltage) the mass spectra of neutrals were acquired in the range of 1–100 amu.

In order to get better insight into the behaviour of plasma generated species high-sensitivity 'time sequence' measurements were performed using the acquisition mode (MID scan). The following procedure was applied for all measurements: firstly, the molecular beam inlet of the mass analyser was shielded (thus blocking the signal

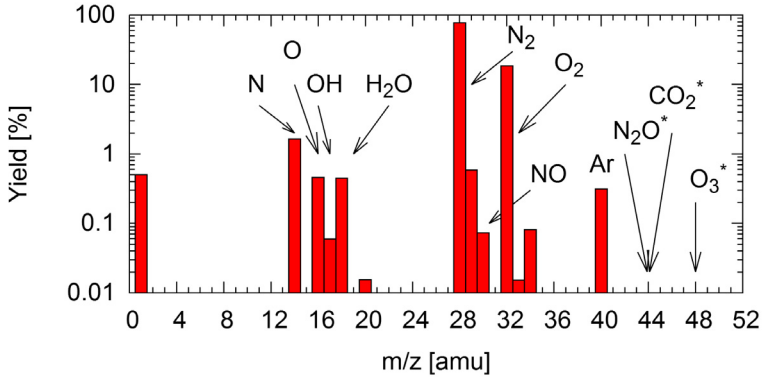

Fig. 2. The mass spectrum of working gas for the following conditions: N_2/O_2 ratio of 80/20 and DCSBD discharge operated at working frequency of DCSBD 15 kHz and voltage amplitude of 11.2 kV. The spectrum is truncated at 52 amu, due to lack of detectable signal at given experimental conditions. Asterisk-marked species are close to the limit of detection at given conditions.

from plasma-background signal acquisition), then the inlet of the MBMS was opened and the system was allowed to reach the equilibrium (≈2 min). After that, plasma was ignited and system was allowed again to reach the equilibrium (≈2 min). Then the discharge was switched off and after the final equilibrium was reached experiment was completed. The whole procedure of a MID scan took approx. 10–12 min. The behaviour of specific radicals could be derived from recorded changes of the signal when DCSBD plasma is on and off. Total variations were determined for O_3 and NO radicals for the pre-selected current at the ionization filament of 50 μA.

3 Results and discussion

According to the described procedures of mass analysis this section is divided into two sub-sections. Firstly, the survey mass spectra are discussed and then results of the high-sensitivity measurements of selected radicals are given and discussed.

From the whole set of studied discharge conditions the limited sub-set was chosen for presentation. For survey spectra analysis, the typical discharge conditions used for plasma treatment of materials were chosen, i.e., the working gas composition of 80% of N_2 and 20% of O_2, as the substitution of the ambient air. The high-voltage amplitude of 11.2 kV at the frequency of 15 kHz were used as the typical working conditions of DCSBD discharge. These results can be compared to the previous measurements made on the industrial-size DCSBD system at ambient air conditions in 2008 [12]. For the time-series measurements of selected radicals the two radicals (O_3 and NO) were selected as the representatives of volatile compounds that have to be controlled and monitored in industrial environment due to their biological effects.

Due to the used mass analysis method the interpretation of the data should be done carefully, concerning the other possible sources of the species, mainly from the reactions inside the MBMS. We based our analysis and conclusions on the published results and protocols on atmospheric pressure mass analysis of plasmas, mainly on the interpretation of the 'time sequence' measurements.

3.1 RGA analysis – mass spectra of the DCSBD discharge

In Figure 2 the mass spectrum of the working gas in the chamber of DCSBD discharge is given. The spectrum represents the discharge operated at frequency of 15 kHz at high-voltage amplitude of 11.2 kV in the gas mixture of 80% N_2 and 20% O_2, i.e., artificial air conditions. The yields in Figure 2 represent relative percentage of distribution of the species. The following formula was used for the calculation of the yields: $Yield = Y^i_{mass} / \sum_i Y^i_{mass}$, where Y^i_{mass} is the count of specific species (like N_2, O, etc.) at the detector (detected as appropriate positive ion there), see [8,11] for details.

The yields of the recorded mass spectra can give us the relative gas composition. From the spectra in Figure 2 it is evident that the dominant species in the discharge were molecular nitrogen and molecular oxygen. Atomic nitrogen and atomic oxygen are present as the result of plasma reactions as well as the NO radical. The OH radical is also present due to plasma reactions as well as the decomposition of water in the MBMS. Having in mind that the spectra were obtained for the electron energies of 70 eV the comparison of the mass spectra with and without ignited discharge is necessary.

In Figure 3 effect of the discharge on gas composition is shown. In the upper part of Figure 3 the comparison of working gas composition not-influenced (labelled 'PL OFF') and influenced (labelled 'PL ON') by the discharge is given.

Although the yields of species like N, O, or NO are relatively high, the relative gas composition of the rest of the species with/without plasma differs only very slightly, typically less than 1% of the relative composition (see lower part of Fig. 3). This could be mainly contributed to the fact that the most of detected species were produced in the ionizer. The system was also not able to sample

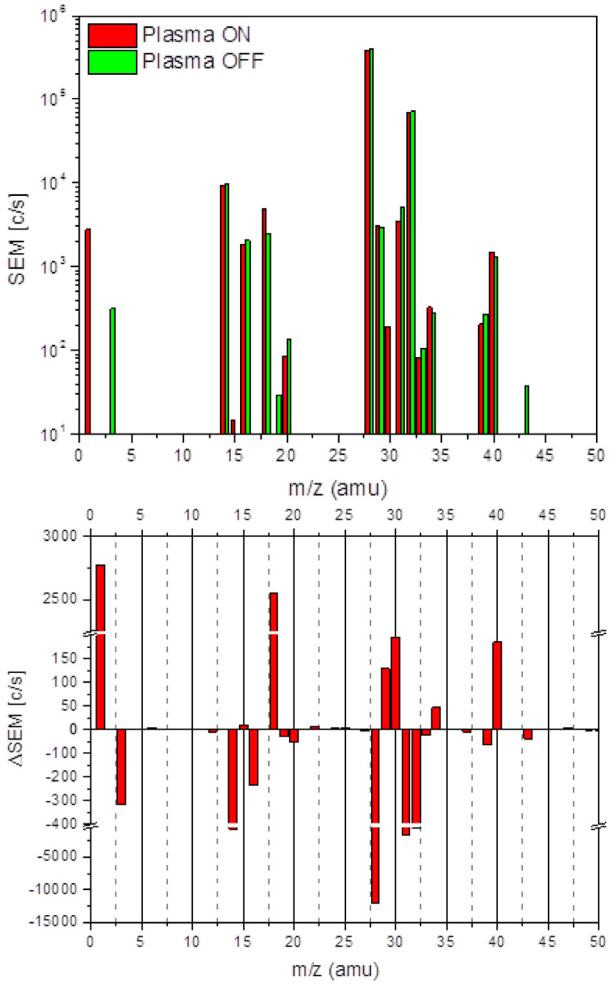

Fig. 3. The survey spectrum of working gas when the DCSBD discharge was turned on/off for the following conditions: N_2/O_2 ratio of 80/20 and working frequency of DCSBD 15 kHz (top); the corresponding difference of counts with/without plasma (bottom).

the gas directly from the plasma layer of DCSBD. The sampling of discharge atmosphere had to be realized keeping a minimum distance between the DCSBD discharge and the grounded MBMS front plate to avoid arcing to the grounded MBMS plate. Thus the post-plasma reactions of direct products of the DCSBD plasma-chemical reactions with the surrounding gas in the discharge chamber could occur also. This limits a better understanding of the reactions directly in the DCSBD plasma, but does not limit the goal of presented research, i.e., the research of the industrially important by-products of the DCSBD plasma deployment.

Although the background signal in the RGA analysis was relatively high, it can still give us an overview of the plasma influence on gas composition.

The absolute difference of MBMS signals with and without plasma is given in the lower part of Figure 3. Positive difference represents an increase of the signal of the radical after plasma ignition. We can see that the gas composition differs significantly for the N_2 and O_2 signals, as these molecules are decomposed in the plasma. The increase of NO indicates production of these radicals in the plasma.

Stoffels et al. (see [7,18]) came to the (same) conclusion that NO is produced abundantly in the plasma and N_2 is lost due to the dissociation of the molecules in plasma itself. They have done extensive investigation for the various plasma parameters by using both methods presented in Section 2.2. In experiments conducted by Stoffels and Aranda Gonzalvo plasma needle was used as the plasma source and measurements were done, like in our case, by using HIDEN HPR60 mass spectrometer. The plasma needle is a source which is known not to produce significant amount of O_3 molecules and Stoffels and co-workers did not observe signal due to this molecule. In our case DCSBD produces significant amounts of ozone and therefore we have employed the same 'time sequence' method to record it. But the ozone molecule is not the most important and especially not the only relevant molecule for bio applications of plasma discharges. Actually its presence diminishes the use of plasmas if one needs to operate it in the vicinity of humans. The advantage of adopted MBMS technique (among other techniques able to give us the information on the ozone production) is in its ability to give us the information for all the desired molecules (RONS-reactive oxygen and nitrogen species) in real time and at the same time, which was our goal. When it comes to OH radicals we cannot certainly attribute their production to the plasma reactions, based on the conducted experiments. Its creation in the plasma was confirmed by mass spectrometry or other methods (see, e.g. [7,23–26], or EPR (Electron Paramagnetic Resonance) technique [27]), but in presented experiments we have used the pure oxygen and nitrogen gasses and we did not vary, nor measure the residual humidity of the processing gas. From the observation that the OH radical mass signal does not respond to the great extent on the presence of the discharge or not we can estimate that it is likely that the OH radicals could arise from the residual moisture inside the MBMS chamber.

3.2 MID scan – high-sensitivity measurement of selected species

While the results of mass spectra presented above gave us an overall view of the main species present in the discharge chamber, the nitrogen oxides and ozone affect the industrial environment even in much smaller concentrations (below the limit of detection used in obtaining mass spectra). Thus more sensitive measurements were performed only for the selected 'important' species, i.e., N_2, O_2, N, O, NO, NO_2, N_2O and O_3[2]. In the following, two representatives were selected for discussion, the ozone (O_3) and the nitric oxide (NO).

[2] The OH radical was measured also, but the production of OH was attributed to the MBMS residual gas water impurities, because of the time-series behaviour of OH radical did not exhibit the influence on the plasma presence in the discharge chamber.

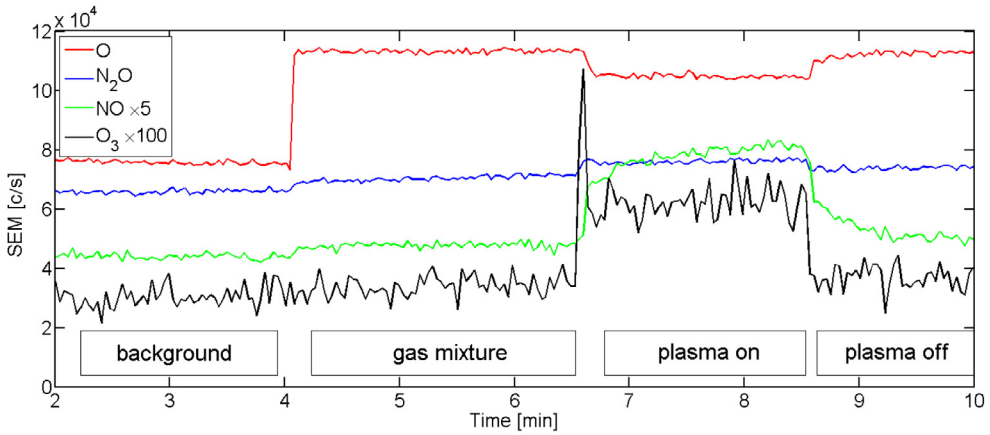

Fig. 4. The typical representative of the 'MID scan', i.e. the constant tracking of the selected species, four stages of experiment were marked using the labelled boxes. The conditions were as follows: gas mixture 80% N_2 and 20% O_2, DCSBD voltage frequency 15 kHz, ionization filament current 50 μA.

In Figure 4 a typical representative of the 'MID scan', i.e., the 'time sequence' measurement of selected species is given. The four stages of the measurement can be identified (see the boxes in Fig. 4): the residual gas traces inside MBMS (labelled 'background') and the processing gas composition (labelled 'gas mixture') and the influence of the discharge presence (labelled 'plasma on', resp. 'plasma off'). For the following calculations absolute differences of the averaged signals of the 'plasma on' and 'plasma off' stages were used. In Figure 4 at the beginning and at the end of the 'plasma' stage the inertia of the mass signal can be seen. The attribution of this behaviour to the parameters of the discharge or the whole measurement system is not clear at this moment and further analysis will be necessary.

In Figure 5 the results of the 'MID scan' data processing are given for the ozone (O_3) and nitric oxide (NO). The influence of experimental conditions is presented using absolute differences of the averaged signals of the 'plasma on' and 'plasma off' stages.

The first sub-figure (upper) shows the behaviour of ozone (O_3) production with the respect to the discharge conditions. The drop of the ozone production with the increase of discharge repetition rate (frequency) is clearly visible namely for oxygen-rich mixtures of operating gas. The same effect of the decrease of ozone production with increasing frequency was observed also in [30], but there the maximum frequency of 2 kHz was used and the decrease was not so pronounced as it was seen for studied DCSBD. The microdischarge of DBD can be treated as a small reactor, in which the plasma-chemical reactions occurs [1]. Assuming the average energy transferred per individual microdischarge of DBD partially heats-up the discharge channel [28] then the increase of the repetition rate (discharge frequency) could result in the increase of the average discharge channel temperature. Pietch and Gibalov stated in [29] that the increase of energy density is associated with the increase of processing gas temperature, to which the ozone producing chemical reactions are strongly dependent. The same temperature effect was observed

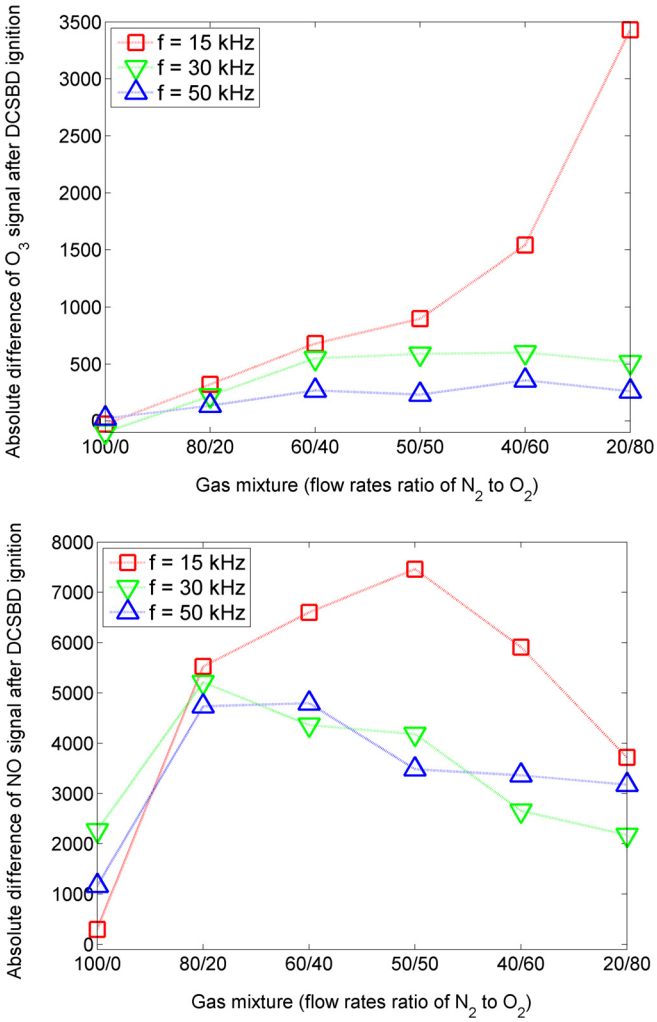

Fig. 5. The absolute difference of the MBMS signal after plasma ignition in the discharge chamber for ozone (top) and nitric oxide (bottom) as the results of 'MID scan' ('time sequence' measurement) signal analysis. For given species the dependence of their production is given with the respect to the discharge conditions shown in the figures.

also, e.g., in [31]. In [32] the decomposition of ozone was attributed rather to the repetitive exposure of the gas volume to the discharge in a microdischarge channel. The temperature and gas flow effect on ozone production studied in [33] indicated, that the ozone production must be treated as a complex interplay of the discharge condition hardly attributable to particular separated quantity. The possible mechanisms of the drop of the production of ozone in studied DCSBD discharge could therefore be attributed to the growth of energy density at higher frequencies, that leads to increase of the gas temperature through direct and/or indirect plasma-induced heating and/or to the higher plasma-exposure time at higher repetition frequency conditions, under the same gas residence time in the chamber (constant gas flow rate).

For low oxygen concentrations (labelled '100/0') only a few percent of remnant oxygen is present. For increasing amount of oxygen in the discharge chamber, the difference in ozone production due to variation in the frequency is evident. The DCSBD operated at lowest frequency, i.e., 15 kHz, produces considerably higher amount of ozone, than for 30 and 50 kHz. The behaviour of nitric oxide (NO) with the respect to the variation in frequency and gas mixture is given in the second sub-figure (lower). Production of NO has a peak depending on the abundance and with the peak position varying with the frequency. NO production is the greatest at the lowest frequency. The maximum of the production of nitric oxide for the lowest frequency is for the '50/50' gas mixture. In case of 30 kHz and 50 kHz the maximum of NO production is for the '80/20' gas mixture. For detailed analysis of RONS generation and equilibrium concentrations the full plasma-kinetic model should be assembled, which is beyond the scope of this paper.

4 Conclusion

The mass spectrometry of DCSBD discharge generated at atmospheric pressure condition was performed. The effects of working gas composition (mixtures of oxygen and nitrogen) and the high voltage frequency were studied on the production of reactive oxygen and nitrogen species (RONS), e.g., N, NO_x or O_3, as they play important role in the plasma interactions with the living organisms and tissues. The results confirmed the substantial effects of the high voltage frequency and oxygen/nitrogen flow ratio on the production of RONS. The ozone (O_3) and nitric oxide (NO) molecules production was highest at the lowest frequency of 15 kHz from the studied range of 15–50 kHz. This demonstrated that the production of these species could be suppressed or enhanced with the selection of the frequency of the input high voltage and gas mixture.

Author contribution statement

All authors contributed equally to the paper.

This research has been supported by the project CZ.1.05/2.1.00/03.0086 funded by European Regional Development Fund and project LO1411 (NPU I) funded by Ministry of Education Youth and Sports of Czech Republic (J.C., A.B., M.C.). N.S., N.P. and Z. Lj. P. are grateful for the support from MESTD, Republic of Serbia projects ON171037 and III41011.

References

1. U. Kogelschatz, Plasma Chem. Plasma Process. **23**, 1 (2003)
2. P. Bruggeman, R. Brandenburg, J. Phys. D: Appl. Phys **46**, 464001 (2013)
3. M. Šimor, J. Ráheľ, P. Vojtek, M. Černák, A. Brablec, Appl. Phys. Lett. **81**, 2716 (2002)
4. J. Čech, J. Hanusová, P. Sťahel, M. Černák, Open Chemistry **13**, 528 (2015)
5. M. Černák, D. Kováčik, J. Ráheľ, P. Sťahel, A. Zahoranová, J. Kubincová, A. Tóth, Ľ. Černáková, Plasma Phys. Control. Fusion **53**, 124031 (2011)
6. J. Čech, P. Sťahel, Z. Navrátil, Eur. Phys. J. D **54**, 259 (2009)
7. E. Stoffels, Y.A. Gonzalvo, T.D. Whitmore, D.L. Seymour, J.A. Rees, Plasma Sources Sci. Technol. **16**, 549 (2007)
8. J.D. Skalny, J. Orszagh, N.J. Mason, J.A. Rees, Y.A. Gonzalvo, T.D. Whitmore, Int. J. Mass Spectrom. **272**, 12 (2008)
9. J. Benedikt, D. Ellerweg, A. von Keudell, Rev. Sci. Instrum. **80**, 055107 (2009)
10. S. Lazović, N. Puač, G. Malović, A. Đorđević, Z. Lj. Petrović, Chem. Listy **102**, 1383 (2008)
11. G. Malović, N. Puač, S. Lazović, Z. Lj. Petrović, Plasma Sources Sci. Technol. **19**, 034014 (2010)
12. S. Lazović, N. Puač, N. Radić, T. Hoder, G. Malović, J. Ráheľ, M. Černák, Z. Lj. Petrović, Publ. Astron. Obs. Belgrade **84**, 401 (2008)
13. D. Maletić, N. Puač, S. Lazović, G. Malović, V. Schulz-von der Gathen, Z. Lj. Petrović, Plasma Phys. Contr. Fusion **54**, 124046 (2012)
14. N. Škoro, K. Spasić, N. Puač, G. Malović, Z. Lj. Petrović, in *Proceedings of 20th International Conference on Gas Discharges and their Applications*, Orléans, France (2014), p. 486
15. K. Spasić, N. Škoro, N. Puač, G. Malović, Z. Lj. Petrović, in *27th Summer School and International Symposium on the Physics of Ionized Gases (SPIG 2014)*, Belgrade, Serbia (2014), p. 439
16. D. Rapp, G.P. Englande, D.D. Briglia, J. Chem. Phys. **42**, 4081 (1965)
17. D.C. Frost, C.A. McDowell, Proc. of the Royal Society of London. Series A, Mathematical and Physical Sciences **236**, 178 (1956)
18. E. Stoffels, Y.A. Gonzalvo, T.D. Whitmore, D.L. Seymour, J.A. Rees, Plasma Sources Sci. Technol. **15**, 501 (2006)
19. T.R. Hogness, E.G. Lunn, Phys. Rev. **30**, 26 (1927)
20. N.J. Mason, W.R. Newell, J. Phys. B **22**, 2297 (1989)
21. G. Allcock, J.W. McConkye, Chem. Phys. **34**, 169 (1978)
22. J.W. McConkey, C.P. Malone, P.V. Johnson, C. Winstead, V. McKoy, I. Kanik, Phys. Rep. **466**, 1 (2008)
23. S. Yonemori, Y. Nakagawa, R. Ono, T. Oda, J. Phys. D. Appl. Phys. **45**, 225202 (2012)

24. R. Ono, T. Oda, in *33rd IAS Annual Meeting*, New York, USA (1998), Vol. 3, p. 1777
25. P. Bruggeman, D.C. Schram, Plasma Sources Sci. Technol. **19**, 045025 (2010)
26. T. Verreycken, R.M. van der Horst, A.H.F.M. Baede, E.M. Van Veldhuizen, P.J. Bruggeman, J. Phys. D: Appl. Phys. **45**, 045205 (2012)
27. N. Puač, M. Miletić, M. Mojović, A. Popović-Bijelić, D. Vuković, B. Miličić, D. Maletić, S. Lazović, G. Malović, Z. Lj. Petrović, Open Chem. **33**, 332 (2015)
28. J. Ráheĺ, Zs. Szalay, J. Čech, T. Morávek, Eur. Phys. J. D **70**, 92 (2016)
29. G.J. Pietsch, V.I. Gibalov, Pure Appl. Chem. **70**, 1169 (1998)
30. N. Mericam-Bourdet, M.J. Kirkpatrick, F. Tuvache, D Frochot, E. Odic, Eur. Phys. J.: Appl. Phys. **57**, 30801 (2012)
31. H. Kobayashi, T. Tandou, H. Nagaishi, K. Suzuki, N. Negishi, Jpn J. Appl. Phys. **51**, 8HC04 (2012)
32. S. Jodzis, in *Proceedings of Int. Symp. on High Pressure Low Temperature Plasma Chemistry HAKONE XIII*, Kazimierz Dolny, Poland (2012), p. 53
33. S. Pekárek, J. Mikeš, Eur. Phys. J. D **68**, 310 (2014)

5th Central European Symposium on Plasma Chemistry

Balatonalmádi, Hungary, 25-29 August 2013

Final scientific programme & Book of abstracts

ISBN 978-615-5270-04-8

5th Central European Symposium on Plasma Chemistry

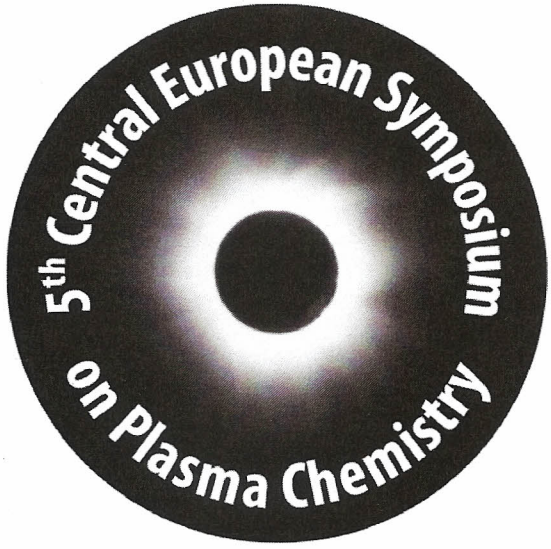

Final scientific programme
&
Book of abstracts

Balatonalmádi, Hungary, 25-29 August 2013

Published by:

Research Centre for Natural Sciences, Hungarian Academy of Sciences
H-1025 Budapest, Pusztaszeri út 59-67., HUNGARY

Wigner Research Centre for Physics, Hungarian Academy of Sciences
H-1121 Budapest, Konkoly Thege Miklós út 29-33. , HUNGARY

Diamond Congress Ltd., Conference Secretariat
H-1012 Budapest, Vérmező út 8., HUNGARY
www.diamond-congress.hu

Lectored by: Kinga Kutasi, Klára Szentmihályi, Zoltán Donkó
Edited by: Róbert Hohol, Zsuzsanna Heiszler

ISBN 978-615-5270-04-8

O-BM9
MASS SPECTROSCOPY OF AN ATMOSPHERIC PRESSURE PLASMA BULLET

N. Selaković, D. Maletić[1], N. Puač, S. Lazović, G. Malović, Z. LJ. Petrović

Institute of Physics, University of Belgrade, Belgrade, Serbia

nele@ipb.ac.rs

Wide range of potential applications of plasma sources operating at atmospheric pressure, particularly in medicine and biology, has led to a large expansion in their development. Before using a new plasma source for treatment of bio-samples it is necessary to make detailed diagnostics of the plasma and, most importantly, examine its chemical composition. We have used Hiden HPR 60 mass-energy analyzer for the time-resolved measurements of the ionic species originated from atmospheric-pressure plasma jet.

Plasma jet was made of Pyrex glass tube with two transparent electrodes (15 mm wide) made of polyester (PET) foil. The gap between the electrodes was 15 mm. This source operated at excitation frequency of 80 kHz and applied voltage was in the range of 6-10 $kV_{peak\text{-}to\text{-}peak}$. The feeding gas was helium with flow rate of 4 slm. In all experiments distance between the plasma source and HPR60 orifice was 15 mm. We also used plastic side-covers around plasma source to prevent plasma flickering due to ambient air disturbance. The applied current and voltage signal and HPR 60 internal gate signal have been synchronized. The internal gate width of HPR60 analyzer was 0.5 μs.

Mass spectrometer was operated in ion mass spectroscopy mode and we have measured positive and negative ion species coming from the plasma. The detected positive species from the plasma plume are N_2^+(36%), N^+(20%), O_2^+(18.5%), O^+(16.8%), H_2O^+(6.1%) and a few percentage of OH^+, NO^+, N_2H^+ and Ar^+ (see Fig.1). In case of negative ions we have detected O^-(34.3%), OH^-(24.2%), O_2^-(10.5%) and a few percentage of CO_2^-, NO_3^- and NO_2^-. The signal of detected ions was also tracked in time for the duration of 5 periods (5x12.5 μs) of current and voltage signal.

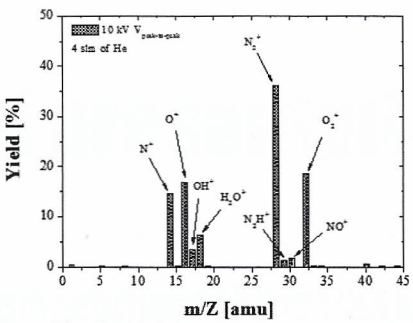

Fig. 1: Mass spectra plot of positive ions

Acknowledgements

This research has been supported by the MESTD, Serbia, under projects ON171037 and III41011.

References

1 *N. Puač, D. Maletić, S. Lazović, G. Malović, A. Đorđević and Z. Lj. Petrović, Applied Physics Letters, 101(2), (2012), 24103.*

ESCAMPIG

Viana do Castelo 2012

XXI Europhysics Conference on the

Atomic and Molecular Physics of Ionized Gases

Tuesday 10 July to
Saturday 14 July 2012

at Castelo de Santiago da Barra
Viana do Castelo, Portugal
http://escampig2012.ist.utl.pt

PROCEEDINGS

Edited by
Pedro G. C. Almeida, Luís L. Alves and Vasco Guerra

Time-resolved images of plasma bullet for different electrode geometries

D. Maletić[(*)1], N. Puač[1], N. Selaković[1], S. Lazović[1, 2], G. Malović[1], A. Đorđević[3] and Z. Lj. Petrović[1]

[1]*Institute of Physics, University of Belgrade, Pregrevica 118, 11080 Belgrade, Serbia*
[2]*Institute Jožef Stefan, Jamova cesta 39, 1000 Ljubljana, Slovenia*
[3]*Faculty of Electrical Engineering, University of Belgrade, Bulevar kralja Aleksandra 73, 11000 Belgrade, Serbia*
[(*)] dejan_maletic@ipb.ac.rs

In this paper we will present time-resolved images of atmospheric pressure plasma jet obtained by using fast ICCD camera for several electrode settings. It will be shown that formation and position of the plasma bullet strongly depends on the electrode geometry. The main purpose of our investigation was the possibility of applying plasma bullet for the treatment of thermo-sensitive samples.

A possibility to obtain the discharges of various geometries at low gas/ion temperatures and at atmospheric pressure would be a good basis for numerous applications in the industry, biology and medicine [1-5]. Here we study properties of an atmospheric pressure plasma jet (APPJ) operating with sinusoidal voltage excitation at a frequency of 80 kHz. Construction of plasma jet [6, 7] allowed easy ICCD camera capturing of the time-resolved images of the discharge between and inside the electrodes, as well as, of the plasma bullet that is formed outside the tube/electrode system. Experimental setup is given in Fig. 1. We will use the common term "plasma bullet" for visible manifestations of plasma because these ionization fronts create appearance of a motion of a bullet even though plasma itself may have a very different motion.

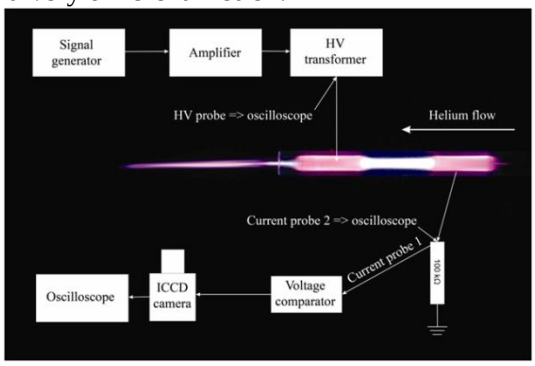

Fig. 1. Experimental setup

The body of a plasma jet was made of Pyrex glass tube 6 mm outer diameter and 4 mm inner diameter. The length of the coated PET electrodes was 15 mm and the distance between them was 15 mm. The distance between the electrodes was kept constant during all measurements. The right electrode was grounded and the other electrode, closer to the end of the glass tube, was the powered one (see Fig. 1.). The calculated mean power transmitted to the plasma was 4 W and the flow rate of the feeding gas (He) was 4 slm. The distance between the powered electrode and the end of the glass tube was varied and ICCD images were taken for distances of 7, 10, 30 and 50 mm. Voltage – current signals are shown in Fig. 2. with trigger position of 11.2 μs.

In order to obtain the time-resolved images we have used integration on the chip because the light emission in a single shot is not always sufficient to obtain clear images with gate widths of less than 25 ns. In Fig. 3. (A, B, C and D) we can see time-resolved image of plasma jet obtained by ICCD camera for 4 different electrode distances to the end of the tube while the rest of the geometry is unchanged. All images were obtained for the same parameters of electrical circuit and ICCD camera settings. It is shown that, when the distances of electrodes to the edge of the tube are shorter, the

plasma bullet is formed (see Fig. 3. – A, B and C). At the same time there is no visible discharge in the powered electrode.

When plasma is moving through the tube, including both electrodes, it is at a much lower speed then the speed of the bullet. With an increase of the distance of the electrodes from the edge of the tube plasma bullet is formed but with lower emission intensity (Fig. 3. – C). For the longest distance bullet is not emerging from the plasma jet body throughout the whole cycle period of 12.5 μs. (Fig. 3. – D) and it simply dissipates.

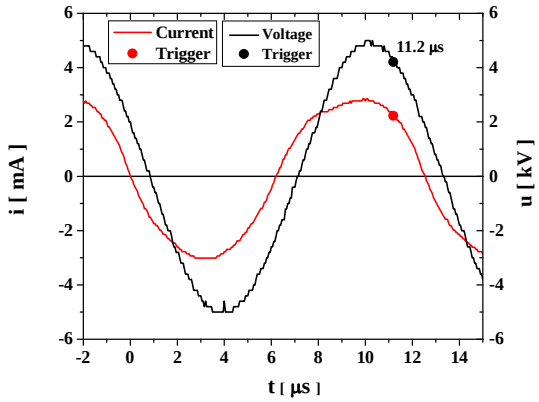

Fig. 2. Current – Voltage signals with 11.2 μs trigger position

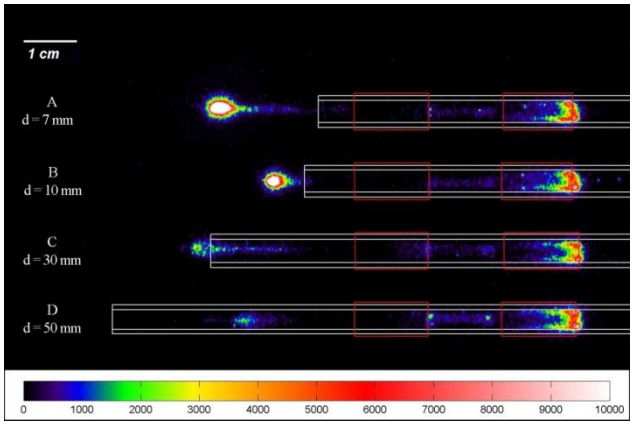

Fig. 3. Time resolved ICCD images for different geometry, delay of 11.2 μs, helium flow rate of 4 slm and average applied power of 4 W. Color bar represents intensities of emission.

This research has been supported by the Ministry of Education and Science Serbia, project III41011 and ON171037.

References

[1] G. Fridman, G. Friedman, A. Gutsol, A. B. Shekhter, V. N. Vasiletsm and A. Fridman, *Plasma Process. Polym.* 5 (2008) 503–533.
[2] M. Laroussi, *IEEE T. Plasma Sci*. 37-6 (2009) 714-725.
[3] E. Robert, E. Barbosa, S. Dozias, M. Vandamme, C. Cachoncinlle, R. Viladrosa, J. M. Pouvesle, *Plasma Process. Polym.* 6 (2009) 795–802.
[4] N. Puač, Z.Lj. Petrović, G. Malović, A. Đorđević, S. Živković, Z. Giba and D. Grubišić, *J. Phys. D Appl. Phys.* 39 (2006) 3514-3519.
[5] S. Lazović, N. Puač, M. Miletić, D. Pavlica, M. Jovanović, D. Bugarski, S. Mojsilović, D. Maletić, G. Malović, P. Milenković and Z. Petrović, *New J. Phys* 12 (2010) 083037.
[6] M. Kong, J. Walsh., *IEEE T. Plasma Sci. 36-4* (2008) 954-955.
[7] J. Shi, F. Zhong, J. Zhang, D. W. Liu and M. G. Kong, *Phys. Plasmas* 15 (2008) 013504.

BULLETIN
OF THE AMERICAN PHYSICAL SOCIETY

67th Annual Gaseous Electronics Conference

November 2-7, 2014
Raleigh, North Carolina

Volume 59, Number 9

APS physics

BULLETIN
OF THE AMERICAN PHYSICAL SOCIETY

Coden BAPSA6 ISSN: 0003-0503
Series II, Vol. 59, No. 16 October 2014
Copyright © 2014 by the American Physical Society

APS COUNCIL 2014

President
Malcolm R. Beasley*, *Stanford University*

President-Elect
Samuel H. Aronson*, *Brookhaven National Laboratory (Retired)*

Vice President
Homer A. Neil*, *University of Michigan*

Executive Officer
Kate P. Kirby*, *Harvard Smithsonian (Retired)*

Treasurer/Publisher
Joseph W. Serene*, *Georgetown University (Emeritus)*

Editor-in-Chief
Gene D. Sprouse*, *Stony Brook University (On Leave)*

Past-President
Michael S. Turner*, *University of Chicago*

General Councillors
Haiyan Gao*, Marcelo Gleiser, Nadya Mason, Pierre Meystre*, Keivan G. Stassun

Division, Forum and Section Councillors
Miriam Forman (*Astrophysics*), Thomas Gallagher (*Atomic, Molecular & Optical Physics*), Jose Onuchic (*Biological*), Amy Mullin (*Chemical*), Frances Hellman* (*Condensed Matter Physics*), Steven Gottlieb (*Computational*), James Wallace (*Fluid Dynamics*), Gay Stewart* (*Forum on Education*), Eric Sorte, (*Forum on Graduate Student Affairs*), Dan Kleppner (*Forum on History of Physics*), Gregory Meisner* (*Forum on Industrial & Applied Physics*) Gong-Kee Kim (*Forum on International Physics*), Lowell Brown (*Forum on Physics & Society*) Anthony Johnson* (*Laser Science*), James Chelikowsky (*Materials*), David McIntyre (*Northwest Section*), Wick Haxton* (*Nuclear*), Philip Michael Tuts (*Particles & Fields*), TBD (*Physics of Beams*), Vincent Chan* (*Plasma*), Mark Ediger (*Polymer Physics*), Nan Phiney (*California Section*)

**Members of the APS Executive Board*

Scientific Program Coordinator:
Don Mewha

APS MEETINGS DEPARTMENT
One Physics Ellipse
College Park, MD 20740-3844
Telephone: (301) 209-3286
Fax: (301) 209-0866
Email: meetings@aps.org
Terri Gaier, *Director of Meetings & Conventions*
Christine Lenihan, *Meeting Planner*
Ebony Montgomery, *Meetings Assistant*
Vinaya Sathyasheelappa, *Senior Meeting Planner*
Don Wise, *Senior Registrar*

International Councillors
Macia Barbosa
Annick Suzor-Weiner*
Kiyoshi Ueda

Chair, Nominating Committee
Paul L. McEven

Chair, Panel on Public Affairs
Robert Jaffe

ADVISORS
Representatives from other Societies
Fred Dylla, *AIP*; Gay Stewart, *AAPT*

International Advisor
Robert Fedosejevsk, Canadian Association of Physicists

Staff Representatives
Tracy Alinger, *Director of Information Technology (College Park)*, Mark Doyle, *Director of Journal Information Systems*, Amy Flatten, *Director of International Affairs*, Terri Gaier, *Director of Meetings*; Barbara Hicks, *Associate Publisher*, Ted Hodapp, *Director of Education and Diversity*; Trish Lettieri, *Director of Membership*; Darlene Logan, *Director of Development*; Michael Lubell, *Director of Public Affairs*; Dan Kulp, *Editorial Director*; Christine Giaccone, *Director of Journal Operations*; Michael Stephens, *Controller and Assistant Treasurer*

Administrator for Governing Committees
Ken Cole

Please Note: APS has made every effort to provide accurate and complete information in this *Bulletin*. However, changes or corrections may occasionally be necessary and may be made without notice after the date of publication. To ensure that you receive the most up-to-date information, please check the meeting Corrigenda distributed with this *Bulletin* or the "Program Changes" board located near Registration.

various properties of negative planar fronts. We discuss the practical and theoretical aspects of applicability of each fluid model.

[1]Dujko *et al.*, J. Phys. D **46**, 5202 (2013).

11:45

DT2 8 Investigating the guiding of streamers in nitrogen/oxygen mixtures with 3D simulations* JANNIS TEUNISSEN, *Centrum Wiskunde & Informatica, The Netherlands* SANDER NIJDAM, *Eindhoven University of Technology, The Netherlands* EIICHI TAKAHASHI, *National Institute of Advanced Industrial Science and Technology, Japan* UTE EBERT, *Centrum Wiskunde & Informatica and Eindhoven University of Technology, The Netherlands*

Recent experiments by S. Nijdam and E. Takahashi have demonstrated that streamers can be guided by weak pre-ionization in nitrogen/oxygen mixtures, as long as there is not too much oxygen (less than 1%). The pre-ionization was created by a laser beam, and was orders of magnitude lower than the density in a streamer channel. Here, we will study the guiding of streamers with 3D numerical simulations. First, we present simulations that can be compared with the experiments and confirm that the laser pre-ionization does not introduce space charge effects by itself. Then we investigate topics as: the conditions under which guiding can occur; how photoionization reduces the guiding at higher oxygen concentrations and whether guided streamers keep their propagation direction outside the pre-ionization.

*JT was supported by STW Project 10755, SN by the FY2012 Researcher Exchange Program between JSPS and NWO, and ET by JSPS KAKENHI Grant Number 24560249.

SESSION DT3: EFFECTS OF PLASMAS ON BIOLOGICAL CELLS

Tuesday Morning, 4 November 2014; Room: State D at 10:00; Mounir Laroussi, Old Dominion University, presiding

Invited Papers

10:00

DT3 1 Application of atmospheric plasma sources in growth and differentiation of plant and mammalian stem cells* NEVENA PUAC, *Institute of Physics, University of Belgrade*

The expansion of the plasma medicine and its demand for in-vivo treatments resulted in fast development of various plasma devices that operate at atmospheric pressure. These sources have to fulfill all demands for application on biological samples. One of the sources that meet all the requirements needed for treatment of biological material is plasma needle. Previously, we have used this device for sterilization of planctonic samples of bacteria, MRSA biofilm, for improved differentiation of human periodontal stem cells into osteogenic line and for treatment of plant meristematic cells. It is well known that plasma generates reactive oxygen species (ROS) and reactive nitrogen species (RNS) that strongly affect metabolism of living cells. One of the open issues is to correlate external plasma products (electrons, ions, RNS, ROS, photons, strong fields etc.) with the immediate internal response which triggers or induces effects in the living cell. For that purpose we have studied the kinetics of enzymes which are typical indicators of the identity of reactive species from the plasma created environment that can trigger signal transduction in the cell and ensue cell activity. In collaboration with Suzana Zivkovicm, Institute for Biological Research "Sinisa Stankovic," University of Belgrade; Nenad Selakovic, Institute of Physics, University of Belgrade; Milica Milutinovic, Jelena Boljevic, Institute for Biological Research "Sinisa Stankovic," University of Belgrade; and Gordana Malovic, Zoran Lj. Petrovic, Institute of Physics, University of Belgrade.

*Grants III41011, ON171037 and ON173024, MESTD, Serbia.

10:30

DT3 2 Minimally-Invasive Gene Transfection by Chemical and Physical Interaction of Atmospheric Pressure Plasma Flow* TOSHIRO KANEKO, *Department of Electronic Engineering, Tohoku University*

Non-equilibrium atmospheric pressure plasma irradiated to the living-cell is investigated for medical applications such as gene transfection, which is expected to play an important role in molecular biology, gene therapy, and creation of induced pluripotent stem (iPS) cells. However, the conventional gene transfection using the plasma has some problems that the cell viability is low and the genes cannot be transferred into some specific lipid cells, which is attributed to the unknown mechanism of the gene transfection using the plasma. Therefore, the time-controlled atmospheric pressure plasma flow is generated and irradiated to the living-cell suspended solution for clarifying the transfection mechanism toward developing highly-efficient and minimally- invasive gene transfection system. In this experiment, fluorescent dye YOYO-1 is used as the simulated gene and LIVE/DEAD Stain is simultaneously used for cell viability assay. By the fluorescence image, the transfection efficiency is calculated as the ratio of the number of transferred and surviving cells to total cell count. It is clarified that the transfection efficiency is significantly increased by the short-time (<4 sec) and short-distance (<40 mm) plasma irradiation, and the high transfection efficiency of 53% is realized together with the high cell viability (>90%). This result indicates that the physical effects such as the electric field caused by the charged particles arriving at the surface of the cell membrane, and chemical effects associated with plasma-activated products in solution act synergistically to enhance the cell-membrane transport with low-damage.

*This work was supported by JSPS KAKENHI Grant Number 24108004.

ICPIG 2017

XXXIII INTERNATIONAL CONFERENCE ON PHENOMENA IN IONIZED GASES

CONFERENCE PROCEEDINGS

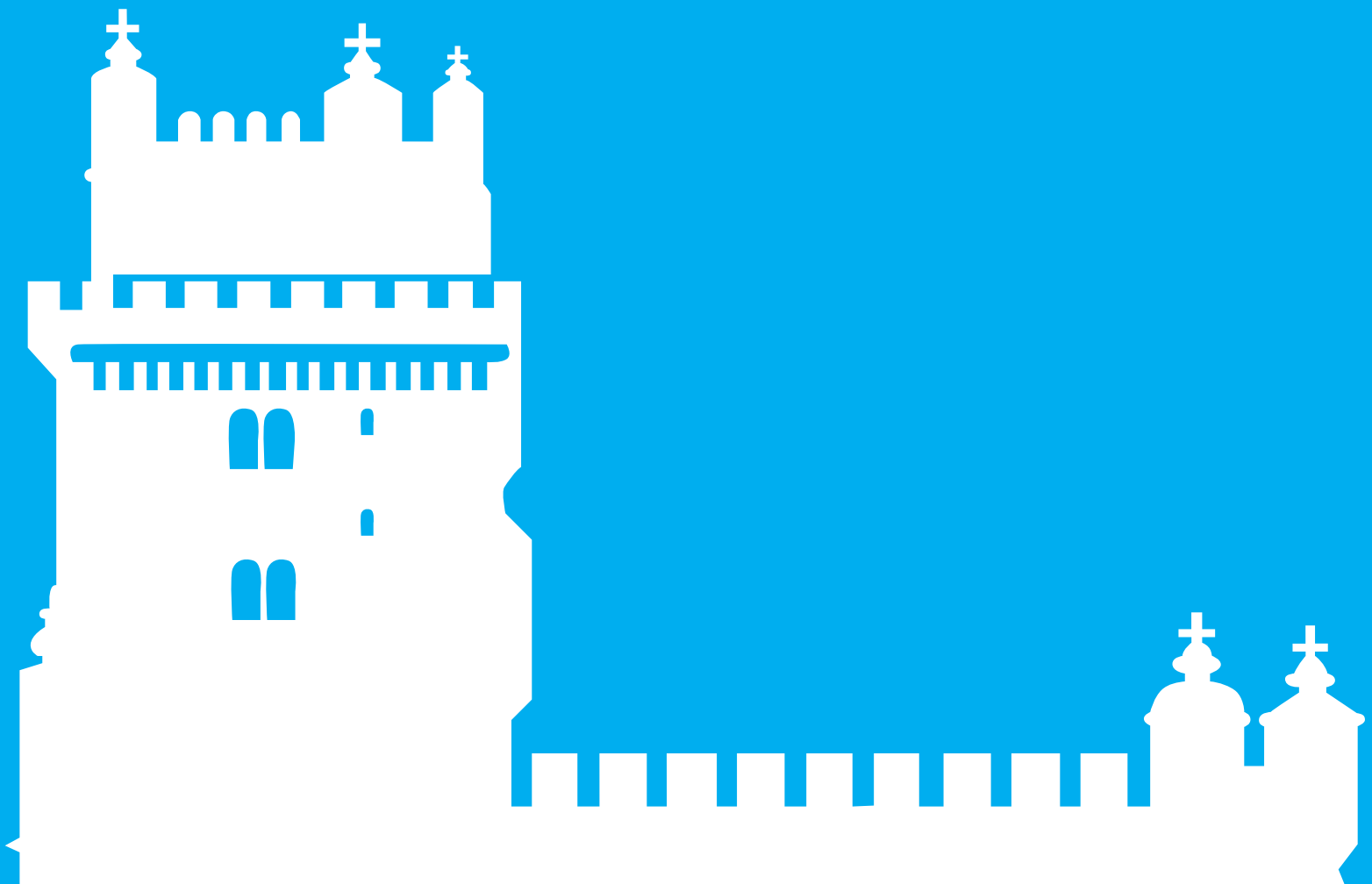

Influence of humidity on formation of pulsed atmospheric pressure plasma streamers

N. Selaković[1], J. Voráč[2], N. Puač[1], G. Malović[1], P. Dvořák[2] and Z. Lj. Petrović[1,3]

[1] *Institute of Physics, University of Belgrade, Pregrevica 118, 11080 Belgrade, Serbia*
[2] *Department of Physical Electronics, Faculty of Science, Masaryk University, Kotlářská 2, Brno 611 37, Czech Republic*
[3] *Serbian Academy of Sciences, Knez Mihailova 35, 11000 Belgrade, Serbia*

Atmospheric pressure plasma jet (APPJ) falls into one of the most promising non-equilibrium low temperature plasma sources which are convenient for multiple applications. In order to achieve the best possible results in applications and explain the mechanisms that lead to the modification of the samples it is necessary to perform a detailed diagnostics of plasma source. Many studies showed that the low-frequency plasma jet's plume is made of fast pulsed atmospheric pressure plasma streamers (PAPS). In this study we show that the change in the concentration of water vapour within the tube, where the feeding gas flows, significantly affect the formation of PAPS.

1. Introduction

The expansion of low temperature atmospheric pressure plasma sources used in the treatment of heat-sensitive samples carries step forward in future bio technologies, methods of healing, etc. These kind of plasmas are particularly suitable for treatment of the samples that do not tolerate vacuum and, more importantly, they produce a huge number of reactive chemical species in its composition.

We have designed and performed detailed diagnostics of atmospheric pressure plasma jet sources with several types of electrode geometries [1]. It is shown that the formation and propagation of PAPS is influenced by electrode geometry, but also by the presence of the water vapour in the helium flow. The propagation of PAPS as a function of humidity of working gas was observed by using an ICCD camera.

2. Experimental set-up

In this experiment we used APPJ [2] that operates at 80 kHz and at 6.5 kV of applied voltage. We have used transparent PET foils coated with indium tin oxide as the powered and the grounded electrode (15 mm wide). The electrodes were wrapped around the Pyrex glass tube (O.D. 6 mm and I.D. 4 mm). As a feeding gas we have used 4 slm of helium and mixture of helium and water vapour. To perform humidity measurements within the flow tube we set up Vaisala DMT143 dewpoint transmitter in front of the glass tube. For PAPS evolution we set up the ICCD camera that recorded the discharge axially along the glass tube and the plume.

3. Results

During the active discharge (water vapour not added in mixture) we noticed that the humidity measured in the helium flow is decreasing and the concentration of H_2O molecules changes from 400 to 25 ppm**.** Around 100 ppm of H_2O we observe shorter range of PAPS. At the concentration of 30 ppm PAPS starts to lose its original shape and it becomes increasingly blurred. At concentration of about 20 ppm, the PAPS appear blurred. On the contrary, a high concentration of water molecules (above 1000 ppm obtained with mixture of helium and water vapour) creates a saturated environment in which discharge starts to be quenched.

This research has been supported by the MESTD Serbia, project III41011 and ON171037 and project LO1411 (NPU I) funded by the Ministry of Education Youth and Sports of the Czech Republic

3. References

[1] N. Puač, D. Maletić, S. Lazović, G. Malović, A. Đorđević and Z. Lj. Petrović Appl Phys Lett. 101 (2012) 24103 (2).

[2] D. Maletić, N. Puač, N. Selaković, S. Lazović, G. Malović, A. Đorđević and Z. Lj. Petrović Plasma Sources Sci. Technol. 24 (2015) 025006 (9pp).

69TH IUVSTA WORKSHOP ON OXIDATION OF ORGANIC MATERIALS BY EXCITED RADICALS CREATED IN NON-EQUILIBRIUM GASEOUS PLASMA

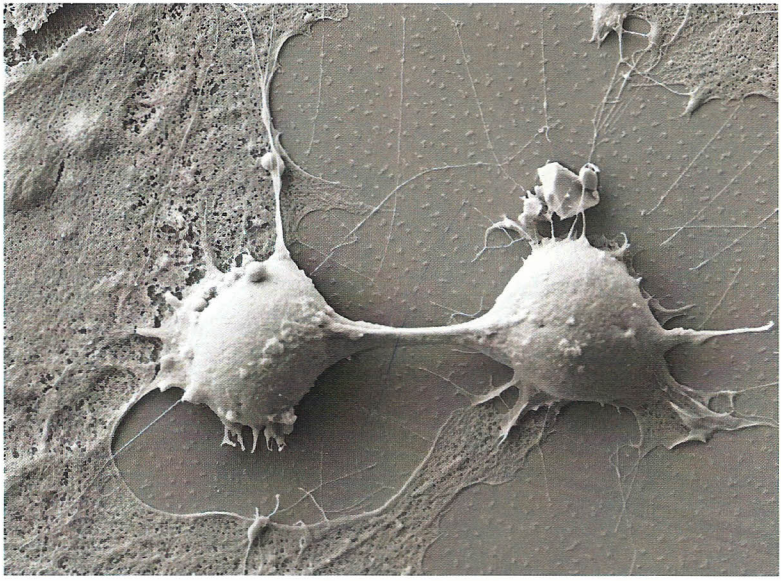

Book of abstracts

69TH IUVSTA WORKSHOP ON OXIDATION OF ORGANIC MATERIALS BY EXCITED RADICALS CREATED IN NON-EQUILIBRIUM GASEOUS PLASMA

ABSTRACTS

December 9th — December 13th 2011, Crklje na Gorenjeskem, Slovenia

© DVTS 2012 All rights reserved.

All rights reserved. No part of this publication may be reproduced, stored in a retrieval system or transmited in any form or by any means, electronic, mechanical, photocopying, recording or otherwise, without the prior permission of the publisher.
No responsibility is assumed by publisher for any injury and/or damage to persons or property as a matter of products liability, negligence or otherwise, or from any use or operation of any method, products, instructions or ideas contained in the material herein.

Editors of Proceedings: Miran Mozetič and Uroš Cvelbar

Published by: Slovenian Society for Vacuum Technique (DVTS Društvo za vakuumsko tehniko Slovenije), Teslova 30, SI-1000 Ljubljana, Slovenia

Conference Chair:

Miran Mozetič (Slovenia)

Program Committee :

Miran Mozetič, Slovenia (Program chair)
Giorgos Evangelakis, Greece (Program vice chair)
Igor Levchenko, Australia
Primoz Eiselt, Austria
Xiaoxia Zhong, PR China
Masaharu Shiratani, Japan
Mohan R. Sankaran, USA
Mahendra K. Sunkara, USA
Francisco Tabares, Spain
Slobodan Milosevic, Croatia
JJ Shi, PR China
Petr Slobodian, Czech Republic
Shuyan Xu, Singapore

Organizing Committee:

Uroš Cvelbar, Slovenia (Organizing chair)
Ita Junkar , Slovenia (Secretary)
Kristina Eleršič, Slovenia
Saša Lazović, Slovenia
Gregor Filipič, Slovenia
Martina Modic, Slovenia
Gregor Primc, Slovenia
Aleksander Drenik, Slovenia

Organizer:

Društvo za vakuumsko tehniko slovenije (DVTS) - Slovenian Society for Vacuum Technique, Teslova 30, SI-1000 Ljubljana, Slovenia

Sponsors:

International Union for Vacuum Science, Technique and Applications (IUVSTA)
Slovenian Research Agency (ARRS)
Jožef Stefan Institute, Ljubljana, Slovenia
Plasmait

Properties and bio-medical applications of non-thermal plasma

S. Lazović[1,2], N. Puač[1], S. Živković[3], S. Jevremović[3], D. Maletić[1], N. Selaković[1], G. Malović[1], J. Kovač[2], T. Filipič[2], M. Mozetič[2], U. Cvelbar[2] and Z. Lj. Petrović[1]

[1]Institute of Physics, University of Belgrade, Pregrevica 118, Belgrade, Serbia [2]Jožef Stefan Institute, Jamova cesta 39, 1000 Ljubljana, Slovenia [3]Institute for Biological Research 'Siniša Stanković', Bulevar despota Stefana 142, 11060 Belgrade, Serbia

lazovic@ipb.ac.rs

Understanding of the complex mechanisms of interaction between the plasma reactive species and cells is among the major tasks in plasma medicine [1, 2]. Results show that treatment with atmospheric plasma can either improve the growth and development of cells and in some cases induces cells death [3, 4]. In order to investigate this phenomenon, we have used plant callus cells as a model of eukaryotic cells, due to their distinctive features and simplicity in handling. After the plasma treatment with different combination of discharge parameters which yield different plasma parameters (densities of charged species and neutrals, electron energies, UV radiation intensity), we have performed surface analyses (XPS) in order to determine plasma effects on the surface. Consequently we have monitored growth and viability of the callus cells (fresh weight increase, MTT test, fluorescent vital staining techniques).

Plasma treatment of plant tissue is demonstrated on fresh plant calli of Iris germanica var. "HP" (fam. Iridaceae), about 3 mm diameter in size. Calli were grown on Murashige and Skoog (MS) solid medium [5], containing 30 gl-1 sucrose, 7 gl-1 agar, 0.1 gl-1 myo-inositol, 0.1 mgl-1 2.4-dichlorophenoxyacetic acid (2.4-D), 0.1 mgl-1 1-naphthaleneacetic acid NAA, 1 mgl-1 kinetin, 0.25 gl-1 proline and 0.25 gl-1 casein. Callus is a distinctively organized mass of proliferating cells, with specific morphology and anatomy, and may be obtained from almost any type of plant. According to the explants origin (and type of medium) compact or friable calli may be formed [6].

Plasma needle setup used in our previous research [7] was used to treat calli cells. Temperature was monitored not to exceed 40°C and it was found that there is no influence of the helium gas flow and plasma generated UV light (through the quartz window).

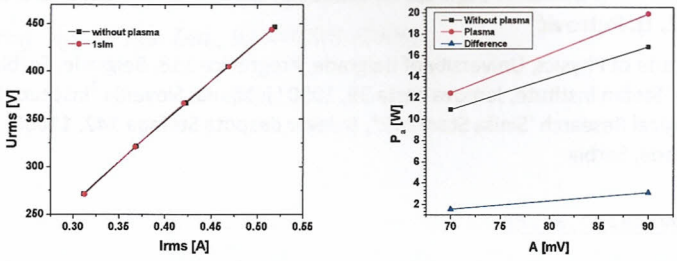

Fig.2. a) V_{rms} as the function of I_{rms}; b) Average power delivered to the plasma (blue line).

Voltage-current characteristics show that the discharge is operating in alpha regime. Derivative probes were used to determine the power delivered to the plasma (see Fig.2. b) blue line). Low powers were used in order to avoid the sample overheating to more than 40°C. It was also found that there is no influence of the helium gas flow and plasma generated UV light.

After the plasma treatment, calli were stained or transferred to fresh half strength MS solid medium (½ of MS salts and vitamins) medium without growth regulators, in order to determine the plasma influence on the fresh weight of the calli. Fresh weight increase of the samples was measured every 7 days during six weeks. Evans blue stain was used for determination of cell death. Calli were transferred to a 2 ml plastic Eppendorf tube and submerged in 0.5 ml of 0.25% Evans blue for 20 min. This led to nonpermeating or exclusion dye leak through ruptured membranes and stained the content of the death cells. Calli were drained and rinsed by distilled water until no further dye eluted from the cells. Untreated plants and calli treated by absolute ethyl alcohol for 6 h represented control and negative control, respectively. Stained calli were observed using light microscopy. Staining of the plant material were repeated six weeks after the plasma treatment using the same protocol. Calli were grown under 16 h day/8 h night photoperiod, light intensity 50 (mol m−2 s−1, and

temperature 25 ± 1 °C. Each treatment was performed in 3 replicates and each experiment was replicated twice.

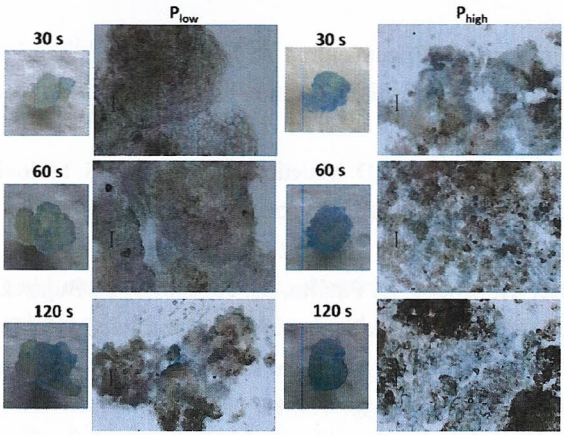

Figure 2. Plasma treatment of iris calli. Samples were stained with 0.25% Evans blue solution for 20 minutes, washed and observed using light microscopy. (Bar = 100 μm).

Parameters such as the power delivered to the plasma, temperature, distance, gas flow rate were measured and optimized so that the treatment of calli of Iris germanica var. "HP" induced minimal injury of the surface plant cells layer, and calli continued their growth. Plasma needle treatment causes enhancement of the fresh weight of the iris calli. Moreover, values of the measured parameter significantly increased with the longer exposure times compared with the untreated samples. Increase of the fresh weight is an implication of calli growth accomplished by a combination of cell division and enlargement. Plasma treatment triggered the enhanced growth of the calli, probably influencing the cell division processes. The cells that divide repeatedly remains essentially meristematic (undifferentiated). These cells are small and oval, forming specific meristematic zones or centers. These zones were not observed in control samples. Furthermore, the XPS results show the increase of O/C ratio which is a sign of surface oxidation of calluses.

Reference

[1] M. G. Kong, G. Kroesen, G. Morfill, T. Nosenko, T. Shimizu, J. van Dijk and J. L. Zimmermann 2009 "Plasma medicine: an introductory review", New J. Phys. Vol. 11, 115012.

[2] D. Dobrynin, G. Fridman, G. Friedman and A. Fridman 2009 "Physical and biological mechanisms of direct plasma interaction with living tissue", New J. Phys. Vol. 11, 115020.

[3] Z. L. Petrović, N. Puač, S. Lazović, D. Maletić, K. Spasić and G. Malović 2012 "Biomedical applications and diagnostics of atmospheric pressure plasma", Journal of Physics: Conference Series Vol. 356, 012001.

[4] S. Lazović, N. Puač, M. Miletić, D. Pavlica, M. Jovanović, D. Bugarski, S. Mojsilović, D. Maletić, G. Malović, P. Milenković and Z. Petrović 2010 "The effect of a plasma needle on bacteria in planktonic samples and on peripheral blood mesenchymal stem cells", New J. Phys. Vol. 12, 083037.

[5] T. S. Murasnige, Folke 1962 "A Revised Medium for Rapid Growth and Bio Agsays with Tohaoco Tissue Cultures", Vol. 15, 473.

[6] K. R. a. Ć. L. Nešković M 2003 Plant Physiology (NNK International) Vol. 387.

[7] N. Puač, Z. L. Petrović, G. Malović, A. Dordević, S. Živković, Z. Giba and D. Grubišić 2006 "Measurements of voltage–current characteristics of a plasma needle and its effect on plant cells", J. Phys. D: Appl. Phys. Vol. 39, 3514-9.

23rd Europhysics Conference on Atomic and Molecular Physics of Ionized Gases

Proceedings

July 12-16, 2016 Bratislava, Slovakia

Proceedings of the 23rd Europhysics Conference on the Atomic and Molecular Physics of Ionized Gases, Bratislava, Slovakia, 12-16 July 2016.

Symposium organised by Department of Experimental Physics, Faculty of Mathematics, Physics and Informatics, Comenius University in Bratislava; Society for Plasma Research and Applications in cooperation with European Physical Society and with support of the Ministry of Education, Science, Research and Sport of the Slovak Republic in hotel Saffron, Bratislava Slovakia, 12-16 July 2016.

All contributions were reviewed by members of the International Scientific Committee.

The XXIII ESCAMPIG (Europhysics Conference on the Atomic and Molecular Physics of Ionized Gases) has been approved by the European Physical Society (EPS). Permission to make digital or hard copies of portions of this work for personal or classroom use is granted without fee provided that copies are not made or distributed for profit or commercial advantage. Abstracting is permitted with credit to the source.

Volume Editors:	V. Medvecká, P. Papp, J. Országh, Š. Matejčík
Publisher:	European Physical Society
Series Editor:	Prof. D. Vernhet, Paris, France
Managing Editor:	P. Helfenstein, Mulhouse
Issued:	July 2016, Bratislava, first issue

EPS ECA (Europhysics Conference Abstracts) vol. 40D

Number of pages: 415

URL: https://www.escampig2016.org

ISBN: 979-10-96389-02-5

Modification of the dentin surface of human teeth by atmospheric pressure plasma needle

Nenad Selaković(*)[1], Jovana Stašić[2], Nevena Puač[1], Maja Miletić[2], Vesna Miletić[2], Gordana Malović[1] and Zoran Lj. Petrović[1,3]

[1] *Institute of physics, University of Belgrade, Pregrevica 118, 11080 Belgrade, Serbia*
[2] *School of Dental Medicine, University of Belgrade, Rankeova 4, 11000 Belgrade, Serbia*
[3] *Serbian Academy of Sciences, Knez Mihailova 35, 11000 Belgrade, Serbia*
(*) nele@ipb.ac.rs

In this study we have performed surface modification of dentin in extracted human teeth by a non-thermal atmospheric pressure plasma treatment. The plasma device that was used in the experiments was plasma needle. The treatments were performed for different powers transmitted to the plasma and at different plasma-to-sample distances. The results show that plasma treatments lead to significant reduction of the contact angle and increase in the surface energy. The focus of this modification was the improvement of surface properties relevant for tooth tissue interaction with dental adhesives.

Plasma needle is one of the most promising low temperature atmospheric pressure plasma sources with a broad spectrum of possible applications in material science, medicine and biology [1-3]. In the experiments presented here we have used plasma needle device to treat the exposed dentin surface of human teeth. The body of the plasma needle is made of Teflon. Inside the body there is a Pyrex glass tube which encompasses a ceramic tube. The central electrode passes through the ceramic tube and exits 1 mm outside of the tube. Helium flows between the glass and ceramic tube with the flow of 1 slm, which was held constant during the entire experiment. The plasma discharge was obtained with sine wave excitation signal at a frequency of 13.56 MHz. The discharge appears as a weak glow with a diameter of 1-3 mm at the tip of the central electrode depending on the distance from the target.

Dentin samples used in the experiment were 1 mm thick discs, cut midcoronally from the crowns of non-carious third molars. Prior to the treatment each sample was stored in distilled water. Immediately before exposing to the discharge they were blot-dried to prevent the contact of plasma with any remaining water on the sample surface.

During the treatments the distance between the plasma needle tip and the surface of the sample was maintained constant at 2 mm, 5 mm or 8 mm, respectively. The power of plasma delivered to the dentin surface was 1 W and 3 W for all distances. The exposure time in case of each treated sample was 30 s. As a control we used untreated samples prepared in the same manner as the treated.

We used DSLR Nikon D7100 with Nikkor Micro 105mm f/2.8D lenses and Nikon Auto extension ring PN-11 in order to obtain images of liquid drops profiles on the dentin surface. These images were used in order to determine contact angles. We used distilled water, ethylene glycol and diiodomethane as the reference liquids.

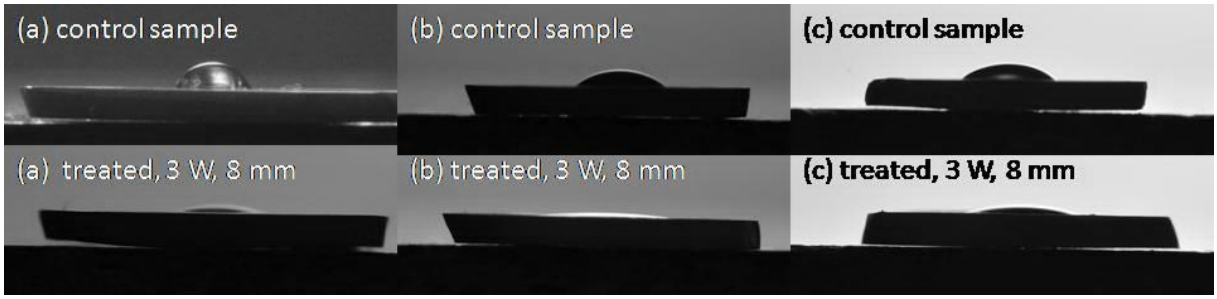

Fig. 1: Images for the contact angle for the three reference liquids: (a) distilled water, (b) ethylene glycol and (c) diiodomethane

In the Fig. 1, we can see the profile of liquid drops that were placed on the untreated and treated (8 mm, 3 W) dentin surface. One can see that after the plasma needle treatment of dentin the contact angle decreased (compare upper and lower part of Fig 1.) and at the same time surface energy drastically increased. Obviously, plasma needle treatment causes physico-chemical changes in the micromechanical structure of dentin. These changes lead to an increase of the surface energy with a potential to allow better interaction between dentin and adhesive systems used in restorative dentistry.

This research has been supported by the Ministry of Education, Science and Technological Development Serbia, project III41011 and ON171037.

References

[1] R. E. J. Sladek, T. A. Baede, E. Stoffels. *IEEE Transactions on Plasma Science 34*(4) (2006) 1325–1330.

[2] M. Miletić, S. Mojsilović, I. Okić Đorđević, D. Maletić, N. Puač, S. Lazović, D. Bugarski, G. Malović, D. Milenković and Z. Lj. Petrović, *Journal of Physics D: Applied Physics 46*(34) (2013) 345401.

[3] N. Puač, S. Živković, N. Selaković, M. Milutinović, J. Boljević, G. Malović and Z. Lj. Petrović, *Applied Physics Letters 104*(21) (2014) 214106.

ICOPS 2015
Abstract Book

The 42nd IEEE
International
Conference
On Plasma Science
24-28 May 2015
Belek, Antalya, Turkey

MASS SPECTROSCOPY AND ICCD ANALYSIS OF COUPLED AND UNCOUPLED MODE IN A GATLING-GUN LIKE PLASMA SOURCE

Augusto Stancampiano, Matteo Gherardi, Vittorio Colombo
Alma Mater Studiorum – Università di Bologna, viale Risorgimento 2, 40136, Bologna, Italy

Nenad Selaković, Nevena Puač, Zoran Lj. Petrović
Institute of Physics Belgrade, University of Belgrade, Pregrevica 118, 11080 Belgrade, Serbia

A novel type of plasma source, composed of an array of seven plasma jets arranged adjacent to one another similar in shape to a Gatling machine gun, has been recently developed to take advantage of the jet-to-jet coupling phenomenon and generate atmospheric pressure cold plasmas with higher intensity and energy with respect to singular plasma jets[1]. This source can be operated either in "uncoupled" mode, where seven plasma jets are independently produced, or in the "coupled" mode, where plasma jets merge in a single combined very intense jet. Previous experiments demonstrated a higher antibacterial potential and surface activation efficacy of this source when operated in the coupled mode than in uncoupled one[2].

In the present study, the coupling phenomenon occurring in a *Gatling* plasma source driven by high voltage sinusoidal waveforms (80 KHz, up to 6.3 $kV_{peak-peak}$) was investigated using mass spectrometry, iCCD imaging and electric measurements. Different modes of operation were achieved by varying the feeding gas (He) flow between 2 slm (coupled mode) and 7 slm (uncoupled mode). A molecular beam mass spectrometer (HIDEN HPR60) was used to detect mass spectra of plasmas. Residual gas analyses (RGA) mode and secondary ion mass spectrometry mode (SIMS+/-) were used to investigate the mass spectra of neutral species and of positive and negative ions respectively, for different sets of operating conditions in both coupled and uncoupled mode. ICCD analysis and electrical characterization were also performed to investigate the temporal evolution of the plasma structure in the two modes.

Results shows that in the coupled mode ion concentrations are at least one order of magnitude higher as compared to the uncoupled mode for similar operating conditions. Consistently, ICCD acquisitions shows higher emission intensity in coupled than uncoupled mode and differences in plasma front propagation.

1. J. Kim et al, "Intense and Energetic Atmospheric Pressure Plasma Jet Arrays", Plasma Processes Polymers, 2012, 9.
2. V. Colombo et al. "iCCD imaging of the transition from uncoupled to coupled mode in a plasma source for biomedical and materials treatment applications", IEEE Transactions on Plasma Science, 2014, 42, 10.

* Work partially supported by COST Action MP1101. NS, NP and ZLjP grateful to the projects ON171037 and III41011, MESTD, Serbia.

27th Summer School and International Symposium on the Physics of Ionized Gases

August 26-29, 2014, Belgrade, Serbia

CONTRIBUTED PAPERS

&

ABSTRACTS OF INVITED LECTURES, TOPICAL INVITED LECTURES, PROGRESS REPORTS AND WORKSHOP LECTURES

Editors:
Dragana Marić
Aleksandar R. Milosavljević
Zoran Mijatović

Institute of Physics, Belgrade
University of Belgrade

Serbian Academy
of Sciences and Arts

www.spig2014.ipb.ac.rs

27th Summer School and International Symposium on the Physics of Ionized Gases

SPIG 2014

CONTRIBUTED PAPERS

&

ABSTRACTS OF INVITED LECTURES,
TOPICAL INVITED LECTURES, PROGRESS REPORTS
AND WORKSHOP LECTURES

Editors

Dragana Marić, Aleksandar R. Milosavljević and
Zoran Mijatović

Institute of Physics, Belgrade
University of Belgrade

Serbian Academy
of Sciences and Art

Belgrade, 2014

CONTRIBUTED PAPERS & ABSTRACTS OF INVITED LECTURES, TOPICAL INVITED LECTURES, PROGRESS REPORTS AND WORKSHOP LECTURES
of the 27th Summer School and International Symposium on the Physics of Ionized Gases

August 26 – 29, 2014, Belgrade, Serbia

Editors:

Dragana Marić, Aleksandar R. Milosavljević and Zoran Mijatović

Publishers:

Institute of Physics,Belgrade
Pregrevica 118, P. O. Box 68
11080 Belgrade, Serbia

Klett izdavačka kuća d.o.o.
Maršala Birjuzova 3-5, IV sprat
11000 Belgrade

Computer processing:

Sanja D. Tošić, Nikola Škoro and Miloš Ranković

Printed by

CICERO
Belgrade

Number of copies

300

ISBN 978-86-7762-600-6

©2014 by the Institute of Physics, Belgrade, Serbia and Klett izdavačka kuća d.o.o. All rights reserved. No part of this book may be reproduced, stored or transmitted in any manner without the written permission of the Publisher.

METHICILIN RESISTANT *STAPHYLOCOCCUS AUREUS* INHIBITION ZONE AREAS OBTAINED BY A PLASMA NEEDLE TREATMENT

Nenad Selaković[1], Nevena Puač[1], Maja Miletić[2], Irena Živanović[3], Ivana Dakić[3], Gordana Malović[1], Dragana Vuković[3] and Zoran Lj. Petrović[1]

[1]*Institute of Physics, University of Belgrade, Pregrevica 118, 11080 Belgrade, Serbia*
[2]*Faculty of Dental Medicine, University of Belgrade, dr Subotića , 11000 Belgrade, Serbia*
[3]*Institute of Microbiology and Immunology, Faculty of Medicine, University of Belgrade, dr Subotica 1, 11000 Belgrade, Serbia*

Abstract. Plasma needle, nonequilibrium plasma source that operates at atmospheric pressure, was used for treatments of methicilin resistant *Staphylococcus aureus* (MRSA). Free radicals and other ion species formed inside the gas mixture of helium and air in the plasma needle discharge are cause for the inactivation of bacteria. In this paper we will show how the inhibition zone areas depend on the applied plasma power, distance of the plasma source relative to the sample and the exposure time.

1. INTRODUCTION

The expansion of the relatively new field of medicine, plasma medicine, is reflected in the development of new plasma devices operating at atmospheric pressure that can be used in the treatment of biological samples. Some of these atmospheric plasma sources, such as plasma jet, plasma needle, DBD and plasma torch [1-4] have been already used and investigated for possible application in sterilization of wounds and medical equipment, treatment of dental caries, faster coagulation of blood, inactivation of cancer cells [5-8], etc.

Plasma needle, originally introduced by Stoffels [9], is atmospheric pressure plasma source suitable for the treatment of biological samples. We have developed slightly advanced version of the plasma needle and, so far, used it for sterilization of planctonic samples of bacteria, differentiation of human periodontal stem cells into osteogenic line and for plant stem cells – calli. [10-12]. Plasma needle is mild source of plasma, but with abundant chemistry that is essential for successful treatments. One of the most important limits that has to be determined is the area of the treatment i.e. the range of the radical and ion species from the plasma. Therefore, we have used MRSA samples in order to determine

zone of inhibition for different treatment times, powers and distances of the source from the sample.

2. EXPERIMENT

Plasma needle is made of glass tube with o.d. of 6 mm and i.d. of 4 mm. Ceramic tube (o.d. ~1 mm) with tungsten wire is placed inside the glass tube. Tungsten wire serves as powered electrode. Helium flows between the ceramic and glass tube. During all experiments helium flow was kept constant at 1 slm. The plasma appears on the tip as a faint glow with a diameter around 1 mm. We power this plasma device with sine wave signal at 13.56 MHz. Electrical circuit of plasma needle contains signal generator, linear amplifier and matching box.
The MRSA isolate used in this study was recovered from a surgical wound and identified as MRSA by by BD Phoenix Automated Microbiology System (Becton Dickinson Diagnostic Systems, Sparks, MD). Bacterial suspension were prepared by suspending overnight grown culture in sterile physiological saline. The turbidity of bacterial inoculum was adjusted to 0.5 McFarland standard ($\approx 10^8$ CFU/mL) by using a Densimat photometer (BioMeriex, France). After that suspension was spread evenly on the surface of a solid growth media in Petri dishes and exposed to the plasma needle.

We divided each Petri dish into the 9 areas and each area was exposed to the treatment. The experimental parameters that we varied were distance between tip of the needle and sample surface (2 mm and 4 mm), exposure time (60 s, 180 s and 300 s) and power delivered to the plasma (1.5 W-3 W). All treatments were done in triplicate. As control we have used untreated samples and helium treated samples when there was no ignition of the discharge.

3. RESULTS AND DISCUSSION

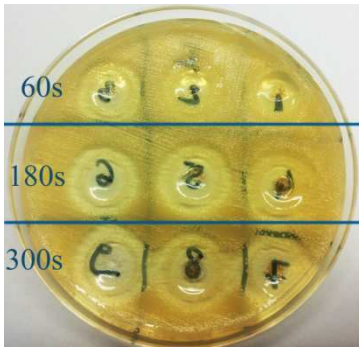

Figure 1. Treated samples of MRSA placed in Petri dish

In the Fig. 1 we can see inhibition zone areas obtained for the power of 1.5 W. Three upper fields were treated for exposure time of 60 s, the middle three fields 180 s and three fields below for 300 s. The needle in this plasma

treatment was set at a distance of 2 mm and it can be seen that the inhibition zone areas have larger diameter compared to the plasma needle.

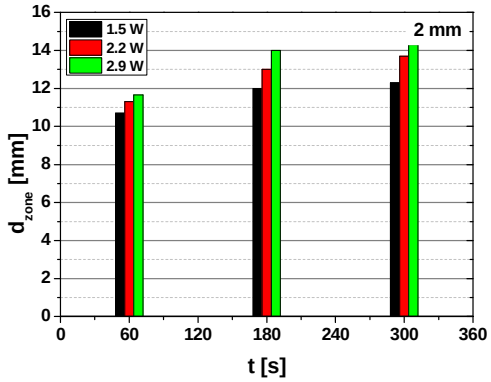

Figure 2. Comparison of MRSA inhibition area diameter for three different applied power of plasma needle and three different exposure times. The distance from plasma to sample was 2 mm.

Fig. 2 shows that the inhibition zone areas expand with the increase of the plasma power and the exposure time. Diameters of the obtained areas are in the range of 10-15 mm. We can see that there is no linear dependence of the measured diameters versus treatment time. With the increase of the treatment time diameters of the inhibition zones saturate at certain values. The higher the power saturation will occur for shorter treatment times. The largest inhibition area is obtained for maximum power 2.9 W, exposure time 300 s and the minimum distance of 2 mm.

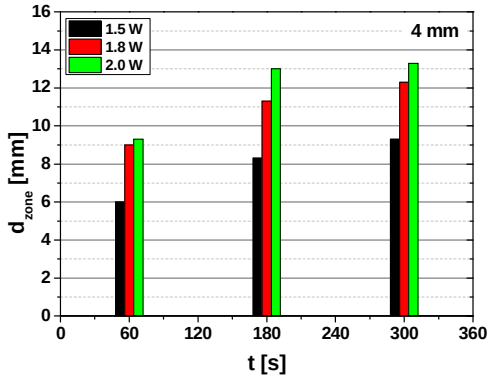

Figure 3. Comparison of MRSA inhibition area diameter for three different applied power of plasma needle and three different exposure times. The distance from plasma to sample was 3 mm.

For treatments with a distance of 4 mm we have observed smaller inhibition zones (see Fig. 3). This can be explain by following. Increase in the distance between the tip of the plasma needle and sample leads to a reduction in power and consequently we have reduced production of chemically reactive species. As in case for 2 mm distance increase in treatment time leads to saturation values of inhibition zones diameters.

4. CONCLUSION

We used the plasma needle in order to determine the surface area of the sample where the plasma makes inhibition effects. It was shown that the obtained inhibition zone areas are much larger than the size of the plasma needle.

Acknowledgements

This study was supported by Grant Nos. III41011, ON171037 and ON173024, MESTD, Republic of Serbia.

REFERENCES

[1] N. Puač, D. Maletić, S. Lazović, G. Malović, A. Đorđević, and Z. Lj. Petrović, Appl Phys. Lett., 101, 24103, (2012).
[2] E. Stoffels, I. E. Kieft, R. E. J. Sladek, E. P. Van Der Laan, and M. Steinbuch, Plasma Sources Sci. Technol. 15, 169, (2006).
[3] I. A. Shkurenkov, Y. A. Mankelevich, and T. V Rakhimova, Eur. Phys. J. D. 62, 213, (2011).
[4] S. Yonson, S. Coulombe, V. Léveillé, and R. L. Leask, J. Phys. D: App. Phys. 39, 3508, (2006).
[5] M. Laroussi, Plasma Processes Polym. 2, 391, (2005).
[6] E. Stoffels, A. J. Flikweert, W. W. Stoffels, and G. M. W. Kroesen, Plasma Sources Sci. Technol. 11, 383, (2002).
[7] G. Fridman, G. Friedman, A. Gutsol, A. B. Shekhter, V. N. Vasilets, and A. Fridman, Plasma Processes Polym. 5, 503 (2008).
[8] B. Gweon, M. Kim, D. Bee Kim, D. Kim, H. Kim, H. Jung, J. H. Shin, andW. Choe, Appl. Phys. Lett. 99, 63701 (2011).
[9] E. Stoffels, Y. A. Gonzalvo, T. D. Whitmore, D. L. Seymour, and J. A. Rees, Plasma Sources Sci. Technol. 15, 501, (2006).
[10] S. Lazović, N. Puač, M. Miletić, D. Pavlica, M. Jovanović, D. Bugarski, S. Mojsilović, D. Maletić, G. Malović, P. Milenković, and Z. Petrović, New J. Phys.12, 83037, (2010).
[11] M. Miletić, S. Mojsilović, I. Okić Đorđević, D. Maletić, N. Puač, S. Lazović, G. Malović, P. Milenković, Z. Lj Petrović, and D. Bugarski, J. Phys. D: Appl. Phys. 46, 345401, (2013).
[12] N. Puač, S. Živković, N. Selaković, M. Milutinović, J. Boljević, G. Malović, and Z. L. Petrović, Appl. Phys. Lett., 104214106, (2014).

Ministry of Education,
Science and Technological Development
Republic of Serbia

IOP Conference Series

28th Summer School and International Symposium on the Physics of Ionized Gases

Aug. 29 - Sep. 2, 2016, Belgrade, Serbia

CONTRIBUTED PAPERS
&
ABSTRACTS OF INVITED LECTURES, TOPICAL INVITED LECTURES, PROGRESS REPORTS AND WORKSHOP LECTURES

Editors:
Dragana Marić, Aleksandar Milosavljević,
Bratislav Obradović and Goran Poparić

University of Belgrade,
Faculty of Physics

Serbian Academy
of Sciences and Arts

28th Summer School and International Symposium on the Physics of Ionized Gases

S P I G 2016

CONTRIBUTED PAPERS

&

ABSTRACTS OF INVITED LECTURES,
TOPICAL INVITED LECTURES, PROGRESS REPORTS
AND WORKSHOP LECTURES

Editors

Dragana Marić, Aleksandar Milosavljević,
Bratislav Obradović and Goran Poparić

University of Belgrade,
Faculty of Physics

Serbian Academy
of Sciences and Arts

Belgrade, 2016

CONTRIBUTED PAPERS & ABSTRACTS OF INVITED LECTURES, TOPICAL INVITED LECTURES, PROGRESS REPORTS AND WORKSHOP LECTURES

of the 28th Summer School and International Symposium on the Physics of Ionized Gases

August 29 – September 2, 2016, Belgrade, Serbia

Editors:
Dragana Marić, Aleksandar Milosavljević,
Bratislav Obradović and Goran Poparić

Publisher:
University of Belgrade, Faculty of Physics,
Belgrade
Studentski trg 12, P. O. Box 44
11000 Belgrade, Serbia

Computer processing:
Tatjana Milovanov

Printed by
Skripta Internacional, Mike Alasa 54, Beograd

Number of copies
200

ISBN 978-86-84539-14-6
©2016 by University of Belgrade, Faculty of Physics
All rights reserved. No part of this book may be reproduced, stored or transmitted in any manner without the written permission of the Publisher.

LOW TEMPERATURE PLASMA NEEDLE REDUCES THE SURVIVAL OF CANCER CELLS

Nenad Selaković[1], Nevena Puač[1], Nevenka Gligorijević[2], Milena Čavić[2], Gordana Malović[1], Radmila Janković[2], Siniša Radulović[2] and Zoran Lj. Petrović[1,3]

[1] *Institute of Physics, University of Belgrade, Pregrevica 118, 11080 Belgrade, Serbia*
[2] *Institute for Oncology and Radiology of Serbia, Pasterova 14, 11000 Belgrade, Serbia*
[3] *Serbian Academy of Sciences, Knez Mihailova 35, 11000 Belgrade, Serbia*

Abstract. The aim of this study was to investigate whether plasma needle induces cancer cell death. This atmospheric pressure plasma source generates reactive oxygen species (ROS) and reactive nitrogen species (RNS) that are presumed to be major causes of cancer cell death. Here we report the influence of the power transmitted to the plasma and the exposure time on cell survival using two cancer cell lines, A549 and HeLa.

1. INTRODUCTION

The rapid development of plasma medicine, a new promising scientific field, occurred during the last decade. Using plasma physics in a wide range of sophisticated fundamental experiments involving the treatment of cells and tissues opened the door of *in vivo* therapeutic applications. Several atmospheric pressure plasma devices, such as plasma jet, plasma needle, dielectric barrier discharge (DBD) and plasma torch [1-4], have already been used for sterilization of wounds and medical equipment, treatment of dental caries and faster coagulation of blood.[5-7]

Our plasma needle is a more advanced version of the one that was originally presented by Stoffels [8] and we have used it in several applications like sterilization of planktonic bacteria, differentiation of human periodontal stem cells into an osteogenic line and for plant stem cells – calli.[9-11]

Lately, low-temperature plasmas are attracting great attention in the field of oncology [12]. In this study we used the plasma needle for the treatment of two cancer cell lines (HeLa and A549). The plasma needle discharge is a mixture consisting of reactive species and radicals that are formed in contact with the surrounding air and the treated sample. The change of power delivered to the plasma and the exposure time create different amounts of ROS and RNS that are

delivered to the treated cells, so we observed the effect on cell survival for the used set of parameters.

2. EXPERIMENT

The construction of the plasma needle was designed to be suitable for applications in direct contact with the sample. The body of the plasma needle is made of Teflon. Inside the body we put a Pyrex glass tube (o.d. 6 mm and i.d. 4 mm) through which we released 1 slm of helium as the feeding gas. A tungsten wire was used as the central electrode powered with 13.56 MHz sine wave and it was placed within a ceramic tube inside the glass tube. The role of the ceramic tube is to prevent discharge between the central electrode and the glass tube. The ceramic electrode is sticking 1 mm outside of the ceramic and glass tubes so the discharge occurs on its tip as a weak glow.

A549 (lung adenocarcinoma) and HeLa (cervical cancer) cell lines were used as representative cancer cell lines. The cells were maintained in RPMI-1640 medium (Sigma-Aldrich, Co, USA) with 10% heat inactivated newborn calf serum (Sigma-Aldrich, Co, USA) at 37°C in 5% CO2.

The cells were seeded in 96-well cell culture plates, A549 (7000 cells/well), HeLa (4000 cells/well). We have varied two experimental parameters: exposure time (10 s, 30 s and 60 s) and power delivered to the plasma (1.3 W and 2.2 W). The distance between the plasma needle tip and the sample surface was 5 mm and we kept it constant during all experiments. The experiments were performed in triplicates, and untreated cells and medium-treated cells were used as controls.

After the treatment we have measured the cytotoxic activity of plasma needle on HeLa and A549 cell lines using an MTT assay according to the method of Mosmann (1983) and modified by Ohno and Abe (1991).

3. RESULTS AND DISCUSSION

Several different factors can affect the death of cancer cells such as the type of the cell and the type of the treatment (direct and indirect contact with the sample). Here we used the direct contact method of discharge on the sample which is more effective than the indirect contact (discharge in contact with the medium without cells).

In Fig.1 we show images of microtiter plate wells observed by optical microscopy. One can notice a reduction in the number of A549 cells between the control (untreated samples) and the treated samples for different powers of plasma (1.3 W and 2.2 W) and different exposure times (10 s, 30 s and 60 s).

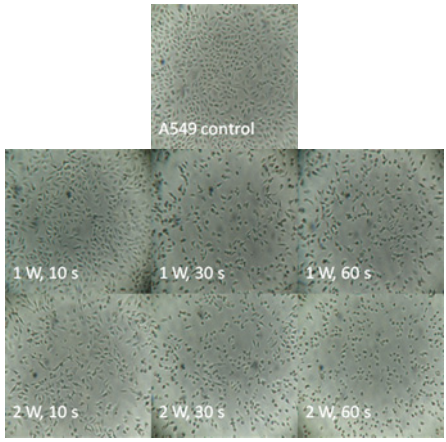

Figure 1. Images of microtiter plate wells obtained by optical microscopy for untreated A549 cells (control) and treated A549 cells for different powers of plasma and exposure times.

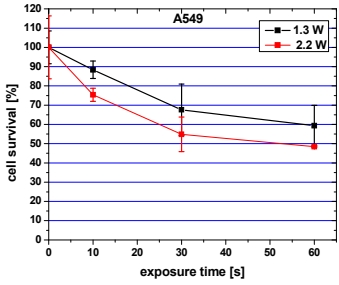

Figure 2. Cell survival comparison of A549 cells for two different applied powers and three different exposure times. The distance from plasma to sample was 5 mm.

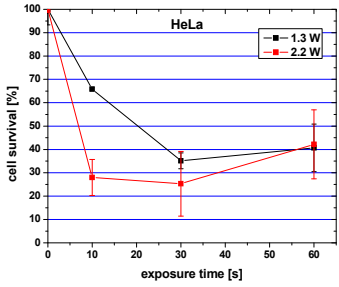

Figure 3. Cell survival comparison of HeLa cells for two different applied powers and three different exposure times. The distance from plasma to sample was 5 mm.

Fig. 2 represents a graphic view of the results of A549 cells already showed in Fig 1. and here one can notice an exponential drop caused by a longer exposure time for two different applied powers of discharge (1.3 W and 2.2 W). From the given chart it is obvious that higher power is more efficient in reducing cancer cell survival.

HeLa cells displayed greater vulnerability to the impact of plasma than A549 cells, especially for the higher power output (2.2 W) where a significant drop in cell survival (Fig. 3.) at the shortest exposure time (10 s) was observed. In both cases (1.3 W and 2.2 W), the effect of reducing cell survival was higher than 50%.

4. CONCLUSION

In this study we used our version of plasma needle for the treatment of two different carcinoma cell lines (HeLa and A549) in order to observe the effect on cell survival. Due to the different nature of the investigated cancer cell lines, which is reflected in a number of differences, among them and in the cells defense system (e.g the cell response to oxidative stress.) [13], these two lines showed different sensitivity to plasma treatment. The HeLa cells were more sensitive than A549 cells on the plasma treatment which was manifested in higher reduction of the cell survival determined by MTT assay.

Acknowledgements

This study was supported by Grant Nos. III41011, ON171037, III41026, and ON173024, MESTD, Republic of Serbia

REFERENCES

[1] N. Puač, D. Maletić, S. Lazović, G. Malović, A. Đorđević, and Z. Lj. Petrović, Appl Phys. Lett., 101, 24103, (2012).
[2] E. Stoffels, I. E. Kieft, R. E. J. Sladek, E. P. Van Der Laan, and M. Steinbuch, Plasma Sources Sci. Technol. 15, 169, (2006).
[3] I. A. Shkurenkov, Y. A. Mankelevich, and T. V Rakhimova, Eur. Phys. J. D. 62, 213, (2011).
[4] S. Yonson, S. Coulombe, V. Léveillé, and R. L. Leask, J. Phys. D: App. Phys. 39, 3508, (2006).
[5] M. Laroussi, Plasma Processes Polym. 2, 391, (2005).
[6] E. Stoffels, A. J. Flikweert, W. W. Stoffels, and G. M. W. Kroesen, Plasma Sources Sci. Technol. 11, 383, (2002).
[7] G. Fridman, G. Friedman, A. Gutsol, A. B. Shekhter, V. N. Vasilets, and A. Fridman, Plasma Processes Polym. 5, 503 (2008).
[8] E. Stoffels, Y. A. Gonzalvo, T. D. Whitmore, D. L. Seymour, and J. A. Rees, Plasma Sources Sci. Technol. 15, 501, (2006).
[9] S. Lazović, N. Puač, M. Miletić, D. Pavlica, M. Jovanović, D. Bugarski, S. Mojsilović, D. Maletić, G. Malović, P. Milenković, and Z. Petrović, New J. Phys.12, 83037, (2010).
[10] M. Miletić, S. Mojsilović, I. Okić Đorđević, D. Maletić, N. Puač, S. Lazović, G. Malović, P. Milenković, Z. Lj Petrović, and D. Bugarski, J. Phys. D: Appl. Phys. 46, 345401, (2013).
[11] N. Puač, S. Živković, N. Selaković, M. Milutinović, J. Boljević, G. Malović, and Z. L. Petrović, Appl. Phys. Lett., 104214106, (2014).
[12] N. Kaushik, N. Uddin, G. B. Sim, Y. J.Hong, K. Y. Baik, C. H. Kim, E. H. Choi, Sci. Rep., *5*, 8587, (2015).
[13] G. Speit and I. Bonzheim, Mutagenesis, 18(6), 545–548, (2003).

CIP - Каталогизација у публикацији
Народна библиотека Србије, Београд

537.56(082)
539.186.2(082)
539.121.7(082)
533.9(082)

SUMMER School and International Symposium on the Physics of Ionized Gases (28 ; 2016 ; Beograd)
Contributed Papers & Abstracts of Invited Lectures, Topical Invited Lectures, Progress Reports and Workshop Lectures / 28th Summer School and International Symposium on the Physics of Ionized Gases - SPIG 2016, [August 29 - September 2], 2016, Belgrade ; editors Dragana Marić ... [et al.]. - Belgrade : University of Belgrade, Faculty of Physics, 2016 (Beograd : Skripta Internacional). - 474 str. : ilustr. ; 24 cm

Tiraž 200. - Str. 5: Preface / editors Dragana Marić ... [et al.]. - Napomene i bibliografske reference uz tekst. - Bibliografija uz svaki rad. - Registar.

ISBN 978-86-84539-14-6
1. Marić, Dragana, 1973- [уредник] [аутор додатног текста]
a) Јонизовани гасови - Зборници b) Атоми - Интеракција - Зборници
c) Плазма - Зборници
COBISS.SR-ID 225356044

ISBN 978-86-7031-242-5

SPIG 2012

26th Summer School and International Symposium on the Physics of Ionized Gases

August 27th -31st, 2012, Zrenjanin Serbia

CONTRIBUTED PAPERS & ABSTRACTS OF INVITED LECTURES AND PROGRESS REPORTS

Editors
M. Kuraica, Z. Mijatović

University of Novi Sad, Faculty of Sciences
Department of Physics
Novi Sad, Serbia

ISBN 978-86-7031-242-5

CONTRIBUTED PAPERS & ABSTRACTS
OF INVITED LECTURES AND PROGRESS REPORTS
of the
26th SUMMER SCHOOL AND INTERNATIONAL
SYMPOSIUM ON THE PHYSICS OF IONIZED GASES

August 27th - 31st, Zrenjanin, Serbia

Editors: Milorad Kuraica
Zoran Mijatović

Publisher:

University of Novi Sad
Faculty of Sciences
Department of Physics
Trg Dositeja Obradovića 3
21000 Novi Sad, Serbia

CIP - Каталогизација у публикацији
Библиотека Матице Српске, Нови Сад

537.56(082)
539.186.2(082)
539.121.7(082)
533.9(082)

SUMMER School and International Symposium on the Physics of Ionized Gases (26 ; 2012 ; Zrenjanin)
Contributed papers & abstracts of invited lectures and progress reports / SPIG 2012 - 26th Summer School and International Symposium on the Physics of Ionized Gases, August 27th-31st, 2012, Zrenjanin Serbia ; editor Z. Mijatović. - Novi Sad : Faculty of sciences, Department of physics, 2012 (Novi Sad : Stojkov). - XVII, 403 str. : ilustr. ; 24 cm

Str. III: Preface / editors. - Napomene i bibliografske reference uz tekst. - Bibliografija uz svaki rad. - Registar.

ISBN 978-86-7031-242-5
I. SPIG (26 ; 2012 ; Zrenjanin) v. Summer School and International Symposium on the Physics of Ionized Gases (26 ; 2012 ; Zrenjanin)
a) Јонизовани гасови - Зборници b) Атоми - Интеракција - Зборници c) Плазма - Зборници
COBISS.SR-ID 272861703

© **2012 Department of Physics, Novi Sad**

All rights reserved.
No part of this publication may be reproduced, stored in retrieval systems, in any form or any means, electronic, mechanical, photocopying or therwise, without the prior permission of the copyright owner.

Printed by:
Štamparija "Stojkov", Novi Sad, Serbia

S3.39 S. Mijović, M. Vučeljić and M. Šćepanović
THE OPTICAL EMISSION SPECTROSCOPY EXPERIMENT OF OPEN AIR PLASMAS 293

S3.40 M. Šćepanović, M. Vučeljić and S. Mijović,
SPECTROSCOPIC TEMPERATURE MEASUREMENTS IN A FREE-BURNING ZINCVAPOR ELECTRIC ARC 297

S3.41 S. N. Stamenković, V. Lj. Marković, S. R. Gocić, A. P. Jovanović, M. N. Stankov and N. D. Nikolić
INFLUENCE OF SURFACE CHARGES ON DC GLOW DISCHARGE IN NEONWITH Au-Ni CATHODE SPOTS 301

S3.42 K. Spasić, S. Lazović, N. Puač, Z. Lj Petrović, G. Malović, M. Mozetič and Uroš Cvelbar
CATALYTIC PROBE MEASUREMENTS OF ATOMIC OXYGEN CONCENTRATION IN LARGE VOLUME OXYGEN CCP 305

S3.43 N. Selaković, D. Maletić, N. Puač, S. Lazović, G. Malović, A. Djordjević and Z. Lj. Petrović
AXIAL PROFILES OF PLASMABULLET WITH DIFFERENT ELECTRODE GAPS 309

S3.44 T. Gajo, I. Savić , R. Kobilarov and Z. Mijatović
STARK WIDTHS OF SEVERALAr II SPECTRAL LINES EMITTED FROM PULSED ARC PLASMAS 313

S3.45 I. Savić, L. Gavanski, S. Djurović, Z. Mijatović and R. Kobilarov
ICCD SPECTROMETER – CHARACTERIZATION OF INSTRUMENTAL LINE PROFILES AND SATURATION LEVEL DETERMINATION 317

S3.46 A. A. Kirillov, Y. A. Safronau, L.V. Simonchik, N. V. Dudchik and O. E. Nezhvinskaya
DC ATMOSPHERIC PRESSURE GLOW DISCHARGE COLD PLASMA FOR BACTERIA INACTIVATION 321

S3.47 M. Savić, M. Radmilović-Radjenović, B. Radjenović
THEORETICAL PREDICTIONS OF THE MICROWAVE BREAKDOWN FIELD 325

S3.48 M. Savić, M. Radmilović-Radjenović, D. Marić, M. Šuvakov, Z. Lj. Petrović
MONTE CARLO SIMULATIONS OF RF BREAKDOWN 329

S3.49 S. Marjanović, A. Banković, M. Šuvakov, T. Mortensen, A. Deller, C. A. Isaac, D. P. van derWerf, M. Charlton, Z. Lj. Petrović
COLLISION-DRIVEN POSITRON CLOUD EXPANSION – EXPERIMENTAND SIMULATION 333

S3.50 S. Marjanović, M. Šuvakov and Z. Lj. Petrović
MONTE CARLO SIMULATION OF POSITRON TRAPPING EFFICIENCY 337

AXIAL PROFILES OF PLASMA BULLET WITH DIFFERENT ELECTRODE GAPS

Nenad Selaković[1], Dejan Maletić[1], Nevena Puač[1], Saša Lazović[1], Gordana Malović[1], Antonije Đordjević[2] and Zoran Lj. Petrović[1]

[1]Institute of Physics, University of Belgrade, Pregrevica 118, 11080 Belgrade, Serbia
[2]School of Electrical Engineering, University of Belgrade, Bulevar kralja Aleksandra 73, 11000 Belgrade, Serbia

Abstract. We used fast ICCD imaging in order to record time evolution of plasma bullet formation. Plasma jet was made of Pyrex glass tube with two transparent electrodes made of polyester (PET) foil whose position can be easily adjusted. The excitation voltage was approximately 10 kVpp at frequency of 80 kHz. The power transmitted to the plasma in all measurements was 4 W. The working gas was helium with constant flow rate of 4 slm. In this paper we shall show the total axial light emission profiles of plasma jet bullets obtained for three different electrode gaps, of 10, 15 and 20 mm.

1. INTRODUCTION

One of the main reasons for the development of new low temperature plasma sources which are working at atmospheric pressure is their simple, non-expensive design with great potential for possible applications. These plasma sources are used for treatment of polymers, cells, tissues, etc. [1-3]. One of the newest scientific fields developed from this high-end research is plasma medicine [4]. Achieving high temperatures of electrons, much higher than the temperatures of ions and ambient gas, is crucial for sustaining stabile non-equilibrium plasmas. In order to reduce the breakdown voltage in these discharges, noble gases are used, usually helium or argon [5]. For powering plasma jets, various types of signals at high frequencies are used [6], as well as different geometries [7, 8]. By choosing different materials for the electrodes, different electrode gaps and sizes, one can significantly change the behavior of plasma jets and control if the plasma jet will form bullets or not. The optimal geometry parameters can be found in order to maximize the distance that plasma bullets can reach. In this paper we present axial profiles for several gaps between the powered and the grounded electrode.

2. EXPERIMENTAL SETUP

The atmospheric pressure plasma jet used in these experiments is shown in Fig. 1. Its body was made of a Pyrex glass tube (O. D. of 6 mm and I. D. of 4 mm) with two transparent thin conductive PET foil electrodes (width of 15 mm) wrapped around the glass tube. The copper foil was used to connect electrodes to an external electrical circuit. The electrode closer to the edge of the glass tube was the powered one, and the other electrode was grounded (see Fig. 1). A resistor of 100 kΩ between the grounded electrode and the ground was connected for current measurements. During all measurements, the helium flow rate was 4 slm. As the power supply, a signal generator was used, and it was connected to a home-made amplifier. The excitation signal was sinusoidal and the working frequency was 80 kHz. Since the maximum value of the voltage at the output of the amplifier is around 1 kV, it was necessary to make a high-voltage transformer to increase the signal from the amplifier up to 10 kV peak-to-peak. The calculated power transmitted to plasma in all measurements was 4 W. The gap between electrodes was 10, 15 and 20 mm. The distance between the powered electrode and the edge of the glass tube was kept constant at 7 mm for all measurements.

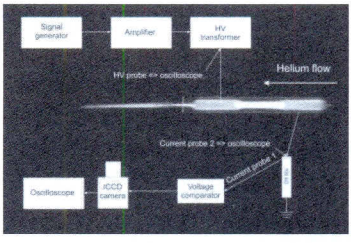

Figure 1. Experimental setup

3. RESULTS AND DISCUSSION

Signals of current and voltage, with trigger positions, are presented in Fig. 2 (left). The voltage signal has pure sine waveform, while the current signal is a somewhat deformed. Three triggering positions of ICCD imaging were selected to present behavior of plasma at different time positions of the whole cycle. The first trigger position is close to the minimum, the second one is near the zero and the third is right after the maximum of the voltage signal. Axial (along the glass tube axis) profiles of plasma emission were calculated from the obtained ICCD images (see Fig. 2 (right)-3). The presented profiles are calculated as a sum of the emission intensity coming from plasma along the axis of the glass tube diameter. In Fig. 2 (right)-3, the right edge of the grounded electrode is chosen to be the reference (zero) position, the positions of the powered and the grounded electrode are marked by vertical solid lines and the edge of the glass tube by a vertical dashed line. The direction of helium flow is from the grounded toward the powered electrode (as shown in Fig. 2 (right)-3).

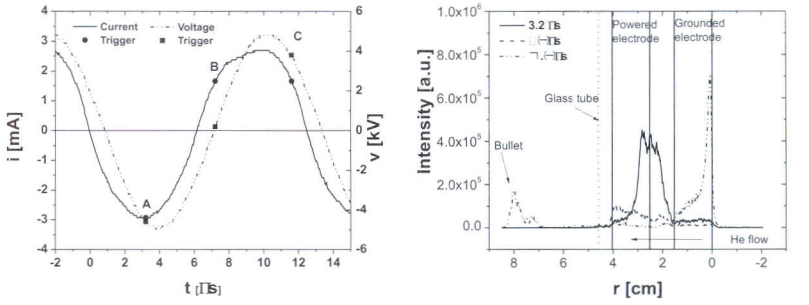

Figure 2. Current and voltage signals with trigger positions for 15 mm electrode gap (left); Axial light emission profiles for 10 mm electrode gap for three different trigger delays (3.2 μs, 7.2 μs and 11.6 μs), 4 slm flow of helium and power of 4 W

Axial profiles of light emission for the gap of 10 mm between electrodes are shown in Fig. 2 (right). For the minimum of the voltage and current signal, the maximum emission intensity coming from the discharge is on the right edge of the powered electrode (Fig. 2 (right), black solid curve). At the same time, the emission intensity in other areas is several orders of magnitude smaller. With increase of the voltage and current signals, plasma is moving towards the left edge of the powered electrode and the emission intensity decreases.

For the delay of 7.2 μs (Fig. 2 (right), black dashed curve) the intensity is very small with the maximum near the left edge of the powered electrode. A plasma bullet is formed at the maximum values of current and voltage signals and it reaches the maximum distance of 3.5 cm from the edge of the glass tube for the delay time 11.6 μs. Also, there is another well-defined maximum at the right edge of the grounded electrode.

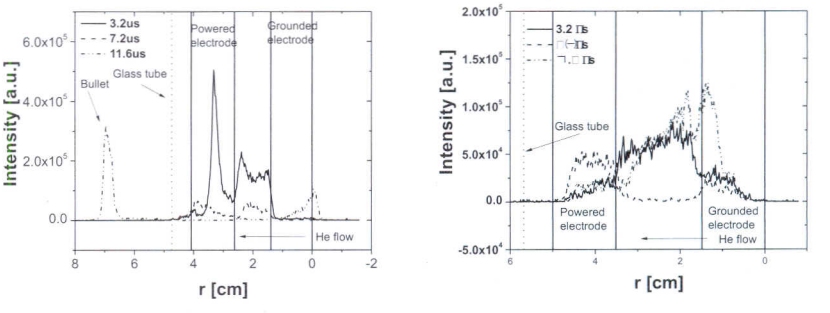

Figure 3. Axial light emission profiles for 15 mm (left) and 20 mm (right) electrode gap for three different trigger delays (3.2 μs, 7.2 μs and 11.6 μs), 4 slm flow of helium and power of 4 W

Axial profiles for the gap of 15 mm are presented in Fig. 3 (left). A well-defined peak of light emission can be seen in the powered electrode, as

well as significant emission between electrodes (for the delay of 3.2 μs, solid black curve). For the delay of 7.2 μs, the intensity significantly drops in and between the electrodes (dashed black curve). For the delay of 11.6 μs, there are two distinct peaks: one inside the grounded electrode and the second one outside the tube approximately at 2.2 cm from the edge of the glass tube. For the 15 mm gap, the bullet is better defined than in the case of other electrode gaps used in this paper.

For the largest electrode gap in Fig. 3 (right), the emission intensity is much smaller than in other two cases. For the delays of 3.2 μs and 7.2 μs, there are no well-defined peaks. For the delay of 11.6 μs, there is no light emission outside the glass tube. This electrode gap is not suitable for treatment of surfaces because plasma does not leave the glass tube.

4. CONCLUSION

Using ICCD imaging it has been shown that the light emission is highly dependent of the electrode geometry. In this study it is has been shown that if it is needed to obtain a well-defined plasma bullet, the most suitable configuration is a gap of 15 mm between the electrodes. In other two configurations, the plasma bullet is distorted or it does not leave the glass tube at all. One of the directions for future research could be to record emission profiles by using filters for different wavelengths.

Acknowledgements

This research has been supported by the Ministry of Education and Science, Serbia, under projects ON171037 and III41011.

REFERENCES

[1] F. Iza, G. J. Kim, S. M. Lee, J. K. Lee, J. L. Walsh, Y. T. Zhang, M. G. Kong, Plasma Process. Polym. 5, 322–344 (2008).
[2] A. Shashurin, M. Keidar, S. Bronnikov, R. A. Jurjus, M. A. Stepp, Appl. Phys. Letters 93, 181501 (2008).
[3] S. J. Kim, T. H. Chung, S. H. Bae, S. H. Leem, Appl. Phys. Letters 97, 023702 (2010).
[4] A. V. Nastuta, I. Topala, C. Grigoras, V. Pohoata, G. Popa, J. Phys. D: Appl. Phys. 44,105204(2011).
[5] H. S. Park, S. J. Kim, H. M. Joh, T. H. Chung, S. H. Bae, S. H. Leem, Phys. Plasmas 17, 033502 (2010).
[6] Q. Xiong, X. P. Lu, K. Ostrikov, Y. Xian, C. Zou, Z. Xiong, Y. Pan, Phys. Plasmas17, 043506 (2010).
[7] E. Karakas, M. Koklu, M. Laroussi, J. Phys. D: Appl. Phys. 43,155202 (2010).
[8] N. Jiang, A.Ji, Z. Cao, J. Appl. Phys. 108, 033302 (2010).